UNIVERSITY OF CALIFORNIA, SAN DIEGO

Ultraviolet Resonance Raman Spectroscopy of the Integral Membrane Protein OmpA: Elucidating Structure and Tryptophan Microenvironment of Folded and Unfolded States

A thesis submitted in partial satisfaction of the requirements
for the degree of Master of Science

in

Chemistry

by

Tiffany Jonean Neary

Committee in charge:

Professor Judy Kim, Chair
Professor Douglas Madge
Professor Ulrich Muller

2008

The thesis of Tiffany Jonean Neary is approved, and it is acceptable in quality and form for publication on microfilm and electronically:

_____

_____

_____

Chair

University of California, San Diego

2008

DEDICATION

This work is dedicated to my parents, Harold and Candice Neary, who have supported me throughout my life. You have provided me with everything I need in life and you have allowed me to pursue my own paths, with little objection. Thank you.

I would also like to devote this to my fiancé, Kevin Rynearson. You have shown me an incredible amount of love, patience, and support. You were always able to make me laugh during stressful times. You help me to appreciate what is important in life.

To Kitty Hawk, thank you for the wisdom and adventures, as I probably would have lost my mind without them. You have helped me find balance. You are my Ying.

Science is not formal logic–it needs the free play of the mind in as great a degree as any other creative art. It is true that this is a gift which can hardly be taught, but its growth can be encouraged in those who already posses it.

Max Born (1882-1970) German Physicist. Nobel Prize, 1954.

TABLE OF CONTENTS

LIST OF FIGURES

LIST OF TABLES

ACKNOWLEDGEMENTS

I would like to acknowledge and thank my PI, Professor Judy Kim, for supporting me during this work. Thank you for taking me in as an undergraduate and allowing me to continue to work in your lab as a master's student. You have stimulated my interests in spectroscopy. I have gained an incredible amount of knowledge from you that I will take with me as I move on in life.

I would also like to thank my OmpA colleague, Katie Sanchez, for always sharing her knowledge with me and nurturing my development in chemistry.

To all the members of the Judy Kim group, Vanessa Oklejas, Diana Schlamadinger, Hannah Shafaat, Jonathan Gable, Tim Tirrell, and Eric Smoll, I thank you. You have all helped me to grow and learn, not just in science but also in life.

ABSTRACT OF THE THESIS

Ultraviolet Resonance Raman Spectroscopy of the Integral Membrane Protein OmpA: Elucidating Structure and Tryptophan Microenvironment of Folded and Unfolded States

by

Tiffany Jonean Neary

Master of Science in Chemistry

University of California, San Diego, 2008

Professor Judy Kim, Chair

A 325 residue integral membrane protein, outer membrane protein A (OmpA), has been investigated using ultraviolet resonance Raman spectroscopy at 207.5 nm and 228 nm to elucidate differences in secondary structure and tryptophan microenvironment of various OmpA mutants. OmpA was investigated in its native form containing five tryptophans, as a trp-less mutant, as five full-length single-trp mutants, and as five truncated single-trp mutants in which the soluble tail (~148 residues) was cleaved from the transmembrane domain (~177 residues). A wavelength-dependence study of a single-trp OmpA mutant was

performed at nine different wavelengths between 206.5-236.5 nm to determine the optimal wavelength that provides the greatest resonance enhancement of the tryptophan modes in OmpA. This wavelength was found to be 228 nm, which is slightly red-shifted from the absorption maximum of tryptophan in solution. Excitation of the protein backbone using 207.5 nm light revealed secondary structure changes between the folded and unfolded states of full-length and truncated single-trp mutants of OmpA, W57 and W57t, respectively, with few noticeable spectral differences between the two mutants. At 228 nm, OmpA wild-type, trp-less and 10 single-trp mutants unfolded in KP_i, folded in SUVs, and folded in OG were examined to identify changes in tryptophan structure and local environment. This study has revealed changes in hydrophobic environments, hydrogen-bonding, and the torsion angle, $|\chi^{2,1}|$.

Introduction and Motivation

Membrane Protein Folding: Why We Care

Protein folding begins with the primary structure of amino acids; the chain of amino acids then folds, resulting in a three dimensional functional structure. The primary structure must adopt the same native conformation every time it folds in order for the protein to be functional. With function relying critically on a protein's structure, it is easy to see why protein folding has intrigued scientists for years and has become a prevalent area of chemistry and biochemistry research.

In recent years, membrane protein folding, specifically, has become a novel area of protein folding studies. As of yet, our knowledge of membrane protein folding is minimal compared to our more extensive knowledge of soluble protein folding. The reason our understanding of membrane protein folding is lacking is due to the difficulty of studying such systems. Some of the difficulties include the hydrophobic nature of integral membrane proteins, the lack of available high resolution structures, the bilayer mechanics and chemistry which make it difficult to find a realistic system to modulate folding events, the low sample yields during expression, and the limited experimental techniques that provide detailed structural information.

Fortunately, scientists are overcoming some of these obstacles in order to study membrane protein folding. For example, we can study β-barrel membrane proteins, which are less hydrophobic than their α-helical bundle counterparts. Also, there has been an increase in high resolution structures available. As of 2003, there have been 75 integral membrane protein structures determined; of

these, only about 12 were β-barrel type.[1, 2] New structures are being solved and are rapidly emerging. Currently, the number of solved structures has risen to ~350, with ~50 being β-barrel type.[3] Additionally, few membrane proteins fold into bilayers easily which has lead to the characterization of realistic membrane protein folding systems.[4] Furthermore, there have been recent advances in new or improved techniques, such as time-resolved tryptophan fluorescence quenching and ultraviolet resonance Raman, which have been able to construct protein folding steps and provide detailed structural information.[5, 6]

Even though membrane protein folding is a challenging topic, it must be done. The benefits of studying such systems far outweigh the difficulties involved. Integral membrane proteins function as a gateway to the cell and have numerous functions including ion-pores, gates, pumps, receptors, membrane anchors, and provide structural support. Estimated at ~1/3 of all cellular proteins, integral membrane proteins are ubiquitous and are often drug targets. Besides the functions that integral membrane proteins provide, misfolding of these proteins is attributed to many diseases, such as cystic fibrosis and Alzheimer's.[7, 8] Therefore, the study of membrane protein folding is necessary, as it relates to these diseases, and such studies will bring us closer to understanding and unraveling the mysteries behind membrane protein folding and misfolding.

There are two types of membrane proteins, α-helical bundles and β-barrels, which follow unique folding mechanisms. A two-stage folding process has been proposed for most α-helical membrane proteins, including bacteriorhodopsin.[9] Due to the hydrophobic nature of α-helical bundle membrane

proteins each helix enters the membrane as a separate unit and then unites in membrane to create a functional folded structure.[10] β-barrel membrane proteins may follow a different folding pathway likely due to their polar side chains.[5] From kinetic and time-resolved tryptophan fluorescence quenching (TDFQ) studies of a model β-barrel membrane protein, outer membrane protein A, it is shown that three distinct steps occur in the folding and insertion process of β-barrel membrane proteins.[2,11] Figure 1 summarizes the folding and insertion mechanism of OmpA.[11] The first step involves the binding of the unfolded protein to a bilayer. In the second step some β–structure is formed and insertion has begun but translocation of the β–strand is not complete. Thirdly, the β–barrel folds as it moves through the bilayer where folding and insertion are completed. Unlike the alpha-helical bundle mechanism of insertion then folding, the β–barrel folding and insertion of OmpA are concerted.

Since membrane proteins carry out their function in association with the lipid bilayer, it is important to discover how protein folding and membrane interactions affect the structural relationship between a protein and a lipid bilayer. The folding interaction of the protein within the bilayer must be characterized in order to fully understand the folding processes in the hopes of solving protein misfolding diseases. One such protein, Outer membrane protein A (OmpA), found in the outer membrane of the Gram-negative bacteria, *Escherichia coli* (*E. coli*), has been well studied. The work presented here provides insight into the structural relationship found when the protein is folded in micelles and bilayers and unfolded, as well as changes in tryptophan microenvironment between the

conformational states.

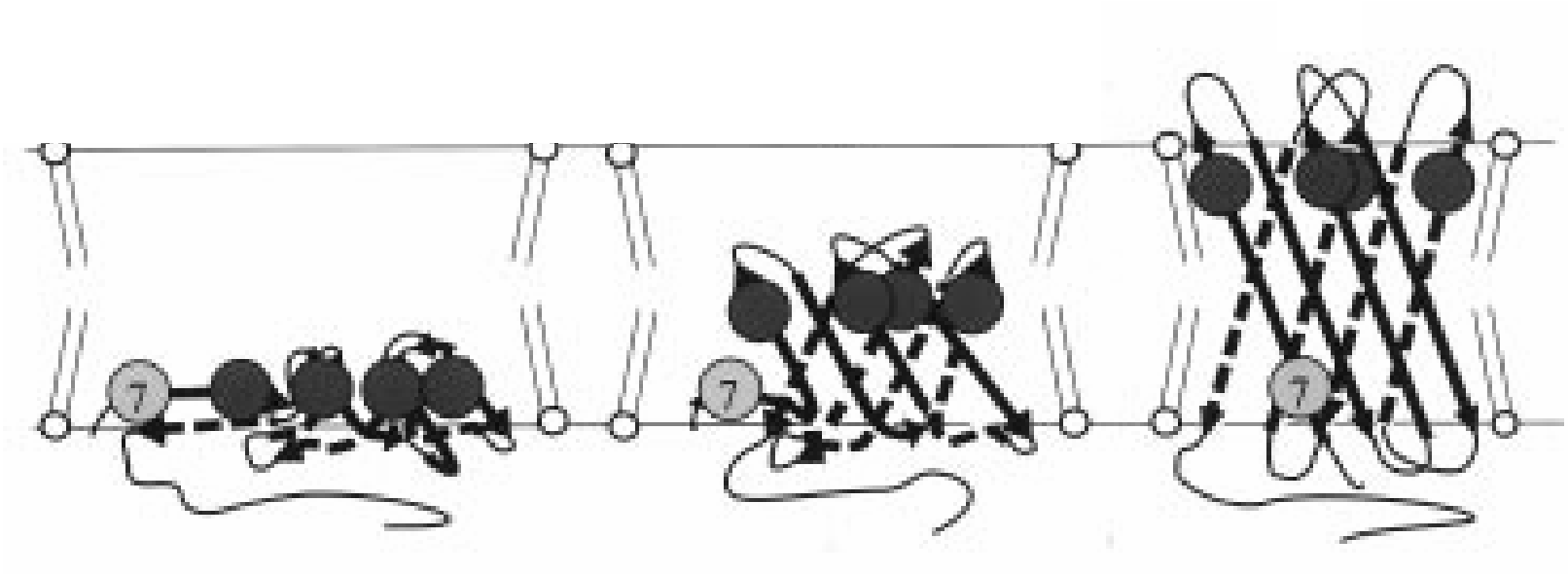

Figure 1. Scheme of the concerted folding and insertion of OmpA into a lipid bilayer, taken from reference 11. Single-tryptophan mutant at residue 7 is shown.

References

1. Stephen H. White. “The Progress of Membrane Protein Structure Determination,” Protein Sci. 13, 7, 1948-1949, 2004.

2. Lukas K. Tamm, Heedeok Hong, and Binyong Liang. “Folding and Assembly of β-barrel Membrane Proteins,” *Biochimica et Biophysica Acta (BBA) - Biomembranes* 1666, 1-2, 250-263, 2004.

3. Stephen H. White. “Membrane Proteins of Known 3D Structure.” <http://blanco.biomol.uci.edu/Membrane_Proteins_xtal.html> 2008.

4. H.D. Hong and L.K. Tamm. “Elastic Coupling of Integral Membrane Protein Stability to Lipid Bilayer Forces,” *Proc. Natl. Acad. Sci. U.S.A*. 101, 12, 4065-4070, 2004.

5. J.H. Kleinschmidt and L.K. Tamm. “Time-Resolved Distance Determination by Tryptophan Fluorescence Quenching: Probing Intermediates in Membrane Protein Folding,” *Biochemistry (N.Y.)* 38, 16, 4996-5005, 1999.

6. H. Vogel and F. Jahnig. ”Models for the Structure of Outer-Membrane Proteins of Escherichia-Coli Derived from Raman-Spectroscopy and Prediction Methods,” *J. Mol. Biol.* 190, 2, 191-199, 1986.

7. C.R. Sanders and J.K. Myers. “Disease-Related Misassembly of Membrane Proteins,” *Annu. Rev. Biophys. Biomol. Struct.* 33, 25-51, 2004.

8. N.N. Dewji and S.J. Singer. “Specific Transcellular Binding between Membrane Proteins Crucial to Alzheimer Disease,” *Proc. Natl. Acad. Sci. U.S.A.* 93, 22, 12575-12580, 1996.

9. J.L. Popot and D.M. Engelman. “Membrane-Protein Folding and Oligomerization - The 2-Stage Model,” *Biochemistry (N.Y.)* 29, 17, 4031-4037, 1990.

10. P.J. Booth. “Unravelling the Folding of Bacteriorhodopsin,” *Biochimica Et Biophysica Acta-Bioenergetics* 1460, 1, 4-14, 2000.

11. J.H. Kleinschmidt, T. den Blaauwen, A.J.M. Driessen, and L.K. Tamm. “Outer Membrane Protein A of Escherichia Coli Inserts and Folds into Lipid Bilayers by a Concerted Mechanism,” *Biochemistry (N.Y.)* 38, 16, 5006-5016, 1999.

Chapter 1: Background and Experimental Set-ups

Acknowledgements

Preparations of the single-trp full-length and truncated site-directed mutagenesis, PCR, and sequencing were previously preformed by lab members Katie Sanchez and Jonathan Gable. It was the stock DNA that I used in the expression of OmpA wild-type and mutants.

I would also like to acknowledge Katie Sanchez for calculating the molar absorpitivity values of OmpA, training me all of the equipment, and her help with protein expression.

1.1 Outer Membrane Protein A (OmpA) Background

OmpA, an integral membrane protein, is a monomer that consists of 325 amino acid residues. Two distinct domains make up OmpA: one domain forms a transmembrane β-barrel made up of 8-standed anti-parallel strands, ~171 amino acid residues, and the second domain, ~154 amino acid residues, resides in the periplasmic tail, which has not been structurally solved (Figure 1.1). The transmembrane region of the β-barrel makes up the N-terminal half, while the C-terminal side comprises the tail which lies in the periplasmic space exposed to the aqueous environment when OmpA is folded in a bilayer. The structure of the transmembrane region has been structurally solved by X-ray crystallography and NMR up to residue 177 (Figure 1.2).[1, 2, 3] The function of OmpA is thought to be mainly structural support; OmpA may stabilize the outer membrane.[4] OmpA has also been thought to be a receptor for bacteriophages and colicines and act as an ion-channel gate.[5, 6, 7]

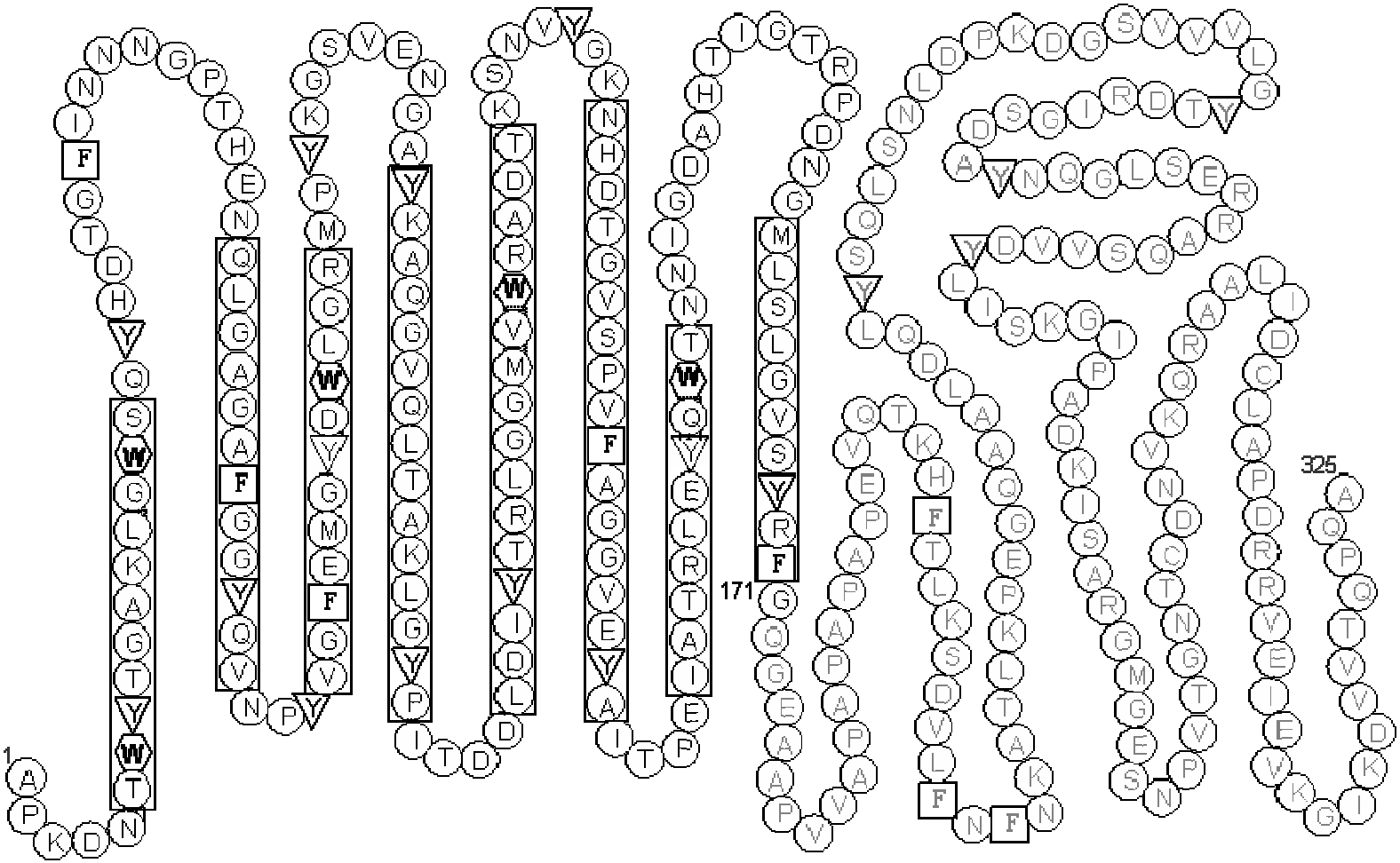

Figure 1.1. Amino acid sequence of wild-type OmpA, given with residue positions 1, 171, and 325. Tryptophan residues are bold and given in hexagons, tyrosine residues are shown in triangles, phenylalanine residues in squares, and all other amino acids are indicated in circles. The large rectangles represent the amino acids involved in forming the β-barrel. The four large loops at the top are located on the extracellular side. There are also three smaller turns on the periplasmic side which lie outside a membrane (not represented). The periplasmic domain is given in gray letters, since the structure is unknown.

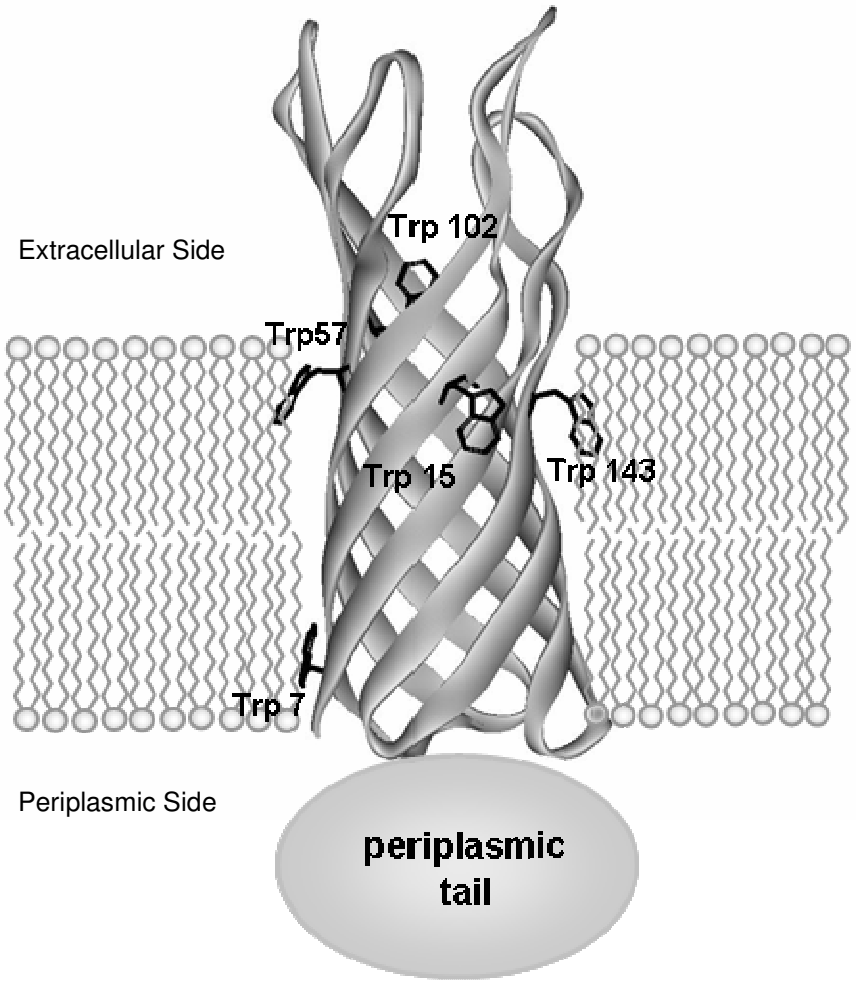

Figure 1.2. Transmembrane domain of OmpA (Residues 1-171; PDB file 1QJP) folded into a bilayer, highlighting the positions of the five native tryptophan residues. The structure of the periplasmic tail is undetermined.

OmpA is an ideal candidate for protein folding studies because the transmembrane domain has been structurally solved. Also, OmpA can be visualized spectroscopically due to the five native tryptophans and it has been used as a model for investigating the insertion and folding process of integral membrane proteins. [1, 3, 8, 9, 10] Furthermore, OmpA is relatively easy to express and folds spontaneously into synthetic bilayers.

OmpA can be studied in its native form, wild-type (WT), with five tryptophans positioned on the transmembrane region. Additionally, OmpA can be mutated to generate five different single-tryptophan (single-trp) mutants in which four of the five native tryptophan residues are mutated to phenylalanine, leaving a single tryptophan (single-trp) residue at position 7, 15, 57, 103, or 143 (called W7, W15, W57, W102, W143, respectively). A sixth mutant that contains zero tryptophans, W0, has also been created. Further modification of OmpA can be accomplished by cleaving the periplasmic domain of the single-trp mutants; these mutants are referred to as truncated mutants W7t, W15, W57t, W102t, and W143t. Four of the five native tryptophan residues lie on the outer portion of the barrel, facing the membrane, except W102, which lies in the interior of the barrel. A tryptophan exists on four of the eight strands of the β-barrel; W7 and W15 are the only two tryptophans which lie on the same strand. In native OmpA there are 17 tyrosine residues and 8 phenylalanine residues included in both the transmembrane and periplasmic domains. The transmembrane region alone contains 13 tyrosine residues and 5 phenylalanine residues.

The folded and unfolded conformational states of OmpA can be

determined by differential gel electrophoretic mobility.[1] When the full-length OmpA is unfolded it shows a characteristic band at ~35kDa (truncated ~19kDa), when folded a band appears at ~30kDa (truncated ~17kDa).

Fluorescence can be used to monitor tryptophan emission of folded and unfolded states.[1, 11] There is a change in quantum yield and frequency of tryptophan emission depending on the environment seen in Figure 3. In a hydrophobic environment, such as in the hydrocarbon core of vesicles, tryptophan shows a maximum wavelength of ~330 nm and increased quantum yield. In a hydrophilic environment, such as in aqueous buffer, the emission maximum exhibits a red shifted maximum of ~355 nm and a decreased quantum yield.

1.2 Sample Preparation

1.2.1 Preparation of OmpA Mutants

Wild-type OmpA was obtained from *E. coli* strain JF701 (Genetic Stock Center, Yale University). Site-directed mutagenesis was performed using the corresponding plasmid encoded to produce five different single tryptophan mutants with single tryptophan residues at positions 7, 15, 57, 102 or 143 and phenylalanine residues in the remaining four native tryptophan positions.[9] Additionally, all five native tryptophan residues were mutated to phenylalanine residues leaving a tryptophan-free mutant.

In order to study the effects of the periplasmic tail on the structure and folding process, truncated versions of each of the single tryptophan mutants were created by inserting a stop codon at position 177 on the plasmids of the single-

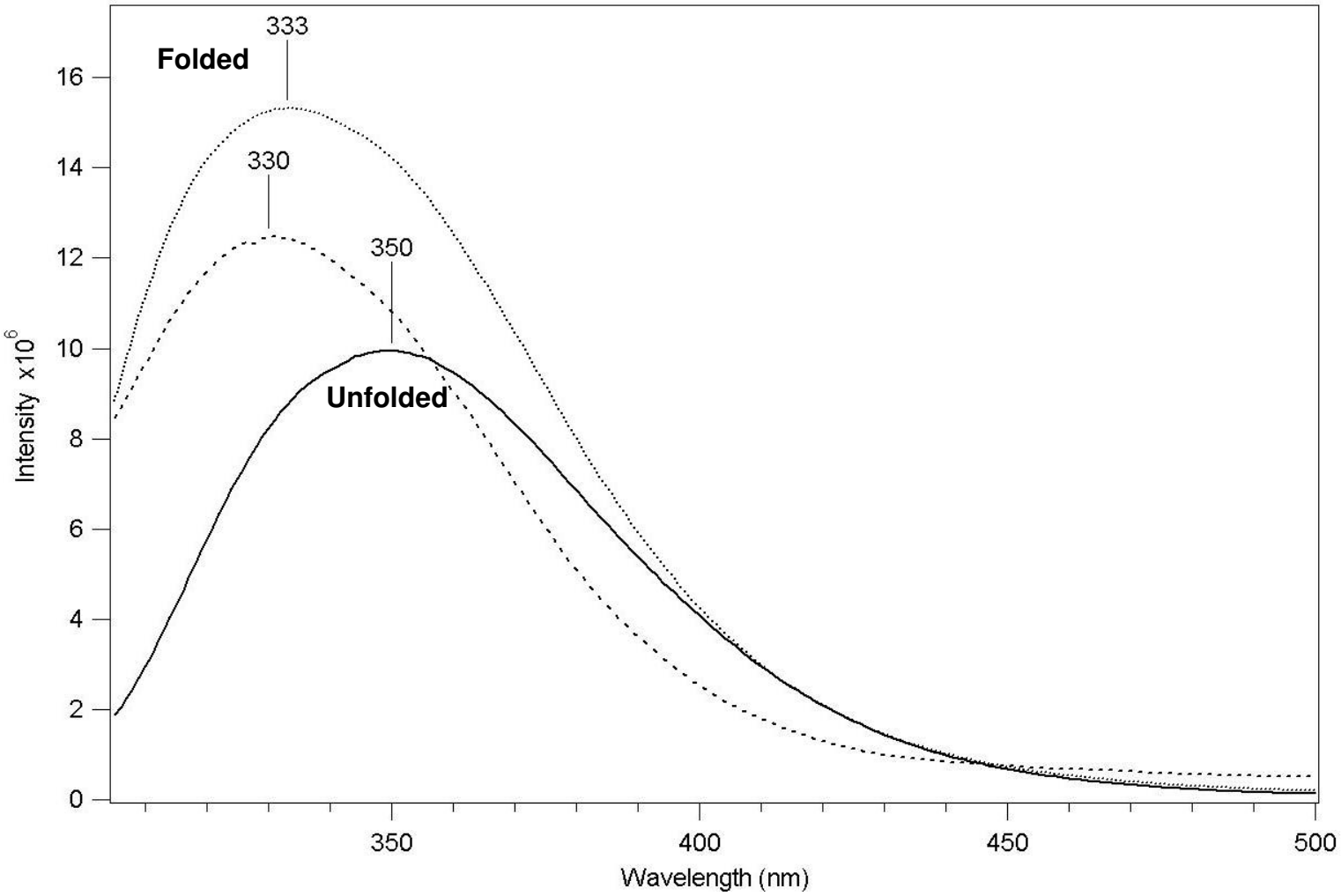

Figure 1.3. Fluorescence spectra of OmpA W57 mutant, folded in micelle (dotted), folded in bilayer (dashed), and unfolded in KP_i (solid). An increase is seen in quantum yield and a blue shift in frequency moving from an unfolded hydrophilic environment to a folded hydrophobic environment.

tryptophan mutants. Cleaving the periplasmic tail created mutants W7t, W15t, W57t, W102t, and W143t.

1.2.2 Expression, Isolation, and Purification of OmpA

The expression of OmpA wild-type and mutants have been previously described and have been adapted.[1, 9, 10] Wild-type, JF701 cells, were grown overnight in 50 mL of sterile media (1% bactotryptone, 0.5% Yeast extract, and 25 μg/mL streptomycin) at 37°C and 180 rmp. When the overnight growth reached an optical density, at 600 nm (OD_{600}), of ~1.5 AU, it was transferred to six flasks containing 1 L of the same media where they continued to grow at 37°C and 180 rmp. The cells were harvested at an OD_{600} of ~1 AU. After the OmpA wild-type cells were harvested they were washed with tris-HCl buffer (10 mM, pH 7.8) and stored at -80°C.

All single-tryptophan and truncated mutants were expressed in *E. coli* strain JF733 (*E. coli* Genetic Stock Center, Yale University). OmpA mutants of JF733 cells were grown overnight at 37°C, 180 rmp, in 300 mL of sterile *Luria-Bertani* (LB) broth (0.5% glucose and 50 μg/mL ampicillin). The cells were washed in sterile LB (50 μg/mL ampicillin) to remove glucose and transferred to six 1 L batches of sterile LB (50 μg/mL ampicillin). Cells were induced with 1mM isopropyl beta-d-thiogalactoside (IPTG) and grown at 37°C and 180 rpm. Because the cells become toxic to themselves shortly after reaching an OD_{600} of 1 AU, the 1 L flasks were harvested by OD_{600} ~1 AU, to ensure no cell death. After the OmpA mutants were harvested, they were washed with tris-HCl buffer (10 mM, pH 7.8), and stored at -80°C until further use.

After the expression, wild-type and mutant OmpA follow the same protocol for isolation and purification. Once the cells were defrosted in an ice bath, a 1:1 mixture of sucrose/tris-HCl (0.75 M sucrose, 10 mM tris-HCl, pH 7.8) and a 1:1 mixture of EDTA/lysozome (20 mM EDTA, 0.5mg/mL lysozome) was added to cell pellet, 110 mL total volume, to help lyse the cells. Then 1 mL of phenylmethanesulphonylfluoride (PMSF) was added. The cells were dissolved in an ice bath before sonication (5 min at 50% duty cycle) with a standard ½" horn tip. The soluble protein supernatant was removed and the fragments containing membrane proteins were collected using two centrifugation steps. First, the lysed cells were centrifuged (15 min, 5000 rpm, 4°C) to remove titanium dust and intact cells. Second, the remaining supernatant was centrifuged (1.5 h, 17 000 rpm, 4°C) to separate the soluble and membrane proteins. Pellets were combined and frozen (-80°C) until further use.

The membrane protein pellet was defrosted in a 50°C water bath containing pre-extraction buffer (3.5 M urea, 20 mM tris-HCl, pH 9). The peripheral membrane protein supernatant was removed and integral membrane proteins were collected via centrifugation (2 h, 17 000 rpm, 4°C). Pellets were collected and stored at -80°C.

The pellet was defrosted in a 50°C water bath. OmpA was isolated using a 1:1 solution of extraction buffer (8 M urea, 20 mM tris-HCl, 0.05% 2-mercaptoethanol, pH 8.5) and 2-propanol, totaling 70 mL. Centrifugation (1.5 h, 17 000 rpm, 4°C) gave the crude OmpA supernatant.

The crude protein was purified via anion exchange chromatography (Q

Sepharose Fast Flow column, GE Healthcare), where a linear concentration gradient of 200 mM NaCl (8 M urea, 15 mM tris-HCl, 0.5% 2-mercaptoethanol, pH 8.5) was used for column elution. Gel electrophoresis (~35kDa for unfolded) was used to determine the purity of the fractions, ~90% pure. The fractions containing purified OmpA were combined. The buffer was exchanged (8 M urea, 20 mM KP_i, pH 7.3) and the protein was concentrated using ultrafiltration (Amicon, PM-10 or YM-10 for full-length, YM-3 for truncated). The protein was stored unfolded at -80°C.

1.2.3 Preparation of Small Unilamellar Vesicles (SUVs)

The SUV preparation was modified from a previously published procedure (3). A lipid solution of 1,2-dimyristoyl-sn-glycero-3-phosphocholine (DMPC, Avanti Polar Lipids) were stored in $CHCl_3$ at -20°C before preparation. A 20 mg/mL DMPC solution in $CHCl_3$ was evaporated for one hour under argon gas allowing the lipids to dry. The lipids were resuspended in KP_i buffer (20 mM, pH 7.3) to a concentration of 5 mg/mL. The solution was sonicated (30 min at 50% duty cycle, ultrasonicator microtip). The DMPC solution of small unilamellar vesicles (SUVs) was filtered using a 0.22 μm filter to remove impurities then run through a gravity flow column (Bio-Rad, 10DG) to obtain SUV sizes of ~ 50 nm diameter. The SUV solution was kept above the lipid phase transition of 24°C and was allowed to equilibrate overnight (> 12 h) at 35°C before using.

1.2.4 OmpA Unfolded Solutions and Reconstitution

Unfolded OmpA was diluted in KP_i (20 mM, pH 7.3) usually resulting in < 1 M urea in solution. Spectroscopic measurements were made immediately after

adding OmpA to KP_i, to ensure that no aggregation took place.

OmpA was reconstituted in either n-octyl-β-D-glucopyranoside (OG) or SUVs following previous procedures[3, 7] (Structures shown in Figure 4). OmpA was added to 10 mg/mL OG (20 mM KP_i, pH 7.3) or to a solution 1 mg/mL SUVs. The solutions containing OmpA and OG equilibrated for at least 30 minutes at room temperature prior to obtaining spectroscopic information. The solutions containing OmpA and SUVs equilibrated for at least 3 h at 35°C before spectroscopic measurements were made.

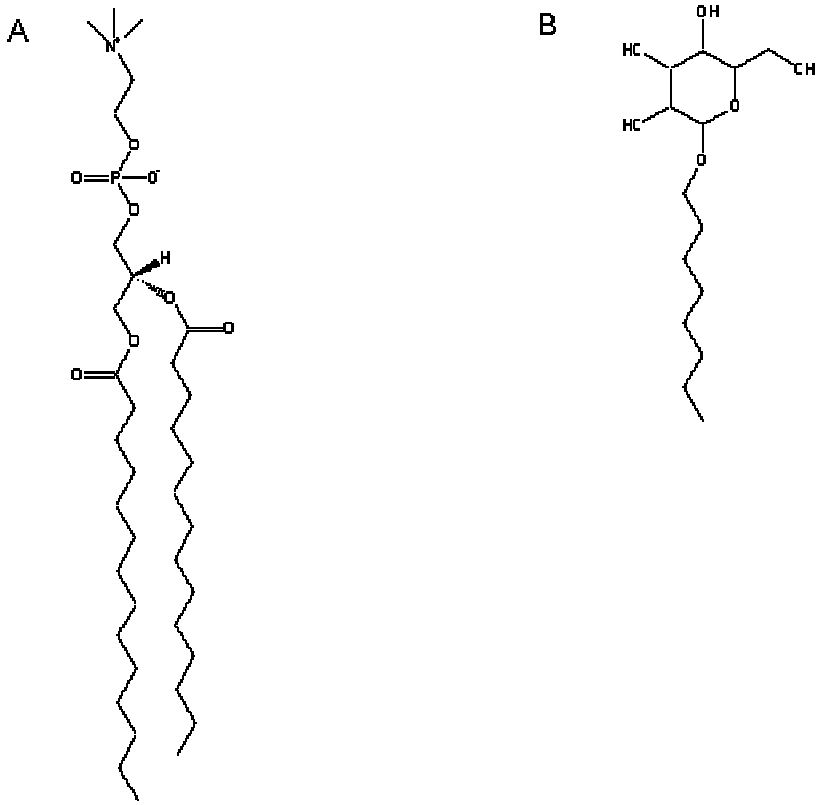

Figure 1.4. Structure of lipid molecules in SUVs (A) and OG (B).

1.3 Spectroscopic Set-ups

1.3.1 Ultraviolet Resonance Raman Laser (UVRR) Spectroscopy

A tunable Ti:Sapphire laser (Photonics Industries) was pumped by an intracavity frequency-doubled Nd:YLF laser (Photonics Industries) providing 1 kHz (40 ns) pulses. The Raman table is illustrated in Figure 5. The excitation wavelength at 228 nm was generated by collimating the fundamental beam of 912 nm and passing through a lithium triborate (LBO) crystal to generate the second harmonic beam. This 456 nm beam was passed through a fourth harmonic generator, a β-barium borate (BBO) crystal, resulting in the excitation wavelength. To obtain the various wavelengths seen in the wavelength dependence, including the 207.5 nm, the fundamental beam was tuned to the appropriate wavelength and sent through the LBO and BBO crystals, to obtain the proper excitation wavelength (fourth harmonic). A Pellin-Broca prism isolated the 228 nm beam before passing through two cylindrical lens, which focused the beam unto a vertical 200 μm inner-diameter (i.d.) fused quartz capillary (100 μm i.d. for wavelength dependence measurements). The Raman scatted light was collected at 135° by a compound lens and focused onto a prefilter, previously described.[12] The photons were dispersed with a SPEX 500 M (JY Horiba) equipped with a holographic grating (3600 groove/mm) and then imaged onto a Pixis 400B CCD detector (Roper Scientific).

The samples and blanks were passed through the capillary at a rate of 0.42 mL/min (0.16 mL/min for the wavelength dependence) and collected after passing through the capillary to assess the extent of photo-degradation from the

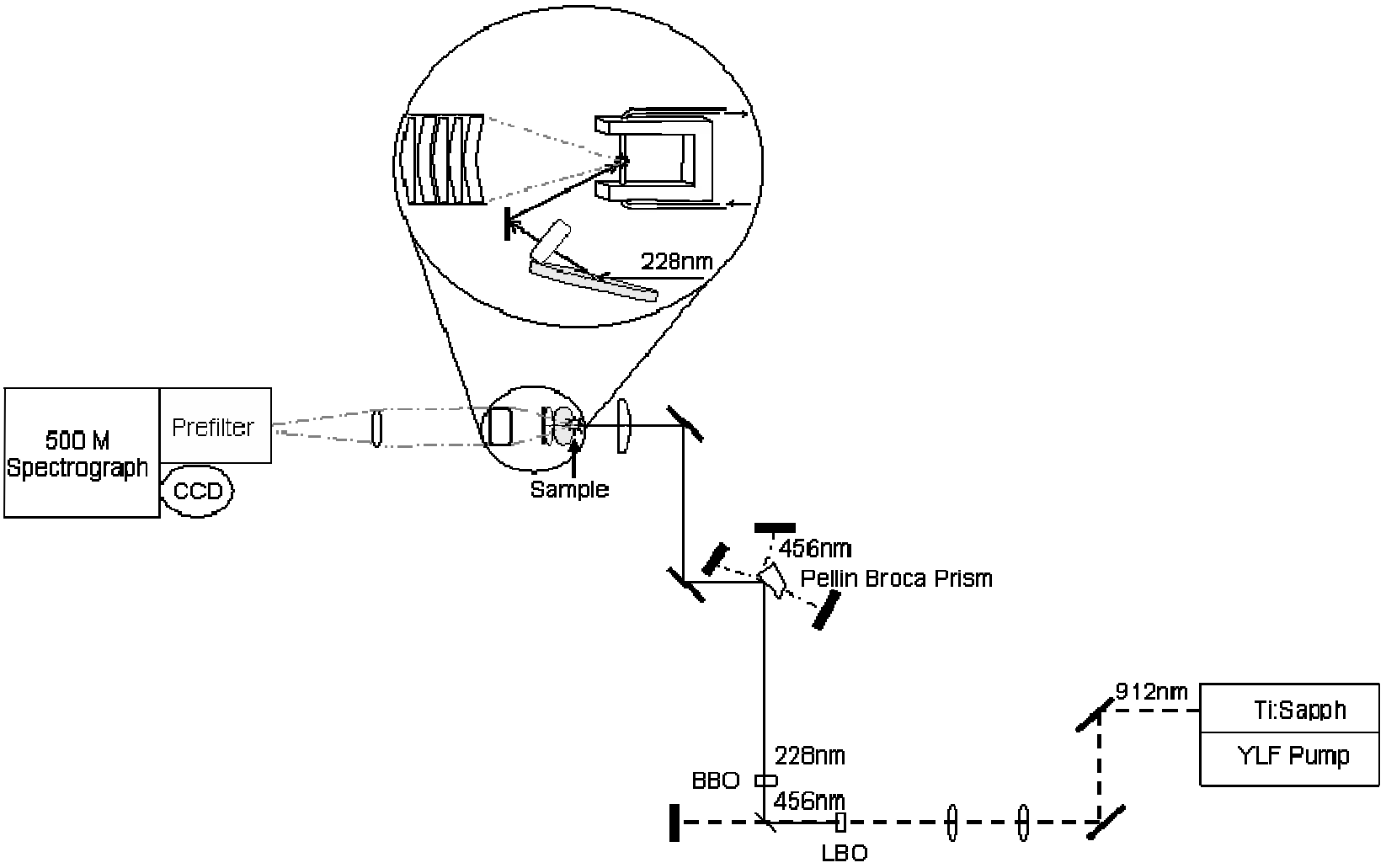

Figure 1.5. Diagram of the laser table and sample set-up.

laser. The displayed Raman spectra were the sum of multiple scans, each 1 minute. The total accumulation time for the 228 nm UVRR spectra was 5 min (15 min for the wavelength dependence). The spectra were calibrated using a standard solution of ethanol and the N_2 peak in order to convert from pixel number to wavenumber. Up to the following nine calibration values were used from ethanol and N_2: 883.3 cm^{-1}, 1051.6 cm^{-1}, 1095.2 cm^{-1}, 1275.6 cm^{-1}, 1453.7 cm^{-1}, 2878 cm^{-1}, 2929 cm^{-1}, 2972 cm^{-1}, and 2331 cm^{-1} (N_2).[13, 14] The number of calibration values used to analyze the data depended on the bandpass and dispersion of the detection system at a given excitation wavelength. The accuracy of the ethanol calibration was ±2 cm^{-1} and the bandpass was ~33 cm^{-1}. Finally, the spectra were analyzed using Igor Pro (WaveMetrics) software.

Signal from the water stretch, ~3300 cm^{-1}, scattering from the capillary at ~484 cm^{-1}, ~602 cm^{-1} and ~792 cm^{-1}, and urea peaks at ~1003 cm^{-1}, ~1151 cm^{-1}, ~1467 cm^{-1}, ~1596 cm^{-1}, and ~1665 cm^{-1} were removed by subtracting the corresponding blanks from the samples until reaching a baseline level. Most of these peaks were removed with the exception of the strong urea peak at ~1003 cm^{-1}, which left a derivative feature upon subtraction. An asterisk will be used to denote this derivative feature which arises during subtraction of urea. The intensity of this derivative is a function of how much urea is in the sample and is due to incomplete subtraction of urea in this area. This area is further complicated by a tryptophan peak at ~1005 cm^{-1}, which is not observable due to urea. All of the OmpA spectra that were analyzed and presented in this thesis were corrected for signal, power, accumulation time, urea concentration, and

protein concentration. An example of the raw OmpA spectra with corresponding blanks and a subtraction is given in figure 6.

1.3.2 Absorption Spectroscopy

The final protein concentration of OmpA was determined by absorption spectroscopy. The ultraviolet–visible (UV-Vis) absorption spectra were collected with an Agilent 8453 UV-Vis spectrophotometer. The following describes the set-up for all absorption measurements measured during the UVRR experiments. A 200 μL quartz cuvette with a pathlength of 1 cm was blanked on 20 mM KP_i, pH 7.3. Absorbance was measured before and after photolysis to examine the integrity of the sample. Protein concentrations were obtained using molar absorpitivity values at 280 nm (ε_{280}) of 54 394 $M^{-1}cm^{-1}$, 32 326 $M^{-1}cm^{-1}$, 26 018 $M^{-1}cm^{-1}$, and 26 809 $M^{-1}cm^{-1}$ for OmpA wild-type, single-tryptophan mutants, single-tryptophan truncated mutants and the zero-tryptophan mutant. Molar absorpitivity values were calculated using Pace's method of average molar absorpitivity per residue.[15]

1.3.3 Steady-State Fluorescence Spectroscopy

A Jobin Yvon-SPEX Flurolog FL 3-11 spectrofluorometer was used to measure tryptophan emission. The following describes the setup for all steady-state fluorescence measurements taken during the UVRR experiments. A 200 μL quartz cuvette was used. The excitation wavelength was 290 nm with a wavelength emission collected in 1 nm increments from 305–500 nm. Integration time was 1 second. The signal was S, PMT HV set to 950 V. When the wavelength-dependence UVRR data of 206.5 – 236.5 nm was performed the

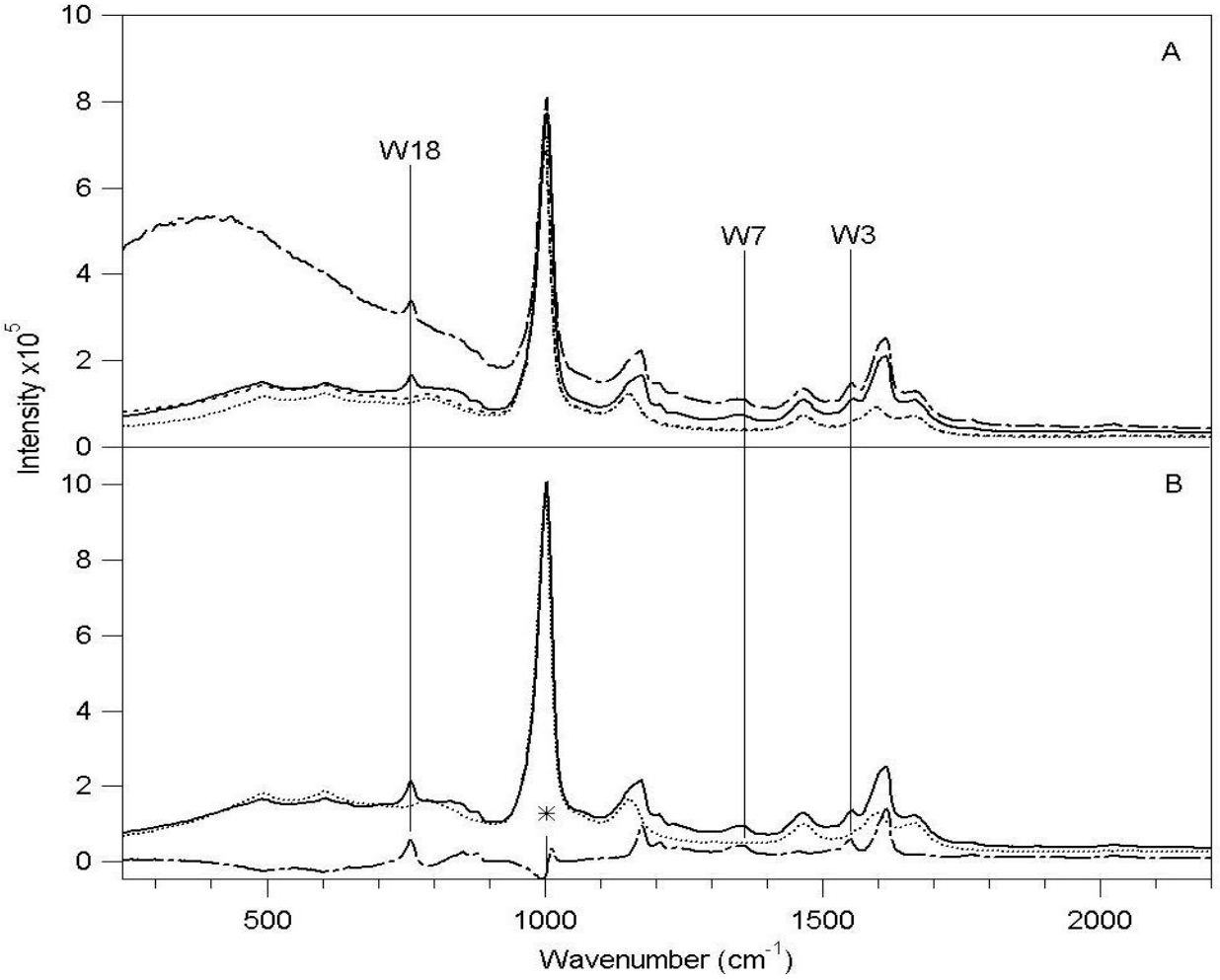

Figure 1.6. (A) The added spectra of SUVs + urea (dashed), KP_i + urea (dotted), W57 in KPi (solid), and W57 in SUVs (dashed and dotted). The tryptophan peaks of the protein can be clearly distinguished in the raw data compared to the blanks. (B) A 1:1 subtraction of [W57 in OG (solid)] minus [OG + urea (dotted)] equals the subtracted spectrum (dashed and dotted).

entrance slits on the fluorometer were 2.00 mm and exits slits were 0.5 mm. For the 228 nm UVRR data, containing samples W0, W7, W102, W143, and WT in all three conditions, KP_i, OG, and SUVs, the entrance and exit slits were 5.00 mm bandpass. The remaining samples, W15, W57, and the truncated mutants in all three conditions, at 228 nm used a 4.00 mm bandpass for entrance and exit slits. The only reason for a change in entrance and exit slits between experiments was due to changing the fluorometer hard drive. Subtraction of the protein samples was done with corresponding blank solutions.

References

1. T. Surrey and F. Jahnig. “Refolding and Oriented Insertion of a Membrane Protein into a Lipid Bilayer,” *Proceedings of the National Academy of Sciences* 89, 16, 7457-7461, 1992.

2. Lukas K Tamm, Ashish Arora, and Jorg H. Kleinschmidt. “Structure and Assembly of β-barrel Membrane Proteins,” *J. Biol. Chem.* 276, 35, 32399-32402, 2001.

3. Lukas K Tamm, Heedeok Hong, and Binyong Liang. “Folding and Assembly of β-barrel Membrane Proteins,” *Biochimica et Biophysica Acta (BBA) - Biomembranes* 1666, 1-2, 250-263, 2004.

4. I. Sonntag, H. Schwarz, Y. Hirota, and U. Henning. “Cell-Envelope and Shape of Escherichia-Coli - Multiple Mutants Missing Outer Membrane Lipoprotein and Other Major Outer Membrane Proteins,” *J. Bacteriol.* 136, 1, 280-285, 1978.

5. H. Hong, G. Szabo and L.K. Tamm. “Electrostatic Couplings in OmpA Ion-channel Gating Suggest a Mechanism for Pore Opening,” *Nature Chemical Biology* 2, 11, 627-635, 2006.

6. R. Morona, C. Kramer, and U. Henning. “Bacteriophage Receptor Area of Outer-Membrane Protein Omp-A of Escherichia-Coli K-12,” *J. Bacteriol.* 164, 2, 539-543, 1985.

7. J. Foulds and C. Barrett. “Characterization of Escherichia-Coli Mutants Tolerant to Bacteriocin Jf246 - 2 New Classes of Tolerant Mutants, *J. Bacteriol.* 116, 2, 885-892, 1973.

8. J.H. Kleinschmidt and L.K. Tamm. “Time-Resolved Distance Determination by Tryptophan Fluorescence Quenching: Probing Intermediates in Membrane Protein Folding,” *Biochemistry (N.Y.)* 38, 16, 4996-5005, 1999.

9. J.H. Kleinschmidt, T. den Blaauwen, A.J.M. Driessen, and L.K. Tamm. “Outer Membrane Protein A of Escherichia Coli Inserts and Folds into Lipid Bilayers by a Concerted Mechanism,” *Biochemistry (N.Y.)* 38, 16, 5006-5016, 1999.

10. J.E. Kim, G. Arjara, J.H. Richards, H.B. Gray,and J.R. Winkler. “Probing Folded and Unfolded States of Outer Membrane Protein A with Steady-state and Time-resolved Tryptophan Fluorescence,” *J. Phys. Chem. B.* 110, 35, 17656-17662, 2006.

11. J.H. Kleinschmidt and L.K. Tamm. "Folding Intermediates of a Beta-barrel Membrane Protein - Kinetic Evidence for a Multi-step Membrane Insertion Mechanism," *Biochemistry (N.Y.)* 35, 40, 12993-13000, 1996.

12. S. Kaminaka, R.A. Mathies. "High-throughput Large-aperture Prism Prefilter for Ultraviolet Resonance Raman Spectroscopy," *Appl. Spectrosc*. 52, 3, 469-473, 1998.

13. Chris W. Brown, John R. Ferraro, and Kaszuo Nakamoto. "Introductory Raman Spectroscopy 2^{sd} ed." Elsevier Science and Technology Books. 2002.

14. G.W. Faris and R.A. Copeland. "Ratio of Oxygen and Nitrogen Raman Cross Sections in the Ultraviolet," *Appl. Opt.* 36, 12, 2684-2685, 1997.

15. C.N. Pace, F. Vajdos, L. Fee, G. Grimsley, and T. Gray. "How to Measure and Predict the Molar Absorption-Coefficient of a Protein *Protein Sci.* 4, 11, 2411-2423, 1995.

Chapter 2: Wavelength-Dependence

Acknowledgements

Data presented in this chapter were collected in collaboration with Katie Sanchez and Hannah Shafaat. This work, in part or in whole, may be used in future publications.

Abstract

A wavelength-dependence UV resonance Raman study of model compounds L-tryptophan, L-tyrosine, L-phenylalanine, and OmpA mutant W57 folded in SUVs and unfolded in KP_i, was conducted at excitation wavelengths from 206.5 nm to 236.5 nm. Tryptophan modes W18, W16, W7, and W3 and phenylalanine modes F1 and F8a were found to be most enhanced with 220 nm excitation while tyrosine modes Y9a and Y8a were enhanced at 228 nm excitation. A red-shift in excitation wavelength to 228 nm was observed for tryptophan modes in OmpA relative to the model compound L-tryptophan in aqueous solution. The 228 nm excitation allows for the selective enhancement of tryptophan in OmpA, which is important for studies in chapter 4.

2.1 Introduction

Resonance Raman enhancement occurs when the frequency of the excitation wavelength closely matches the frequency of an electronic transition. The absorption spectra and electronic transitions for tryptophan, tyrosine and phenylalanine are given in Figure 2.1.[1, 2, 3] Different modes become enhanced to various degrees as the excitation wavelength becomes resonant with different electronic transitions, allowing for selective enhancement of individual aromatic

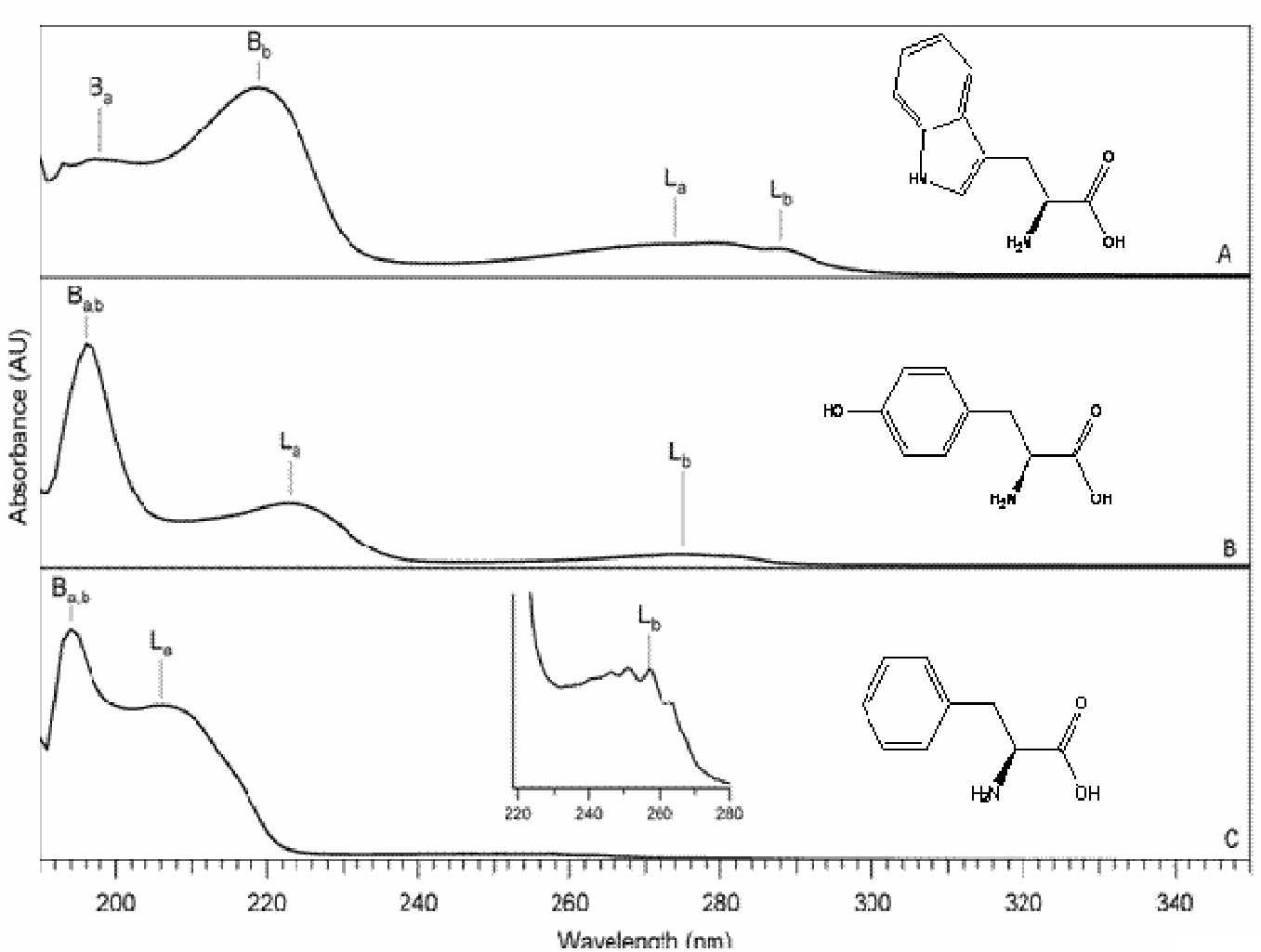

Figure 2.1 UV-Vis absorption spectra of 50 μM tryptophan (A), tyrosine (B), and phenylalanine (C) in 20 mM KP_i with 50 mM ClO^{4-}. Shown of each spectrum is the amino acid structure and the electronic transitions. A close-up of the L_b absorption of phenylalanine is shown.

amino acids or protein backbone.[4] In proteins, the individual aromatic amino acids are enhanced between 225–250 nm, while below 220 nm contributions from the protein amide backbone become enhanced by the 190 nm amide π-π* electronic transition.[4, 5] This wavelength-dependence study of OmpA was important in order to gain selective enhancement of the aromatic amino acid tryptophan, necessary to locate changes in tryptophan structure and local environment in OmpA, discussed in chapter 4.

Typically, excitation profiles are created using an internal standard, where a full analysis of intensities and Raman cross sections can be made. While an internal standard of perchlorate was used in the amino acids, no internal standard was used with OmpA. The internal standards often utilized in our lab overlap with the urea signal and the effects of adding an internal standard to OmpA or SUVs were not studied and hence an internal standard was not added. Additionally, the absence of an internal standard was important in mimicking a natural environment. The aromatic amino acids have been well characterized and analyzed in excitation profiles.[1, 2, 3, 6] The aim of this experiment was not to perform an in-depth analysis, but rather to qualitatively look for tryptophan enhancement in OmpA compared to the aqueous aromatic amino acids in order to choose an excitation wavelength suitable for future studies of OmpA.

As the number of ultraviolet resonance Raman (UVRR) studies increase there is an increased need to study UVRR excitation profiles. Included here is a wavelength-dependence of tryptophan, tyrosine, phenylalanine, and OmpA mutant W57 folded in SUVs and unfolded in KP_i. These five samples have been

investigated at nine different wavelengths between 206.5–236.5 nm. The aromatic amino acids tryptophan, tyrosine, and phenylalanine wavelength-dependence spectra are shown in Figures 2.2, 2.3, and 2.4. The concentrations of amino acids were 50 μM containing 50 mM perchlorate in 20 mM in KP_i solution. The spectra were corrected by subtracting a KP_i blank from the amino acids to remove contributions from the buffer and capillary. The spectra were then normalized to the perchlorate band intensity at ~935 cm^{-1}. The intensities are relative to the perchlorate band are listed in Table 2.1 and illustrated in Figure 2.5. For these experiments the concentration of OmpA was ~20 μM. The subtraction and correction of the OmpA spectra are discussed in chapter 1.

In aqueous solutions the aromatic amino acids show the following wavelength dependence. The tryptophan modes W18, W16, W7, and W3 at ~761 cm^{-1}, ~1013 cm^{-1}, ~1360 cm^{-1}, and ~1550 cm^{-1}, show intensity at 220 nm to be the highest with relative intensities of ~1.2, ~1.4, ~0.4, and 0.6, respectively. The tyrosine bands Y9a and Y8b (~1180 cm^{-1} and ~1611 cm^{-1}) are most intense at 228 nm with relative intensities of ~0.2. Modes F1 and F8a (~1006 cm^{-1} and 1611 cm^{-1}) of phenylalanine give the highest relative intensities at 220 nm of ~ 0.2.

2.2 Aromatic Amino Acids: Tryptophan, Tyrosine, and Phenylalanine

Only two modes in tyrosine and phenylalanine, mentioned above, are resolved in the spectra, likely due to low concentration used. Because of the low concentration and low resolution of the bands, some of the intensities of these modes are similar and may not be fully observed. Nevertheless, the intensities of

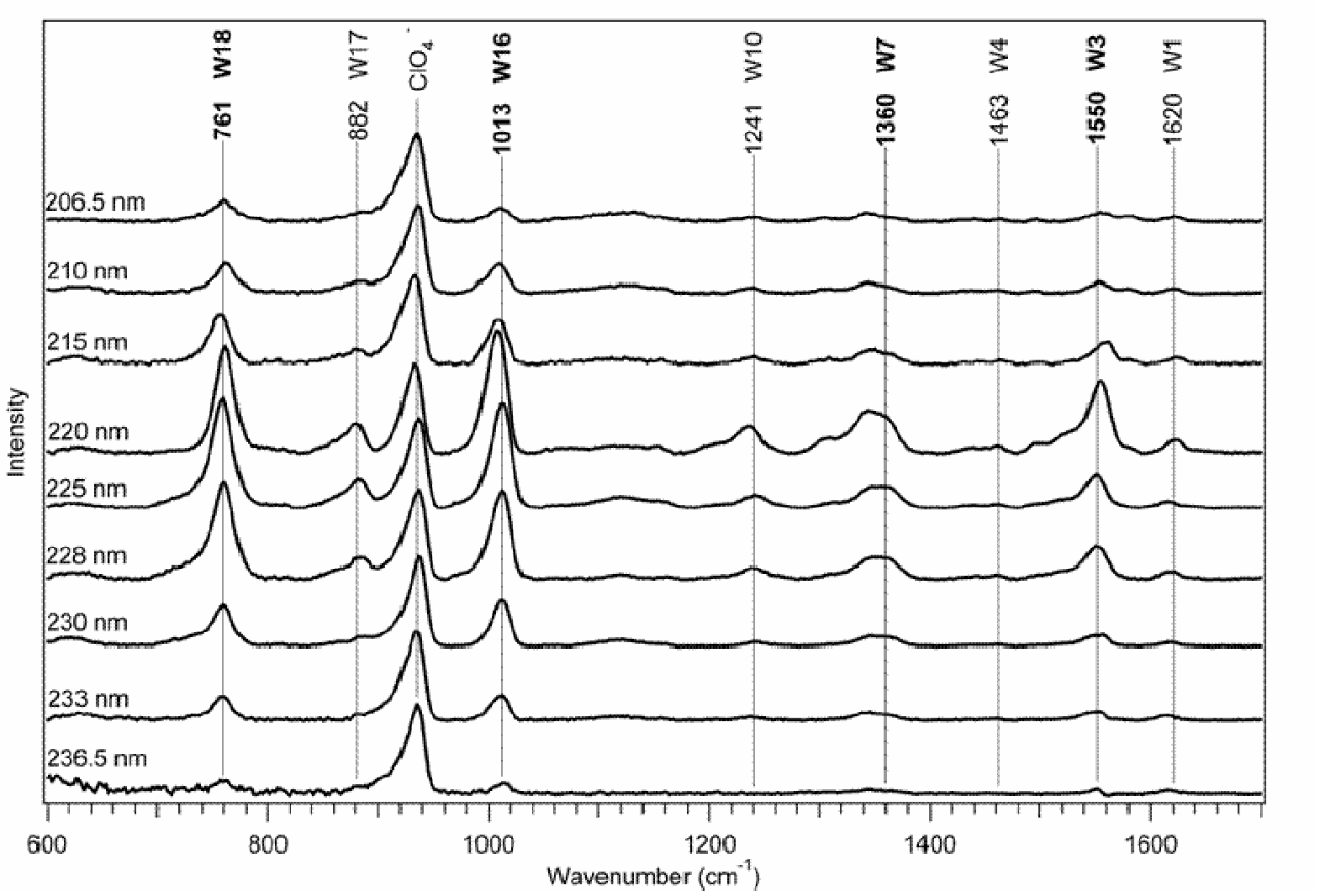

Figure 2.2. UVRR spectra of tryptophan showing excitation at various wavelengths. Intensities of the modes in bold are compared and discussed.

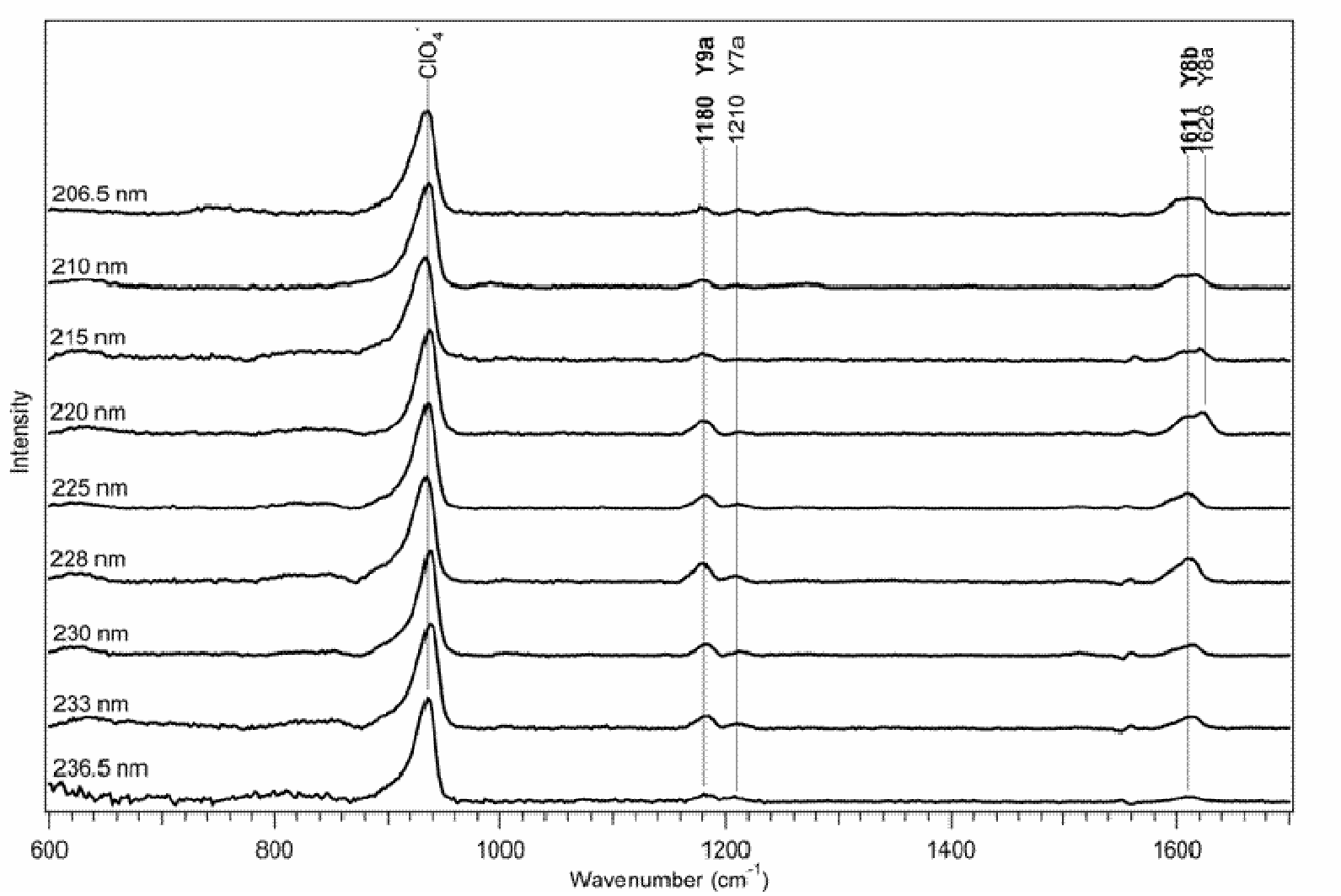

Figure 2.3. UVRR spectra of tyrosine showing excitation at various wavelengths. Intensities of the modes in bold are compared and discussed.

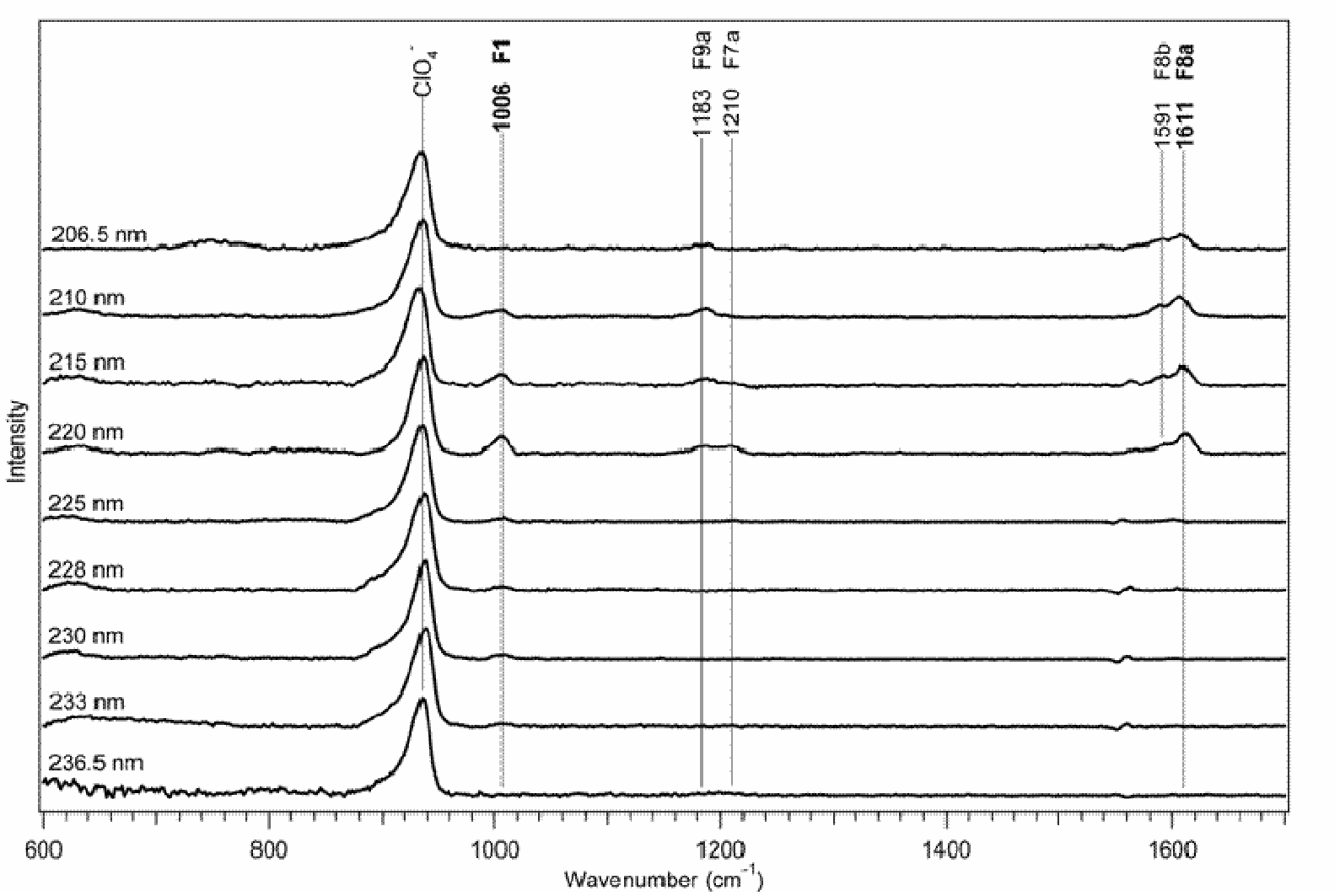

Figure 2.4. UVRR spectra of phenylalanine showing excitation at various wavelengths. Intensities of the modes in bold are compared and discussed.

Table 2.1. Aromatic amino acid intensities for various modes relative to perchlorate. Intensity maxima are given in bold italics.

	Tryptophan Intensities				**Tyrosine Intensities**		**Phenylalanine Intensities**	
Wavelength (nm)	W18	W16	W7	W3	Y9a	Y8a	F1	F8a
206.5	0.24	0.16	0.05	0.09	0.07	0.14	0.02	0.14
210	0.34	0.33	0.07	0.11	0.07	0.11	0.08	0.19
215	0.55	0.49	0.13	0.17	0.07	0.08	0.12	0.19
220	***1.15***	***1.40***	***0.45***	***0.57***	0.13	0.18	***0.19***	***0.21***
225	1.14	1.20	0.23	0.37	0.13	0.15	0.05	0.01
228	1.08	0.96	0.24	0.37	***0.17***	***0.21***	0.05	0.01
230	0.46	0.51	0.11	0.12	0.10	0.08	0.05	0.00
233	0.27	0.27	0.07	0.10	0.12	0.12	0.04	0.00
236.5	0.16	0.11	0.04	0.06	0.19	0.06	0.01	0.00

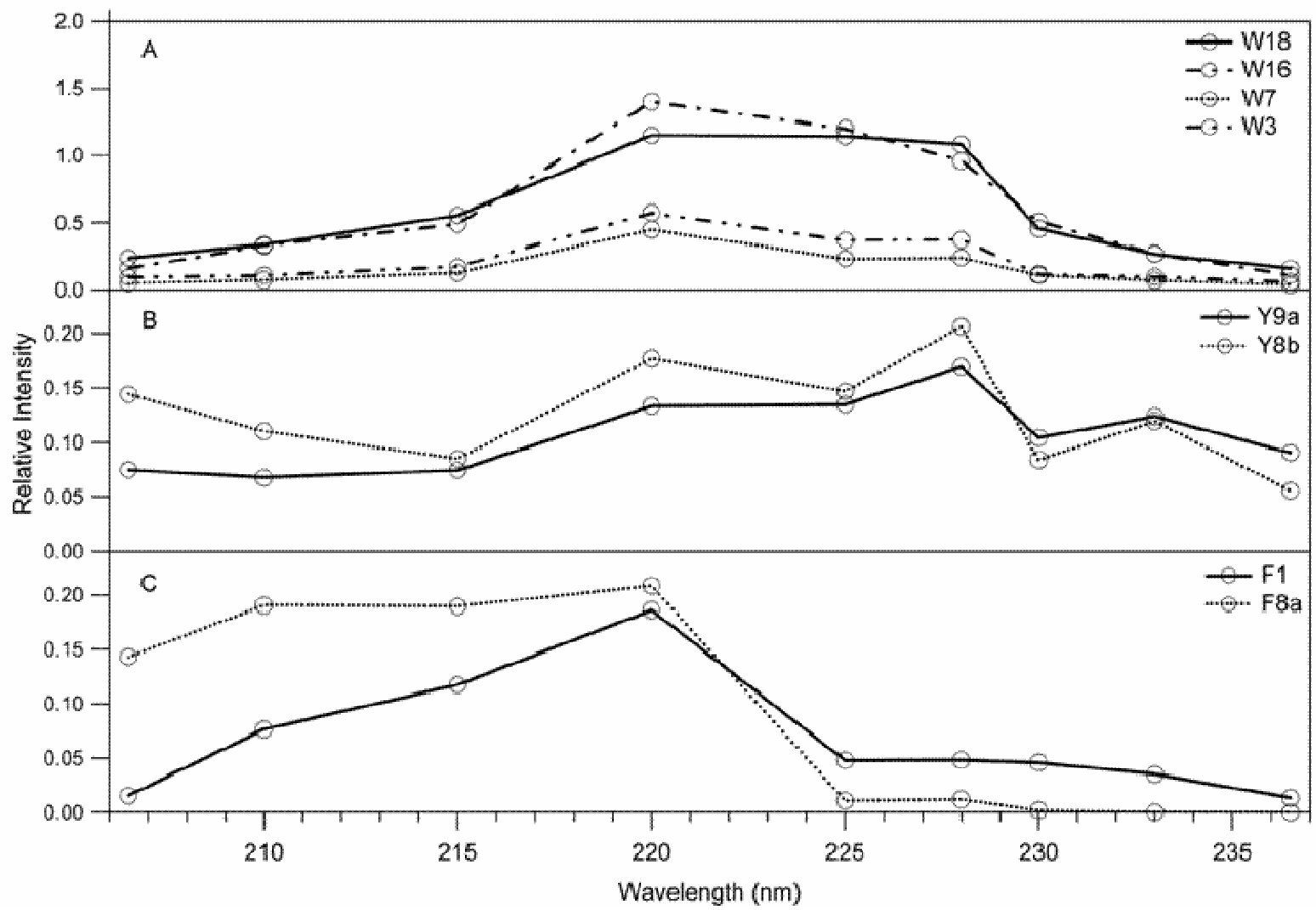

Figure 2.5. Aromatic amino acid mode intensities versus excitation wavelength of (A) tryptophan (B) tyrosine (C) Phenylalanine. Intensities are relative to perchlorate peak.

all three of these aromatic amino acids show agreement with previous studies.[1, 3, 6] The relative intensity of the W18 mode is similar at 220 nm and 225 nm, ~1.2 versus ~1.1. Although the intensities of the W18 mode are very close, the intensity of the W18 mode at 220 nm agrees with the peak increase in intensity of the W7 and W3 modes. An overall enhancement of tryptophan modes occur with 220 nm excitation.

The W18, W7, and W3 modes exhibit the same relative unique intensities when excited at 225 nm and 228 nm. Relative intensities at 225 nm and 228 nm for the W18 mode are ~1.1, for the W7 mode are ~0.2, and for the W3 mode are ~0.4. This result indicates that there is not much difference between the two excitation wavelengths of 225 nm and 228 nm for these modes. However, there is a large difference when the wavelength is shifted to 220 nm, where other tryptophan modes become the most intense. These data are consistent with the fact that tryptophan has a B_b absorption maximum at 218 nm and therefore shows the most enhancement at 220 nm. This work is in agreement with Spiro and Fodor's study, which shows a maximum intensity of tryptophan modes W18, W17, W7, and W3 with 218 nm exciation.[1]

Tyrosine spectra show the Y9a and Y8b modes are intensified at 228 nm with an intensity of ~0.2. The Y8b mode at 220 nm also shows an intensity of ~0.2. The reason for this could be the appearance of the Y8a mode, which appears as a doublet with the Y8b mode at 220 nm. The Y8a and Y9a modes becomes enhanced as it approaches the L_a transition at 223 nm. A peak in intensity at 228 nm, just red of the L_a transition, agrees with Asher and Ludwigs

work, which demonstrate a maximum intensity for tyrosine modes Y9a and Y8b around 230 nm.[6]

Phenylalanine intensities are at a maximum of ~0.2 for modes F1 and F8a, occurring at 220 nm. The F1 mode is strongly resonant with the $B_{a,b}$ transition (~188 nm) and is known to increase in intensity at much shorter wavelengths than examined in this study.[3] The F8a mode is L_a-$B_{a,b}$ mixed but is more vibronically active in the L_a transition.[3] The F8a mode at 220 nm, 215 nm and 210 nm all give an intensity of ~0.2.

2.3 OmpA W57

Figures 2.6 and 2.7 shows W57 folded and W57 unfolded intensity changes for tryptophan are similar. The W18 mode intensity increases to a maximum value at 228 nm excitation. The tryptophan peak at ~1360 cm^{-1} shows a similar trend where there is a pronounced enhancement with 228 nm excitation. The ~1340 cm^{-1} tyrosine/tryptophan combination peak is seen more readily than the tryptophan peak at 1360 cm^{-1} in the wavelength range of 225–236.5 nm. However, at 228 nm the ~1360 cm^{-1} tryptophan peak gains more intensity. Finally, the intensity of the W3 mode is strong evidence that 228 nm is the best region to look for changes in tryptophan frequencies.

Even though no internal standard was used, the increases in tryptophan intensity are real and not due to the Raman signal for that day. The intensities of tyrosine peaks do not follow the same trend as the intensities of tryptophan peaks. If the intensity changes were due to signal for that day then all the peaks would follow that same trend. For example, if the intensity was due to the signal

for the day all the peaks at 228 nm would be highest, which is not the case as seen in the tyrosine peaks around ~850 cm^{-1} and ~1180 cm^{-1}, which are higher in both the 230 nm and 233 nm not the 228 nm spectra, opposite the tryptophan peaks. Also, intensity increases were not due to concentration of protein because the concentrations on either side of 228 nm, at 225 nm and 230 nm, were higher than that of 228 nm and all the spectra have been normalized for protein concentration. The concentrations were 23.3 μM at 225 nm, 17.5 μM at 228 nm, and 19.5 μM at 230 μM. If the higher signal at 228 nm was due to concentration effects, signal acquired with this wavelength would be lower. Additionally, signal, power, accumulation time and concentration were taken into account upon correction and any variations in these factors would likely result in fluctuations in intensities and not be smoothly increasing or decreasing between the wavelength or be consistent between the folded and unfolded spectra. Therefore, 228 nm is seen to provide the most tryptophan signal for probing changes in local environment of OmpA and mutants.

2.4 Comparison of W57 to Aqueous Tryptophan

The absorption spectrum of OmpA, Figure 2.8, is mainly derived from tyrosine and tryptophan electronic transitions, so an excitation wavelength of 220 nm should show enhancement of tryptophan bands in OmpA similar to the excitation profile of tryptophan. However, the UVRR spectra of W57 at 228 nm show the most tryptophan enhancement contrary to aqueous tryptophan at 220 nm. The B_b absorption band of tryptophan is red-shifted in the protein, which explains the red-shifted maximum intensity seen for tryptophan in W57 in the

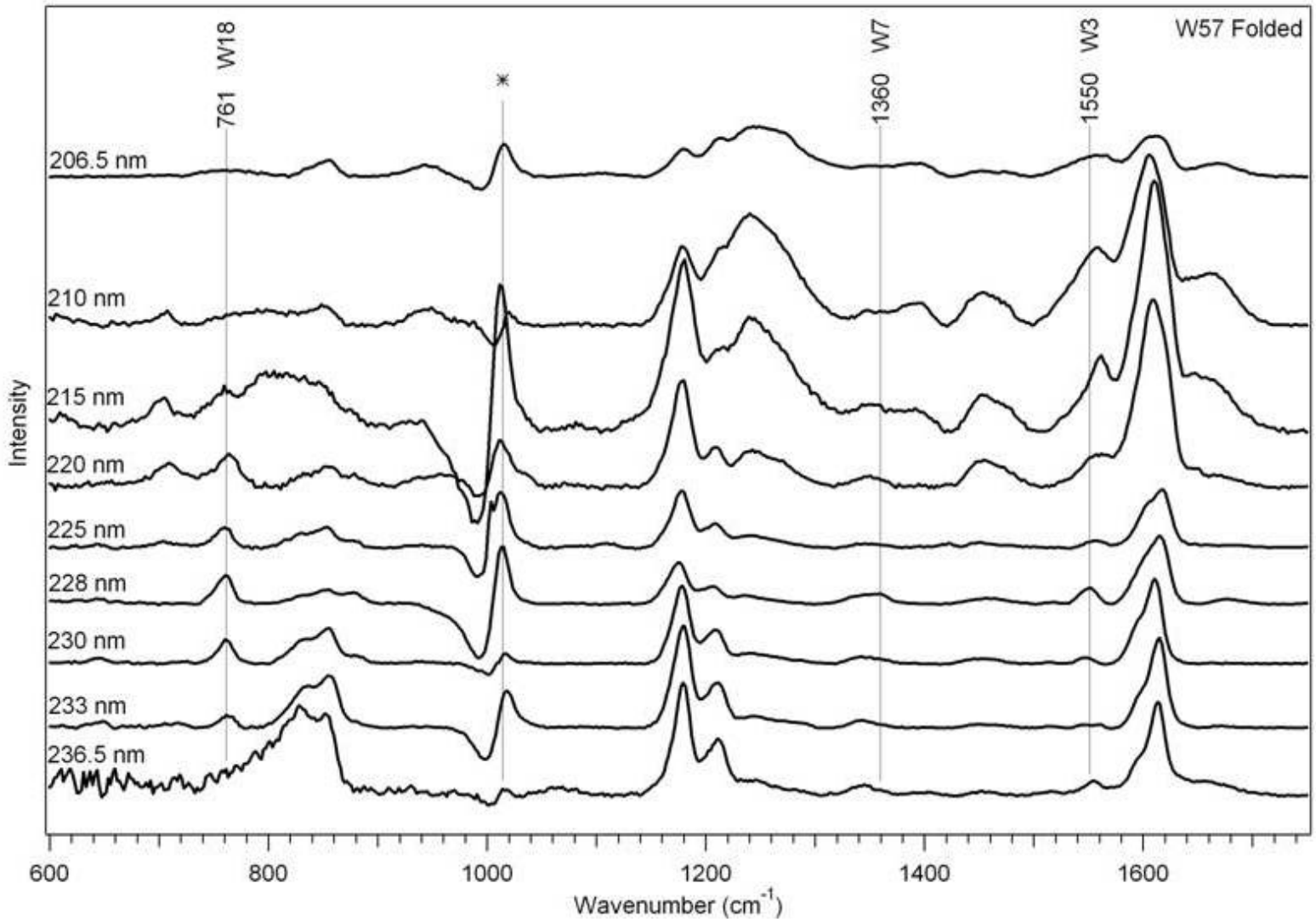

Figure 2.6. UVRR spectra showing the wavelength dependence of OmpA W57 folded in SUVs at various excitations.

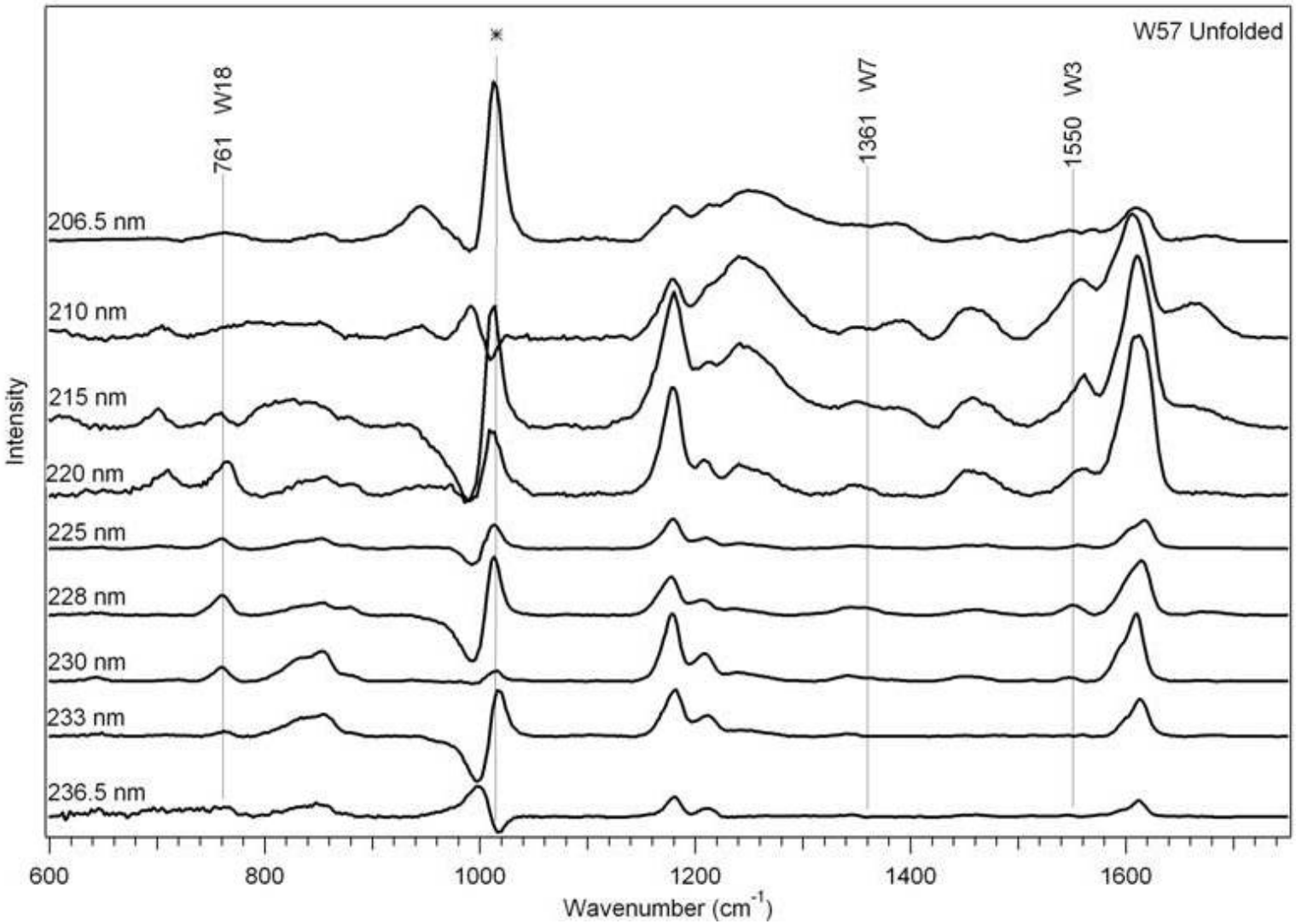

Figure 2.7. UVRR spectra showing the wavelength dependence of OmpA W57 unfolded in KP_i at various excitations.

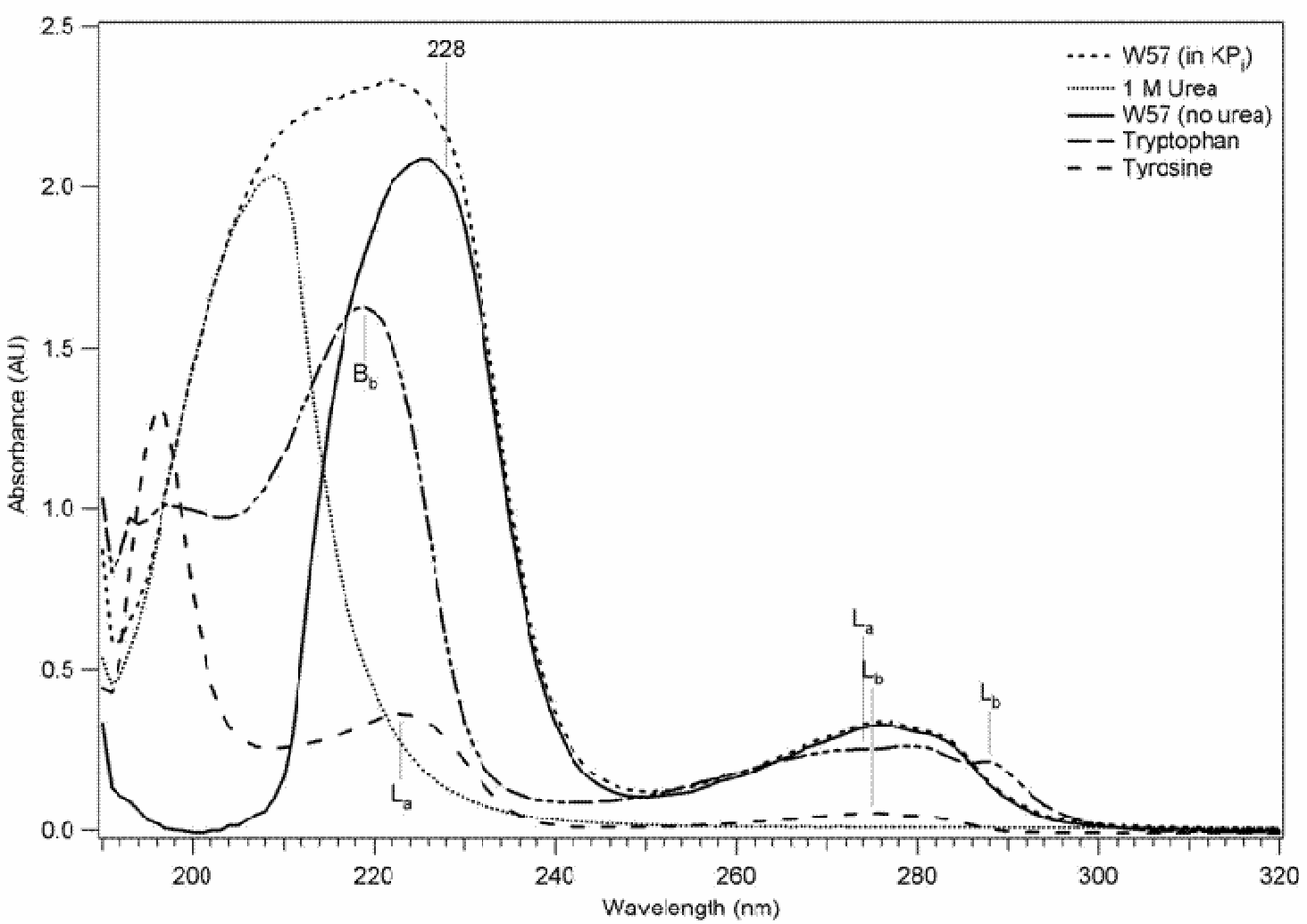

Figure 2.8. UV-Vis absorption spectra of tryptophan (dashed and dotted), tyrosine (medium dashes), OmpA W57 unfolded in KP_i (short dashes), KP_i and urea (dotted), and subtracted spectra (solid) of [W57 in KP_i] minus [KP_i and Urea].

Raman spectra. Asher and co-workers have demonstrated tryptophan and tyrosine red-shifted absorption spectra will result in red-shifted Raman excitation profiles.[7]

Although the W57 spectra show an increase in single from tryptophan modes at 220 nm the spectra are convoluted with amide bands. From 220 nm to 206.5 nm the peaks shift and new features arise due to the protein backbone tryptophan peaks become less intense. Therefore, excitation wavelengths at 220 nm and below are not ideal to investigate the local environment of tryptophan. The wavelength-dependence of OmpA has shown that excitation at 228 nm is the best wavelength to visualize tryptophan signal enhancement rather than the predicted excitation of 220 nm seen in aqueous tryptophan.

References

1. S.A. Asher, M. Ludwig and C.R. Johnson. "UV Resonance Raman Excitation Profiles of the Aromatic-Amino-Acids," *J. Am. Chem. Soc.* 108, 12, 3186-3197, 1986

2. J.A. Sweeney and S.A. Asher. "Tryptophan UV Resonance Raman Excitation Profiles," *J.Phys.Chem.* 94, 12, 4784-4791, 1990

3. S.P.A. Fodor, R.A Copeland, C.A. Grygon and T.G. Spiro. "Deep-Ultraviolet Raman Excitation Profiles and Vibronic Scattering Mechanisms of Phenylalanine, Tyrosine, and Tryptophan," *J.Am.Chem.Soc.*, 111, 15, 5509-5518, 1989

4. Thomas G. Spiro, editor. "Biological applications of Raman Spectroscopy Volume 2: Resonance Raman Spectra of Polyenes and Aromatics." John Wiley and Sons, 1987.

5. Sunho Song, S.A. Asher and A. Sanford. "UV Resonance Raman Studies of Peptide Conformation in Poly(L-Lysine), Poly(L-glutamic acid), and Model Complexes: The Basis for Protein Secondary Structure Determination*," J. Am. Chem. Soc.* 111, 4295-4305, 1988

6. M. Ludwig and S.A. Asher. "Ultraviolet Resonance Raman Excitation Profiles of Tyrosine - Dependence of Raman Cross-Sections on Excited-State Intermediates," *J. Am. Chem. Soc.* 110, 4, 1005-1011, 1988

7. Z.H. Chi, S.A. Asher. "UV Raman Determination of the Environment and Solvent Exposure of Tyr and Trp Residues," *J. Phys. Chem. B.* 102, 47, 9595-9602, 1998

Chapter 3: Secondary Structure Determination at 207.5 nm

Acknowledgements

Data presented in this chapter were collected in collaboration with Katie Sanchez and Hannah Shafaat. This work, in part or in whole, may be used in future publications.

Abstract

UVRR is a powerful technique that can provide detailed secondary structure information when the excitation wavelength is resonant with the π-π* transition of the protein backbone. UVRR with 207.5 nm excitation was used to probe two OmpA mutants, W57 and W57t, folded in SUVs and unfolded in KP_i to elucidate changes in secondary structure. This study revealed that there are minimal differences in the UVRR spectra of the full-length and truncated mutants; however, there are observable spectral differences between the unfolded and folded states.

3.1 Introduction

Secondary structure determination in proteins can currently be accomplished by the methods of X-ray crystallography, nuclear magnetic resonance (NMR), circular dichroism (CD), infrared spectroscopy (IR), and ultraviolet resonance Raman (UVRR). [1, 2, 3, 4] These techniques provide different information and compliment each other allowing for a more complete analysis than any one technique could provide alone. However, while there are inherent limitations in all of these techniques, the use of UVRR in secondary structure determination is on the rise. UVRR lacks the scattering artifacts, such as urea,

associated with CD measurements and does not contain the problematic water vibrations present in IR spectroscopy. This makes UVRR studies a powerful technique.

Characterizing the protein secondary structure is accomplished by looking at the frequencies of the amide backbone vibrations. In order to probe the amide backbone, an excitation wavelength in the deep UV region must be used, so that resonance enhancement with the amide π-π* transition can occur. In UVRR spectra of proteins, there are four key regions that provide insight into secondary structure determination, and are referred to as the amide I, amide II, amide S, and amide III bands. Additionally, there is a fifth region, amide IIP, which is unrelated to secondary structure, but shows frequency dependence with hydrogen bonding to the carbonyl group of proline residues.

3.2 Relationships Between Frequency and Secondary Structure

The amide I band appears from 1625-1750 cm^{-1}. The amide I arises mainly from the amide carbonyl, C=O, stretch (s) with smaller contributions from the C-N s, N-H bend (b), and C-C s.[5] Depending on the frequency of the amide I region, assignments of α-helix, random coil (RC) or unordered, and β–sheet can be determined. There is a shift from a lower frequency of 1651 cm^{-1} for α-helix, through ~1652 cm^{-1} for β–turn, ~1664 cm^{-1} for random coil, and then to a higher frequency for β–sheet at ~1670 cm^{-1}. This frequency shift occurs due to the sensitivity of the C=O stretch to hydrogen-bonding. Hydrogen bonding to the amide carbonyl group causes a shift to higher frequencies.[5] β–sheet structures are seen with the highest frequency because they have the most Intrahelical

hydrogen bonds.[5]

The amide II frequency appears from 1475–1575 cm^{-1}. The amide II is less sensitive to structure than the other amides but still shows distinct frequencies indicating secondary structure elements.[5] The existence of this region is due to a combination of the amide C-N stretching and C-N-H in plane bending.[5] There is a downshift in frequency from random coil at ~1560 cm^{-1}, to ~1551cm^{-1} for β–sheet , and finally to ~1525 cm^{-1} for α-helix.

The amide IIP band is due to the C-N stretching of the proline peptide bond, but a frequency shift occurs when the carbonyl of proline becomes hydrogen bonded.[6] This band appears at ~1445 cm^{-1} with no hydrogen-bonding character, and shifts to ~1460 cm^{-1} with strong hydrogen-bonding to the carbonyl of proline.[6]

A decrease in intensity of amide S region, ~1390 cm^{-1}, is seen in proteins with more α-helix content. The “S” stands for structure sensitive because of the intensity relationship with α-helical structure.[7] The amide S is due to the C_α-H bend and is vibrationally coupled to the amide III.[5] The disappearance of this peak in α-helices is the result of the uncoupling of the amide S and amide III modes when the C_α-H bond is rotated in such a way that the orientation becomes cis to the peptide carbonyl group, where the ψ angle, of the amide III, is restricted to ~60°, in α-helices. [5, 8]

The amide III encompasses a broad region from 1220-1425 cm^{-1}. This region is conformationally sensitive, showing strong frequency and width dependences with secondary structure. The frequency and width dependence

arises from the C-N stretching, N-H in-plane-bending and variations in the Ramachandran dihedral angles, phi (Φ) and psi (Ψ) (Figure 3.1). A large span, 1220-1320 cm^{-1} is seen for unstructured proteins, because of the numerous angles present. At lower frequencies, the most intense peak, ~1235 cm^{-1}, shows the presence of β–sheet structure. Random coil is seen at slightly higher frequencies with an intense peak at ~1250 cm^{-1}, and α-helical structures are seen at the highest frequencies of ~1300 cm^{-1}.

A summary of the vibrational modes and corresponding frequencies given above are shown in Table 3.1. Ultraviolet Raman spectra of proteins have been studied by various groups, which have estimated secondary structure contributions.[5, 9, 10] Basis spectra of pure amide vibrations have been compiled from Raman spectra of α-helix, β–sheet, and unordered proteins, and have been deconvoluted to provide a foundation for determining secondary structure information. The work of Spiro, et. al. is seen in Figure 3.2, with UVRR spectra of pure secondary structure compositions at 206.5 nm.[5] Table 3.2 is modified from reference 5 and lists the deconvoluted amide bands determined from these basis spectra.

3.3 Experimental Background

Two single-trp OmpA mutants, W57 and W57t, were folded into SUVs and unfolded in KP_i buffer. UVRR spectra were collected at 207.5 nm excitation. The aim of this work was to look for secondary structure changes in the folded and unfolded states of an OmpA mutant, and to determine and changes in structure of a full-length mutant and truncated mutant of OmpA. The spectra are seen in

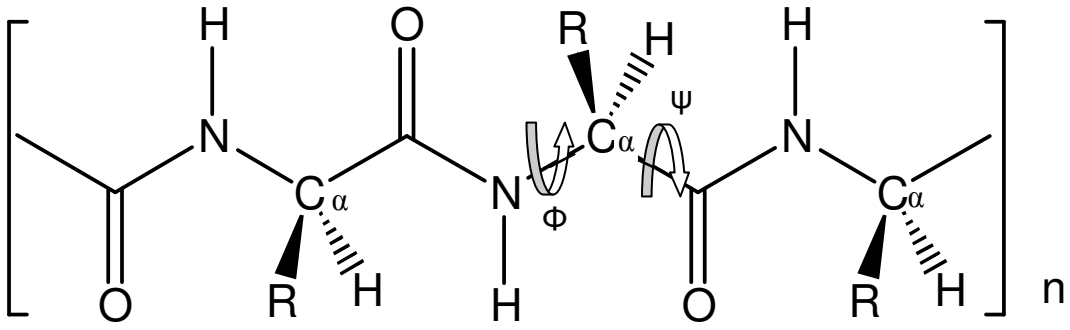

Figure 3.1. Representation of the amide backbone of a protein with "n" number of peptide bonds and R is a side chain of an amino acid. The conformation of the backbone is show with the torsion angles about the Cα-N bond (Φ) and the Cα-C bond (ψ).[11]

Table 3.1. Amide vibrational mode frequencies and vibrational assignments. Abbreviations are: stretch = s, bend = b, in plane bend = ib.

Vibrational Mode	Raman Region (cm^{-1})	Vibration Assignment
Amide I	~ 1625-1750	C=O s, C-N s, N-H b, C-C s
Amide II	~ 1475-1575	C-N s, C-N-H ib
Amide IIP	~ 1445-1460	C-N s of proline
Amide S	~ 1390	C_α-H b
Amide III	~ 1220 - 1425	C-N s, N-H b, ψ and Φ angles

Table 3.2. Results of decomposition from the basis spectra of α-helix, β-sheet, and unordered secondary structures seen in figure 15. Peak height is relative to perchlorate band at ~934 cm^{-1}. The peak positions in parentheses have been reported from other references. This table is modified from reference 4.

	α-helix		β-sheet		Unordered	
Vibrational mode	**Peak Position (cm^{-1})**	**Peak Height (nm)**	**Peak Position (cm^{-1})**	**Peak Height (nm)**	**Peak Position (cm^{-1})**	**Peak Height (nm)**
Amide I	1649 (1650)	91	1630 (1654) 1670 (1666)	65 126	1664 (1665)	72
Amide II	1525 1552 (1545)	48 71	1537 1562 (1551)	112 151	1552 (1560)	76
Amide S	(1393)	(1)	1399 (1395)	68	1386 (1395)	62
Amide III	1254 (1265) 1299 (1294) 1340 (1345)	25 69 40	1241 (1229) 1300 (1289) 1363 (1359)	133 36 62	1253 (1248) 1279 1332	72 32 40

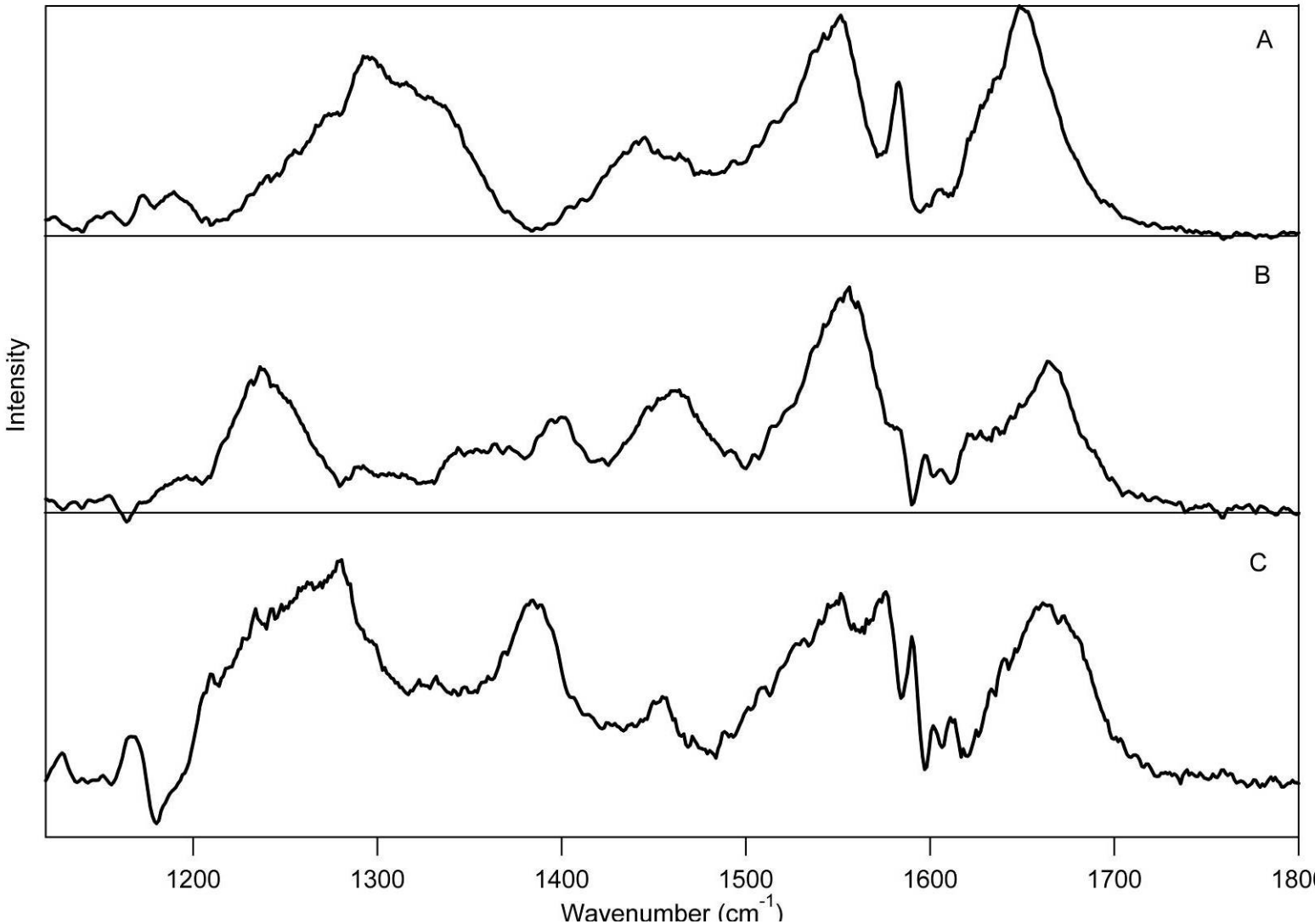

Figure 3.2. UVRR basis spectra of pure α-helix (A), β-sheet (B), and unordered (C) secondary structures at 206.5 nm excitation. Spectra from reference 5.

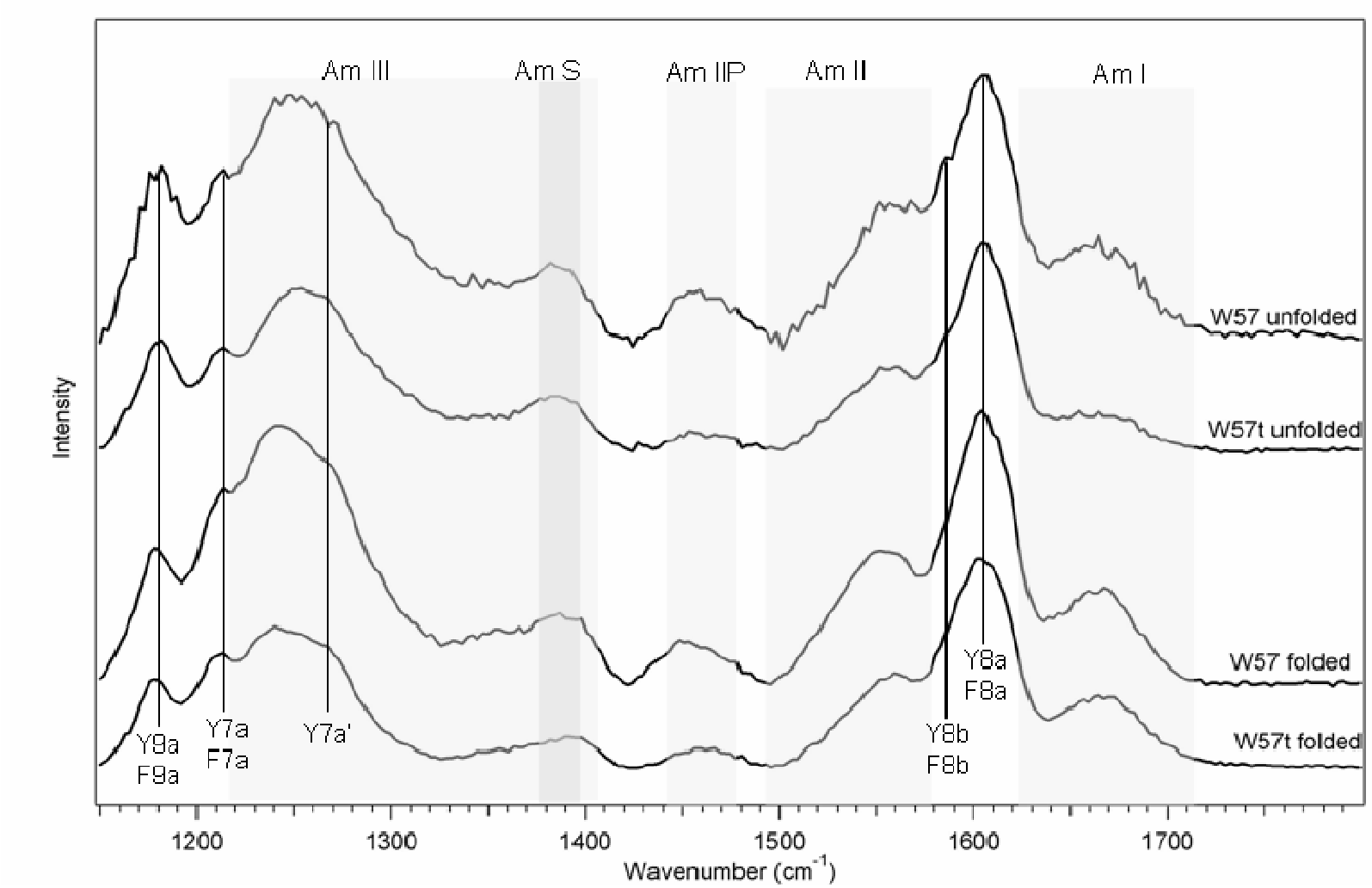

Figure 3.3. UVRR spectra at 207.5 nm of OmpA W57 and W57t unfolded in KPi and folded in SUVs. Amide regions are labeled at the top and are shown in grey. Amide S is shown in a darker grey to distinguish it from amide III. Tyrosine and phenylalanine modes are also indicated and labeled at the bottom.

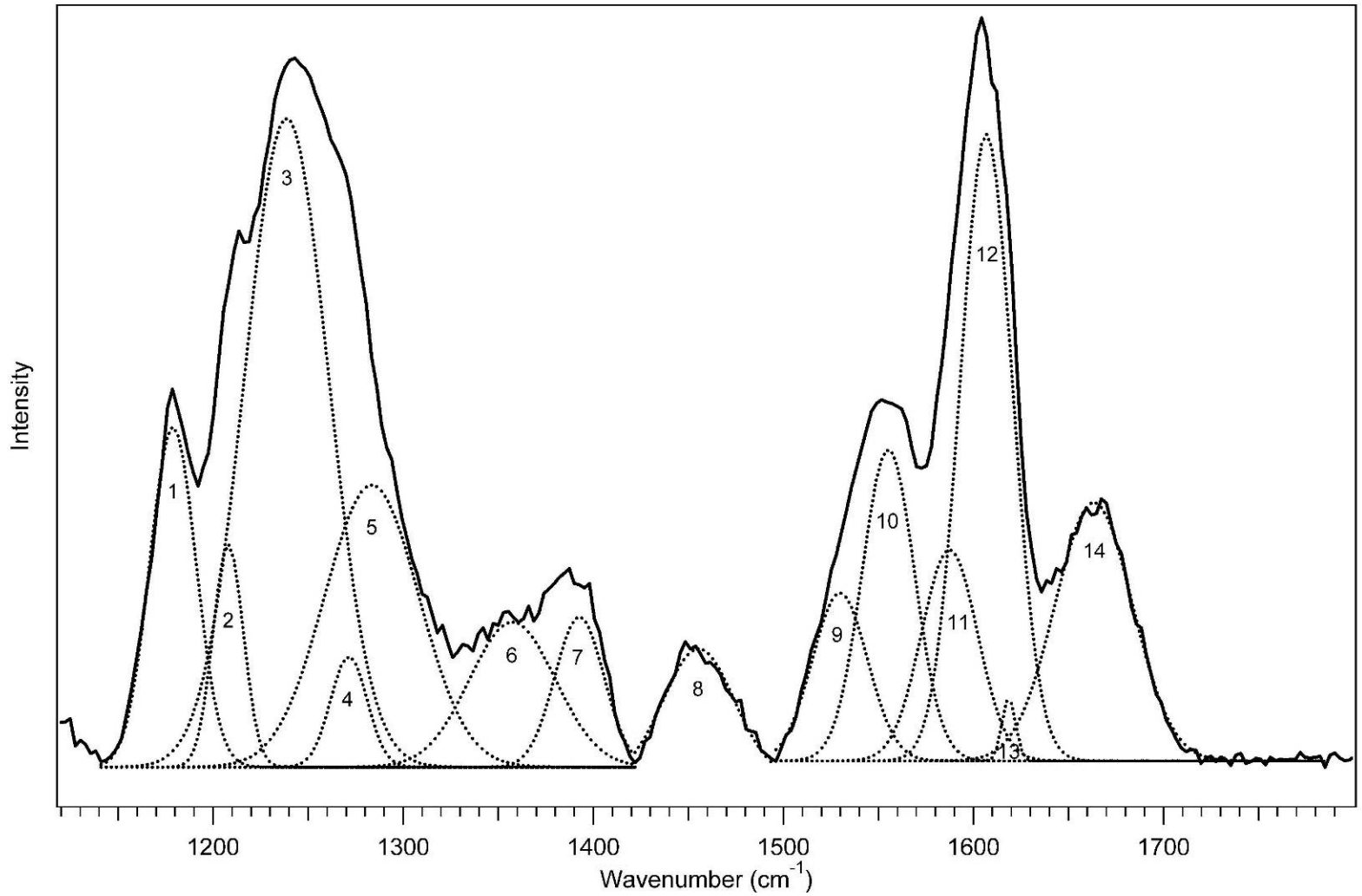

Figure 3.4. UVRR spectra of W57 in SUVs (solid) and the deconvolution of the amide peaks, fit to β-sheet structure, and amino acid bands (dotted). Numeric labels indicate the peak fit: 1 = Y9a/F9a, 2 = Y7a, 3 = amide III, 4 = amide III, 5 = Y7a', 6 = amide III, 7 = amide S, 8 = amide IIP, 9 = amide II, 10 = amide II, 11 = Y8b/F8b, 12 = Y8a/F8a, 13 = amide I, 14 = amide I.

Figure 3.3 with amide regions and aromatic amino acid contributions labeled.

Deconvolution of the amide regions was attempted to provide an estimate of secondary structure contributions; however, overlapping tyrosine and phenylalanine bands contribute to these regions, making definitive assignments difficult. Figure 3.4 shows the fitting of β–sheet structure, using amide peak vibrations given in Table 3.2, to the spectrum of W57 in folded in SUVs. Frequency positions and widths were allowed to vary. Due to the presence of multiple components, including the amide and aromatic amino acids bands, a good fit was unattainable.

Complications involving overlapping tyrosine and phenylalanine peaks made it difficult to remove these amino acid contributions from the protein backbone spectra. Therefore, the spectra shown are not completely pure protein backbone and include some signal from tyrosine and phenylalanine peaks in the amide I, II, and III regions. Tryptophan contributions in the spectra were minimal. This was found by examining the W18, 761 cm^{-1}, peak in the spectra. Looking at the wavelength dependence of aqueous tryptophan (figure 2.2), the W18 mode is the strongest between 215-206.5 nm. In the protein spectra at 207.5 nm the W18 mode is not seen and therefore suggests that tryptophan does not contribute to the peaks observed. Also, 50 μM tryptophan was used in the wavelength dependence compared to ~20 μM tryptophan present in the protein. Furthermore, it has been recognized in other studies that tryptophan, in the deep UV region, has only a minor contribution.[5]

3.4 Frequencies and Secondary Structure of OmpA

A close up of the amide I region of W57 and W57t folded in SUVs and unfolded in buffer is seen in Figure 3.5. The peaks in each spectrum are centered around ~1665 cm^{-1}, with no detectable frequency changes in this region; no observable secondary structure differences between the folded and unfolded conformations of the full-length and truncated mutants is seen. A characteristic peak in β–sheet should appear around ~1630 cm^{-1}; however, this peak cannot be seen because of overlapping tyrosine and phenylalanine bands. Possible secondary structure information determined from the amide I region is inconclusive at this wavelength.

The amide II region of W57 and W57t folded in SUVs and unfolded in buffer is seen in Figure 3.6. The amide II region is broad, and it is difficult to locate a maximum due to contributing amino acids of Y8b and F8b modes, ~1590 cm^{-1}. There appears to be two peaks, ~1549 cm^{-1} and ~1562 cm^{-1}, in all the spectra. The full-length mutant has much broader peaks than the truncated mutant. Some of the broadness in the full-length mutant may be due to an additional five tyrosine residues in the tail, causing the overlapping Y8b mode at ~1562 cm^{-1} to become more intense. There may be small frequency changes in both of these regions, which are unable to be observed. However, when comparing the full-length folded and unfolded mutant, there is a noticeable difference in width of the folded mutant in the lower frequency region (Figure 3.7). β–sheet structures posses an additional peak at ~1537 cm^{-1}. The increase in width is evidence that

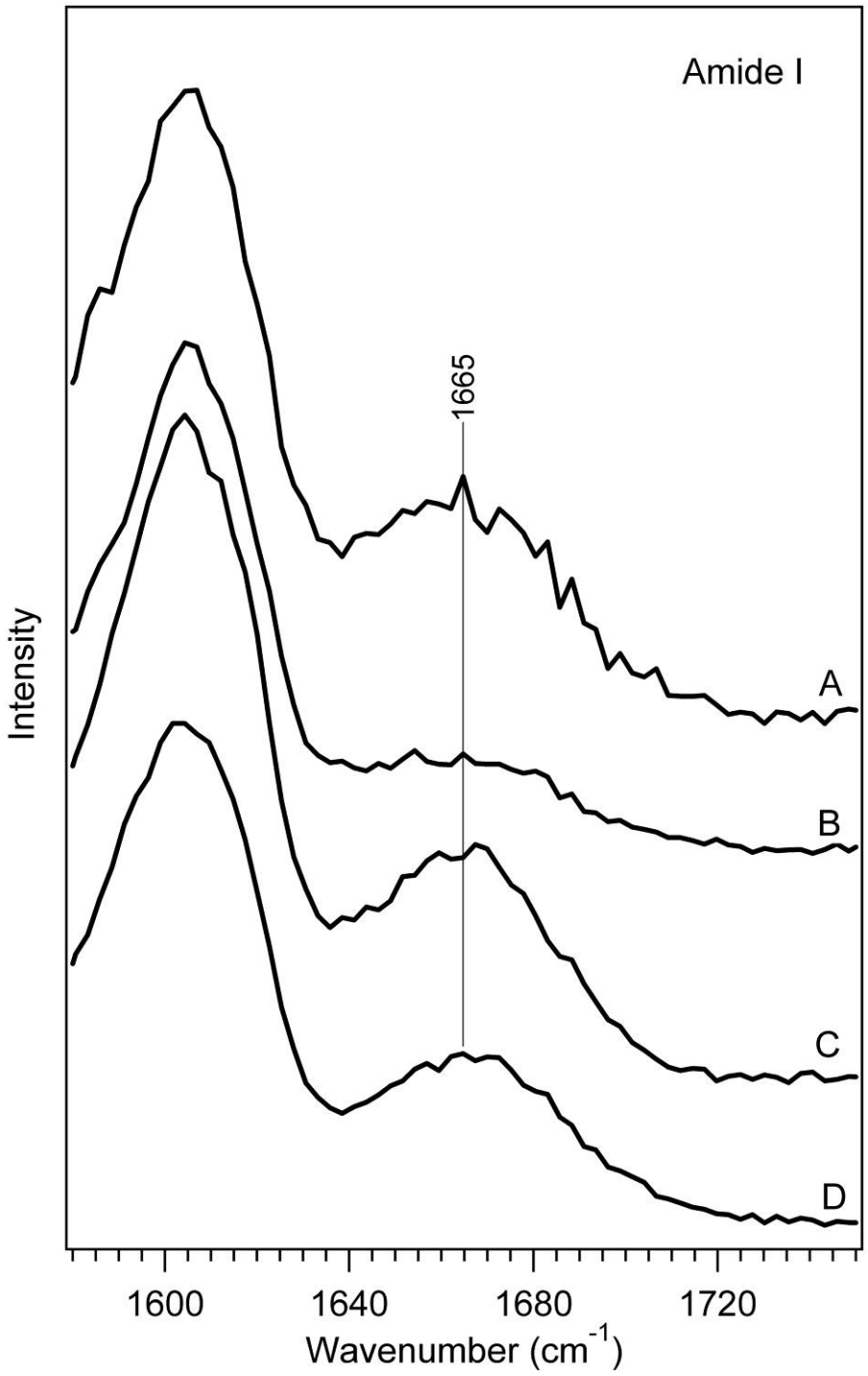

Figure 3.5. Blow-up of the amide I region in the UVRR spectra of W57 unfolded in KP_i (A), W57t unfolded in KP_i (B), W57 folded in SUVs (C) and W57t folded in SUVs (D).

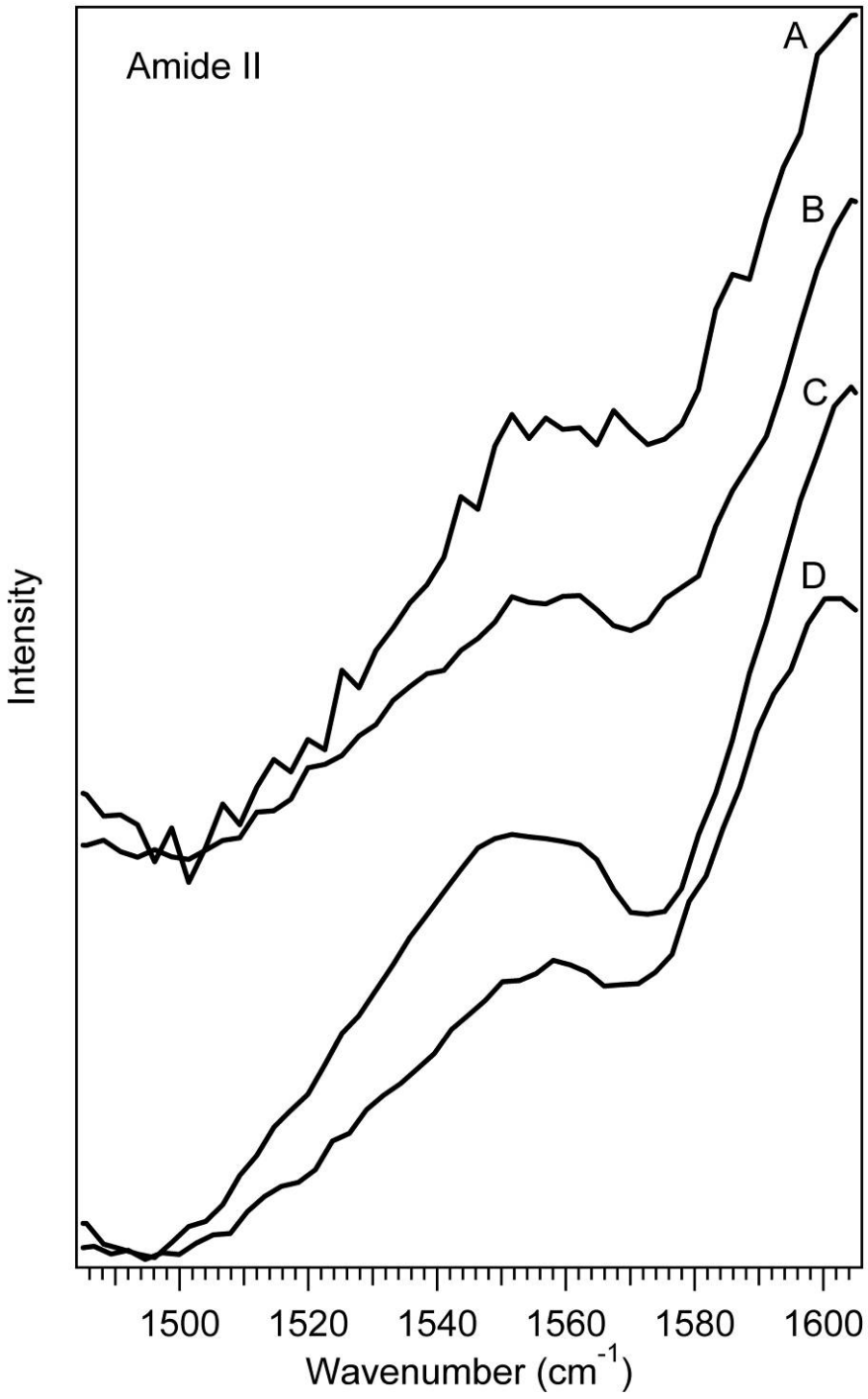

Figure 3.6. Blow-up of the amide I region in the UVRR spectra of W57 unfolded in KP_i (A), W57t unfolded in KP_i (B), W57 folded in SUVs (C) and W57t folded in SUVs (D).

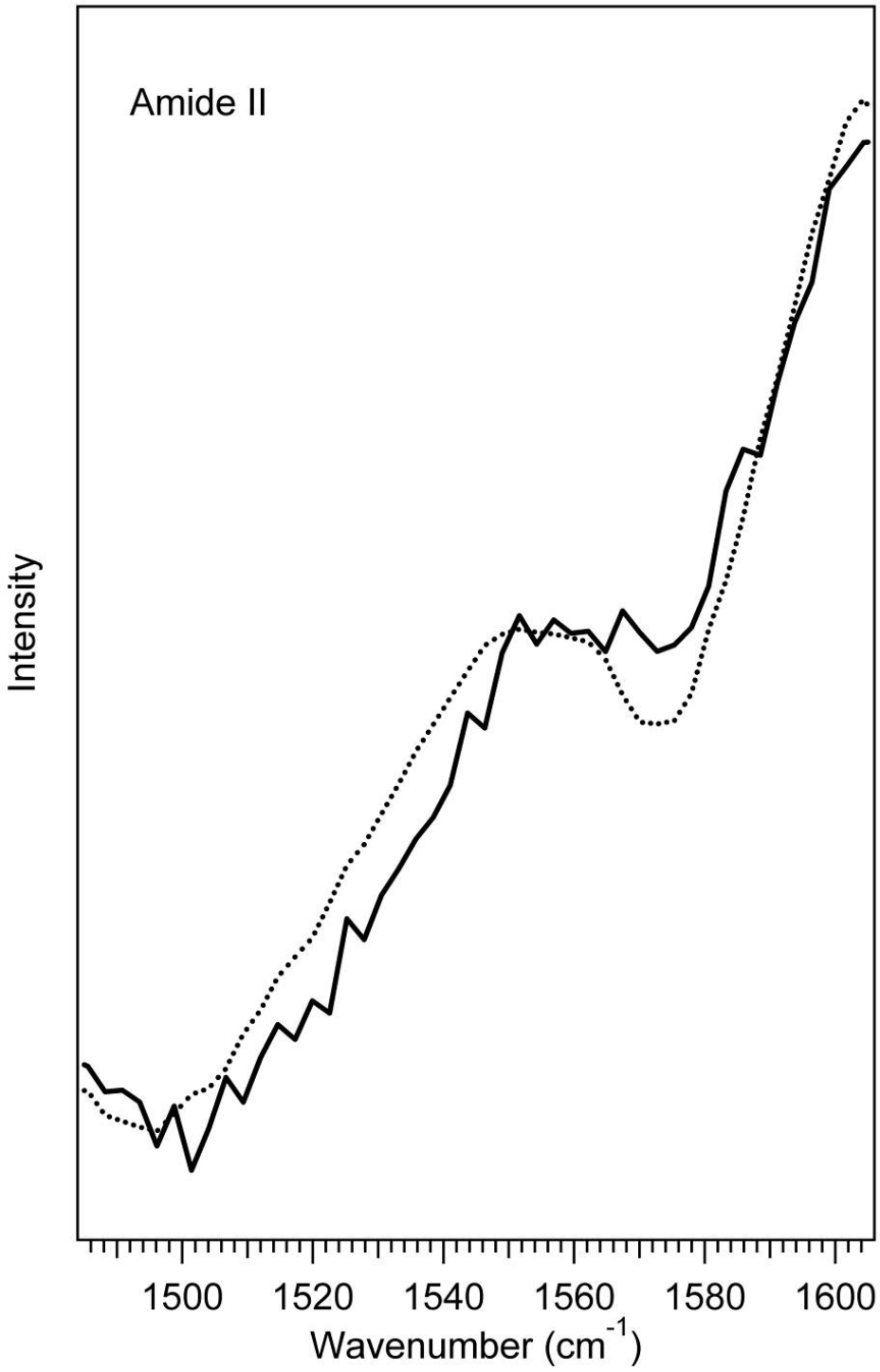

Figure 3.7. UVRR spectra of the amide II region comparing W57 unfolded in KP_i (solid) and W57 folded in SUVs (dotted).

the folded structure of W57 shows β–sheet composition, while W57 unfolded does not.

The amide IIP is the only region which displays differences between the truncated and full-length mutants, regardless of environmental effects (Figure 3.8). There is a ten proline difference between the truncated and full-length mutants. There are nine proline residues in the transmembrane domain and ten additional proline residues that reside in the periplasmic tail, which are cleaved in the truncated mutant. The full-length W57 in KP_i and SUVs show asymmetric peaks shifted to lower frequency, ~1451 cm^{-1}. Compared to W57, the folded and unfolded W57t spectra have smaller, symmetric peaks at a higher frequency of ~1462 cm^{-1}. The breath and shape of the full-length peaks may suggest various hydrogen bonding strengths. The similarity of the truncated mutant in KP_i and SUVs shows that the intramolecular hydrogen bonds between amino acids in the folded protein and the solvent hydrogen bonds in the unfolded protein may be comparable in strength. Additionally, the asymmetric lower frequency peak probably represents the contribution of the ten proline residues in the tail compared to the symmetric peak of the truncated. The truncated mutant in KP_i and SUVs shows stronger hydrogen bonds on the carbonyl of the proline, even though there are less proline residues, which may mean that the proline residues in the tail do not participate in much hydrogen-bonding.

A close-up of the amide S region is shown in Figure 3.9. The presence of the amide S supports the data that shows the structure of OmpA is not α-helical and therefore must be either random coil or β–sheet. Slight frequency shifts

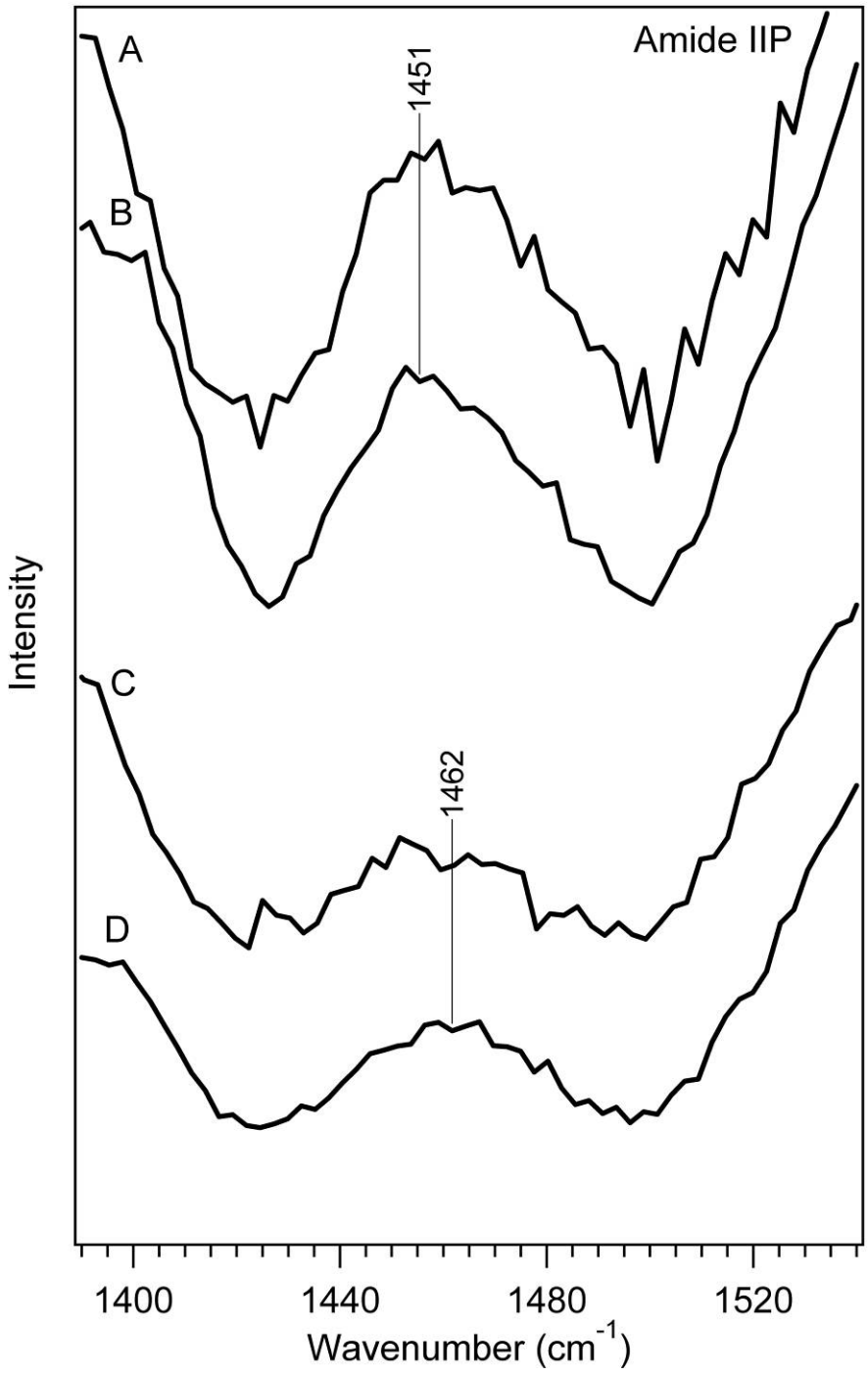

Figure 3.8. Blow-up of the amide IIP region in the UVRR spectra of W57 unfolded in KP_i (A), W57 folded in SUVs (B), W57t unfolded in KP_i (C) and W57t folded in SUVs (D).

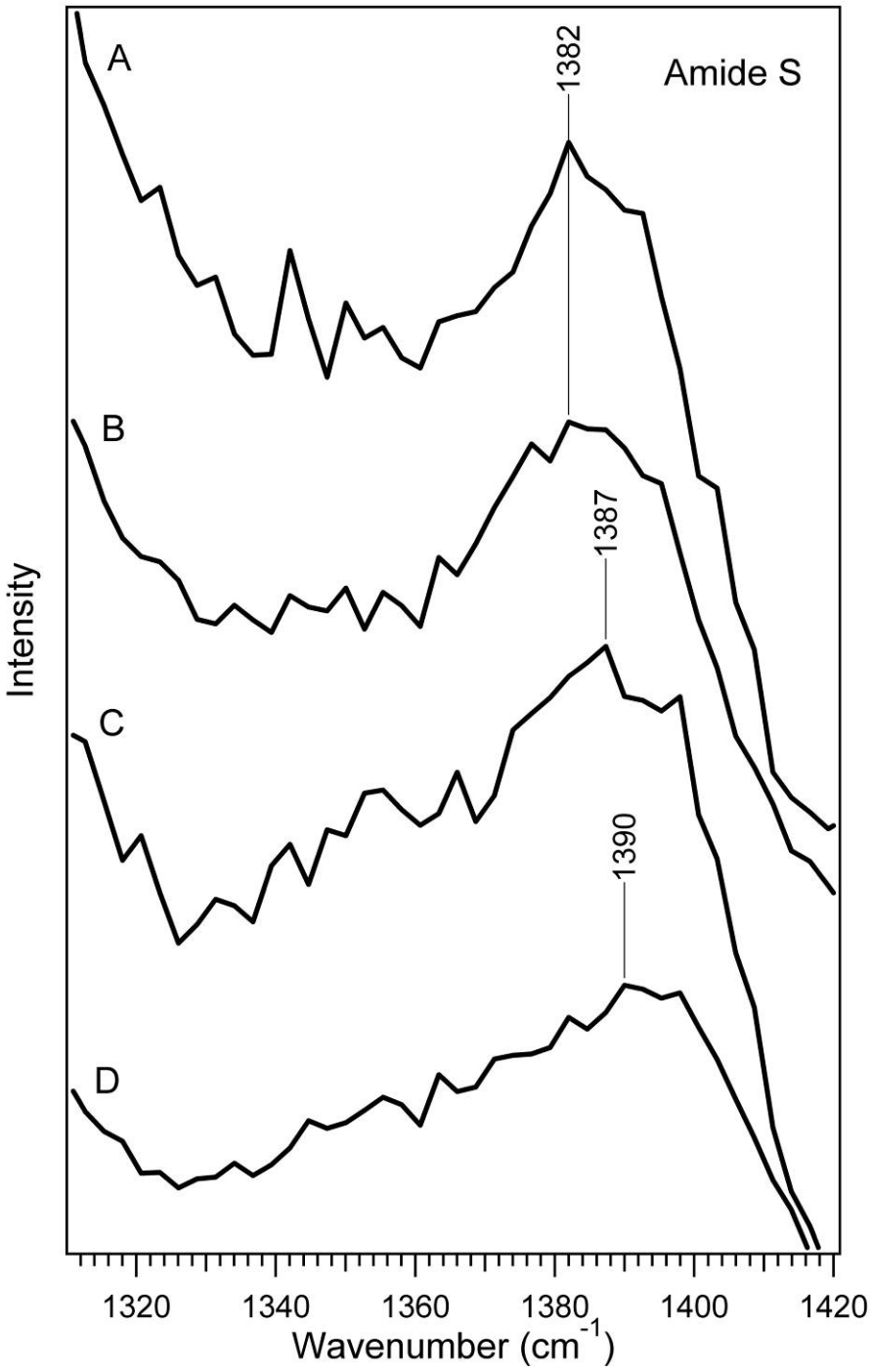

Figure 3.9 Blow-up of the amide S region in the UVRR spectra of W57 unfolded in KP_i (A), W57t unfolded in KP_i (B), W57 folded in SUVs (C) and W57t folded in SUVs (D).

between the unfolded and folded structures are consistent with a change in structure from random coil to β–sheet. A low frequency of ~1382 cm^{-1} found for unfolded protein suggests the structure is unordered, and a higher frequency of ~1387 cm^{-1} and ~1390 cm^{-1} for truncated folded and full-length folded suggests β–sheet structure.

The amide III region is shown in Figure 3.10. W57 and W57t folded have the most intense peak at lower frequencies, ~1240 cm^{-1}. This is consistent with β-sheet structure. On the other hand, the most intense peak in W57 and W57t unfolded show up at slightly higher frequencies compared to the folded mutants, which agrees with an unordered structure.

The amide III shifts could be due to the overlapping tyrosine modes Y9a, Y7a, and Y7a'. These modes have been shown to shift frequency with hydrogen bonding strength. This is unlikely the reason for a shift in the amide III bands. There is a 3 cm^{-1} shift in Y9a mode between the folded mutants at ~1179 cm^{-1} and unfolded mutants at ~1181 cm^{-1}. However, the Y7a mode is clearly seen and no shift is seen in this mode between the truncated and full-length mutants in either the unfolded or folded conformation. There are no shifts for phenylalanine like tryptophan and tyrosine, so the shifts cannot be attributed phenylalanine.

The folded spectra also show evidence of β-sheet structure over the unfolded, unordered spectra in the region of ~1260-1285 cm^{-1}. A more intense shoulder shows up in this region for β-sheet structure and is seen in both the W57 and W57t folded spectra. Although the region around 1355 cm^{-1} is noisy there is a noticeable bulge in the folded spectra in this area. The folded spectra

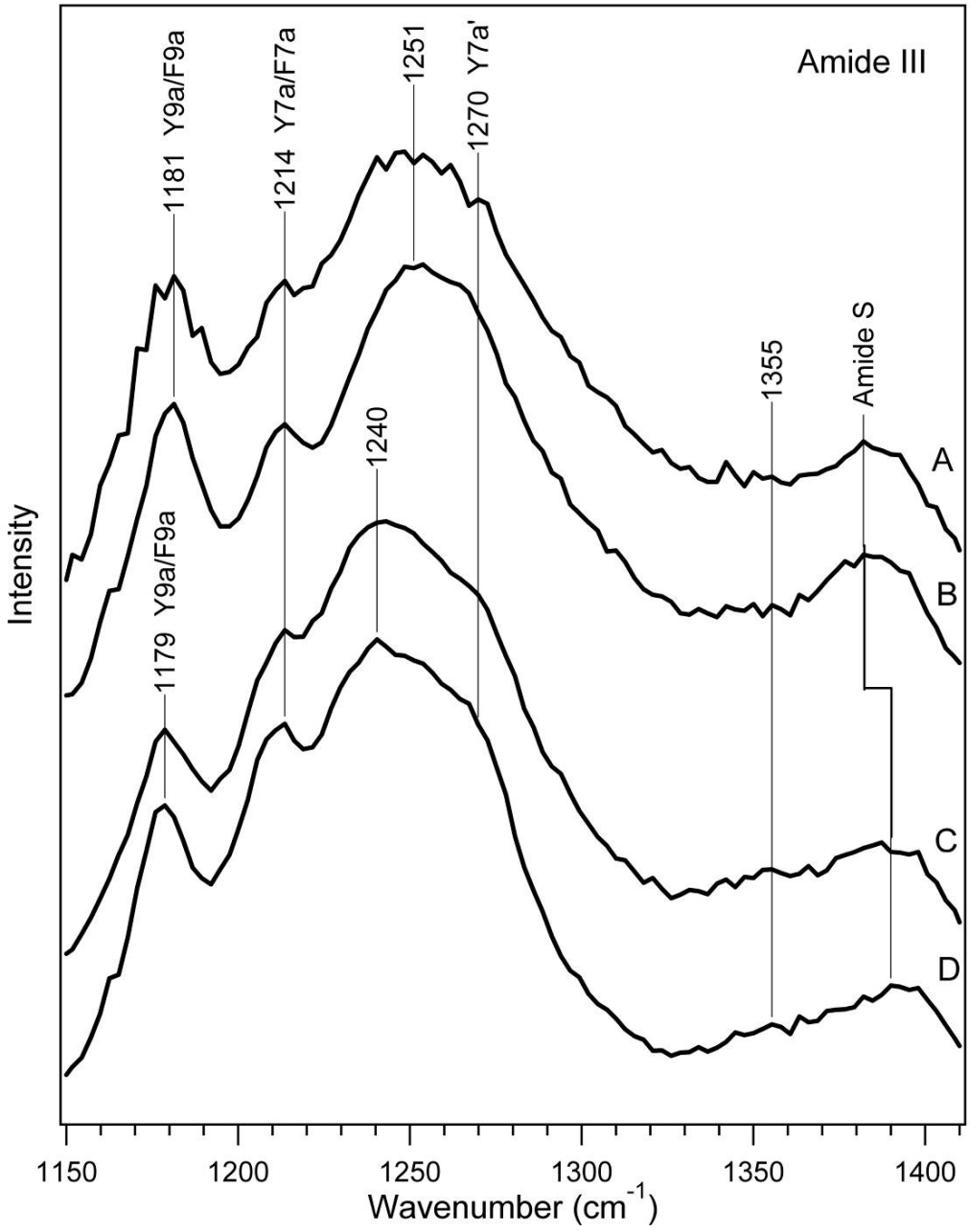

Figure 3.10. Close-up of amide III region in UVRR spectra of W57 unfolded in KP_i (A), W57t unfolded in KP_i (B), W57 folded in SUVs (C) and W57t folded in SUVs (D).

show a slope in this region while the unfolded spectra show a valley. This bulge in the folded spectra is consistent with β-sheet structure.

3.5 Conclusion

UVRR at 207.5 nm is a powerful tool that allows changes in secondary structure to be visualized in OmpA folded and unfolded states. Within the current signal to noise and the contributions from tyrosine and phenylalanine, the UVRR spectra shown here indicate only minor differences in vibrational structure between the folded full-length and truncated mutants. The preliminary conclusion is that unfolded W57 and W57t appear to be structurally similar, with frequencies indicating unordered structure. Also, the folded forms of W57 and W57t have similar secondary structure. On the other hand, the folded and unfolded spectra are quite different and have more significant frequency shifts and shapes, observed in the amide II, amide IIP, amide S, and amide III regions. The folded spectra of W57 and W57t primarily reflect β-sheet structure. An unordered structure is seen for the unfolded W57 and W57t spectra. UVRR at lower wavelengths, <207.5 nm, may be able to distinguish greater differences as the amide bands become more resonance with the π-π* transition at 190 nm.

References

1. J. C. Kendrew, R. E Dickerson, B. E.Strandberg, R. G. Hart, D. R. Davies, D. C. Phillips and V. C. Shore. "Structure of Myoglobin - 3-Dimensional Fourier Synthesis at 2 a Resolution," *Nature* 185, 4711, 422-427, 1960

2. D.W. Peterson, H.J. Zhou, F.W. Dahlquist, and J. Lew. "A Soluble Oligomer of Tau Associated with Fiber Formation Analyzed by NMR," *Biochemistry (N.Y.)* 47, 28, 7393-7404, 2008

3. S.M. Kelly, T.J. Jess and N.C. Price. "How to Study Proteins by Circular Dichroism," *Biochimica Et Biophysica Acta-Proteins and Proteomics* 1751, 2, 119-139, 2005

4. I.K. Lednev, A.S. Karnoup, M.C. Sparrow and S. A. Asher. "Alpha-helix Peptide Folding and Unfolding Activation Barriers: A Nanosecond UV Resonance Raman Study," *J. Am. Chem. Soc.* 121, 35, 8074-8086, 1999

5. C.Y. Huang, G. Balakrishnan and T.G. Spiro. "Protein Secondary Structure from Deep-UV Resonance Raman Spectroscopy," *J. Raman Spectrosc*. 37, 1-3, 277-282, 2006

6. T. Jordan, I. Mukerji, Y. Wang, and T.G. Spiro. "UV Resonance Raman Spectroscopy and Hydrogen Bonding of the Proline Peptide Bond," *J. Mol. Struct.* 379, 51-64, 1996

7. Y. Wang, R. Purrello and T.G. Spiro. "UV Photoisomerization of N-Methylacetamide and Resonance Raman Enhancement of a New Conformation-Sensitive Amide Mode," *J. Am. Chem. Soc.* 111, 21, 8274-8276, 1989

8. Y. Wang, R. Purrello, T. Jordan and T. G. Spiro. "UVRR Spectroscopy of the Peptide-Bond. 1. Amide S, a Nonhelical Structure Marker, Is a C_α-H Bending Mode," *J. Am. Chem. Soc.* 113, 17, 6359-6368, 1991

9. Z.H. Chi, X. G. Chen, J.S.W. Holtz and S.A. Asher. "UV Resonance Raman-Selective Amide Vibrational Enhancement: Quantitative Methodology for Determining Protein Secondary Structure," *Biochemistry (N.Y.)* 37, 9, 2854-2864, 1998

10. S.H. Song and S.A. Asher. "UV Resonance Raman Studies of Peptide Conformation in Poly(L-lysine), Poly(L-glutamic Acid), and Model Complexes - the Basis for Protein Secondary Structure Determinations," *J. Am. Chem. Soc.* 111, 12, 4295-4305, 1989

11. Charlotte W Pratt, Donald Voet, and Judithe G. Voet. “Fundamentals of Biochemistry: Life at the Molecular Level, 2sd ed.” John Wiley and Sons, Inc. 2006.

Chapter 4: UVRR at 228 nm: Probing Tryptophan Microenvironment

Acknowledgments

Data presented in this chapter were collected in collaboration with Katie Sanchez. This work, in part or in whole, may be used in future publications.

Abstract

Tryptophan is an ideal chromophore for studies of protein folding because several tryptophan UVRR peaks report on local hydrophobicity, hydrogen-bonding, and the torsion angle, $|\chi^{2,1}|$. These signatures make it possible to identify changes in the structure and local environment of tryptophan residues in a protein. In this study, OmpA wild-type and the single-trp full-length and truncated mutants unfolded in KP_i, folded in SUV, and folded in OG are compared with 228 nm excitation and illustrate significant changes in tryptophan structure and microenvironment.

4.1 Introduction

UVRR is rapidly becoming a powerful technique for the study of complex biomolecules. Proteins containing the aromatic amino acids, tryptophan, tyrosine, and phenylalanine are particularly interesting because of the role these side chains play in membrane protein folding.[1, 2] Protein interactions with the water-membrane interface uniquely depends on these amino acids. Assembly, folding, and therefore structure and orientation in a membrane can be partially attributed to this interaction.[3] Aromatic amino acid side chains are also known to stabilize the folded structure of integral membrane proteins.[1] An important and informative intrinsic chromophore in the study of protein folding is tryptophan because it

provides a spectroscopic signatures sensitive to hydrophobic environments, hydrogen bonding, and conformations of tryptophan. Therefore, it is possible to identify changes in structure and local environments of tryptophan in folded and unfolded states of proteins.[4, 5, 6, 7, 8] As we have seen in chapter 2, 228 nm excitation provides the greatest enhancement of tryptophan modes in OmpA. The tryptophan modes of interest are W17 (~878 cm^{-1}), W7 (~1340 and 1361 cm^{-1}), and W3 (~1550 cm^{-1}) indicated in the wild-type spectra shown in Figure 4.1. These spectral regions are very informative and are relatively free from tyrosine and phenylalanine signal; the dominating tyrosine and phenylalanine peaks are shown in the W0 spectra of Figure 4.1. The Raman spectra of single-trp full-length and truncated mutants unfolded in KP_i, folded in SUVs and folded in OG are shown in Figures 4.2, 4.3, and 4.4.

4.2 The W17 Mode

The W17 mode is sensitive to hydrogen bonding of the indole N_1H of tryptophan. Specifically, the W17 frequency decreases with increasing hydrogen-bonding strength at the indole N_1H site.[6] According to tryptophan model compounds, the W17 band has been observed at 871 cm^{-1} for strong hydrogen-bonding, 878 cm^{-1} for medium hydrogen-bonding, and 883 cm^{-1} for no hydrogen-bonding.[8]

Contained within the 800-900 cm^{-1} region is the W17 mode adjacent to a tyrosine Fermi doublet. The wild-type and mutant spectra were decomposed into the Fermi resonance of the two tyrosine peaks, a combination Y1 and 2Y16a mode (~831 cm^{-1} and ~854 cm^{-1}), and the W17 peak (~878 cm^{-1}). Additionally a

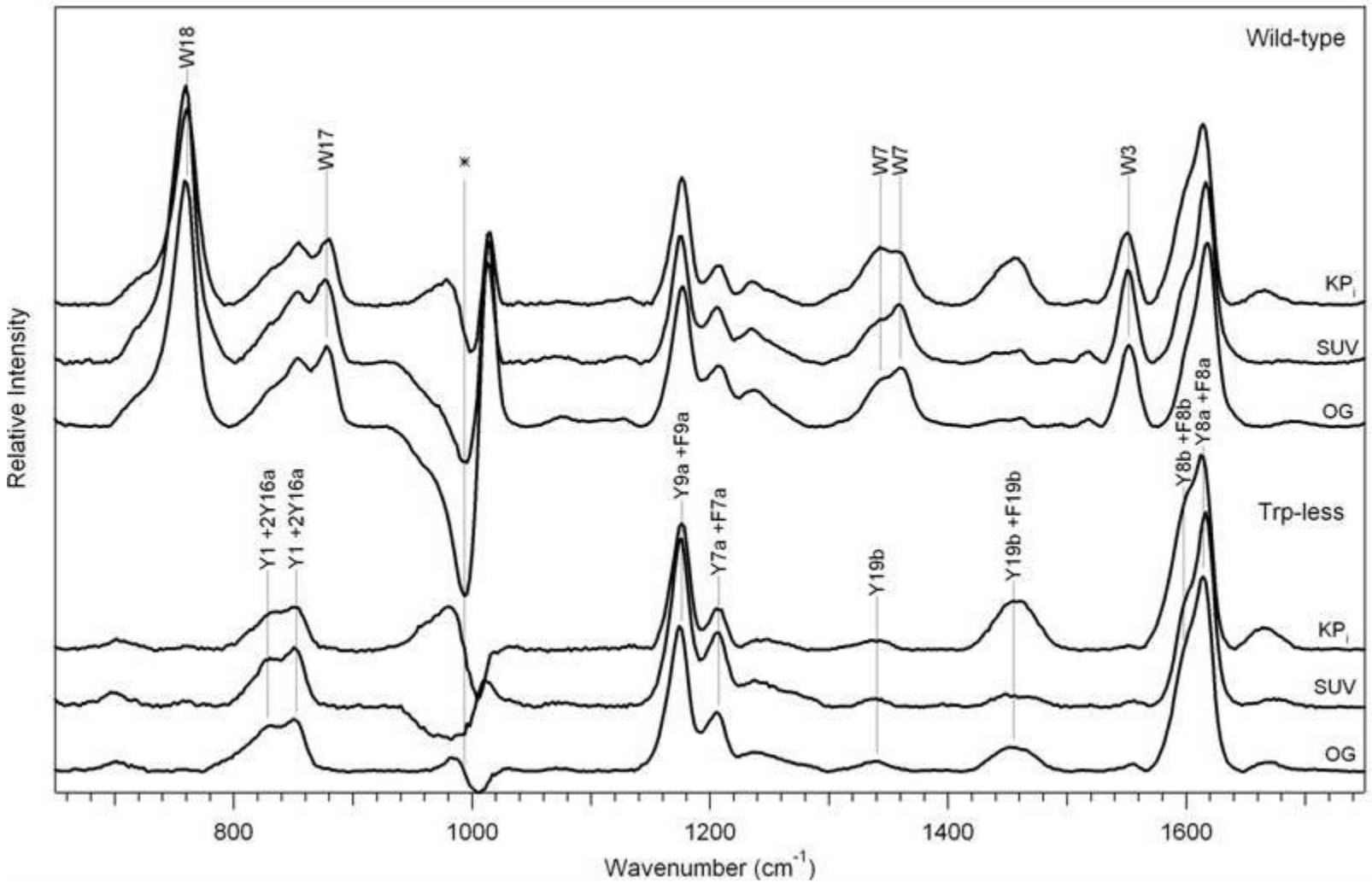

Figure 4.1. UVRR spectra at 228 nm of OmpA wild-type (top) and trp-less (W0, bottom) unfolded in KP_i, folded in SUVs and OG. Tryptophan modes are indicated in the wild-type spectra while tyrosine and phenylalanine modes are indicated in trp-less OmpA.

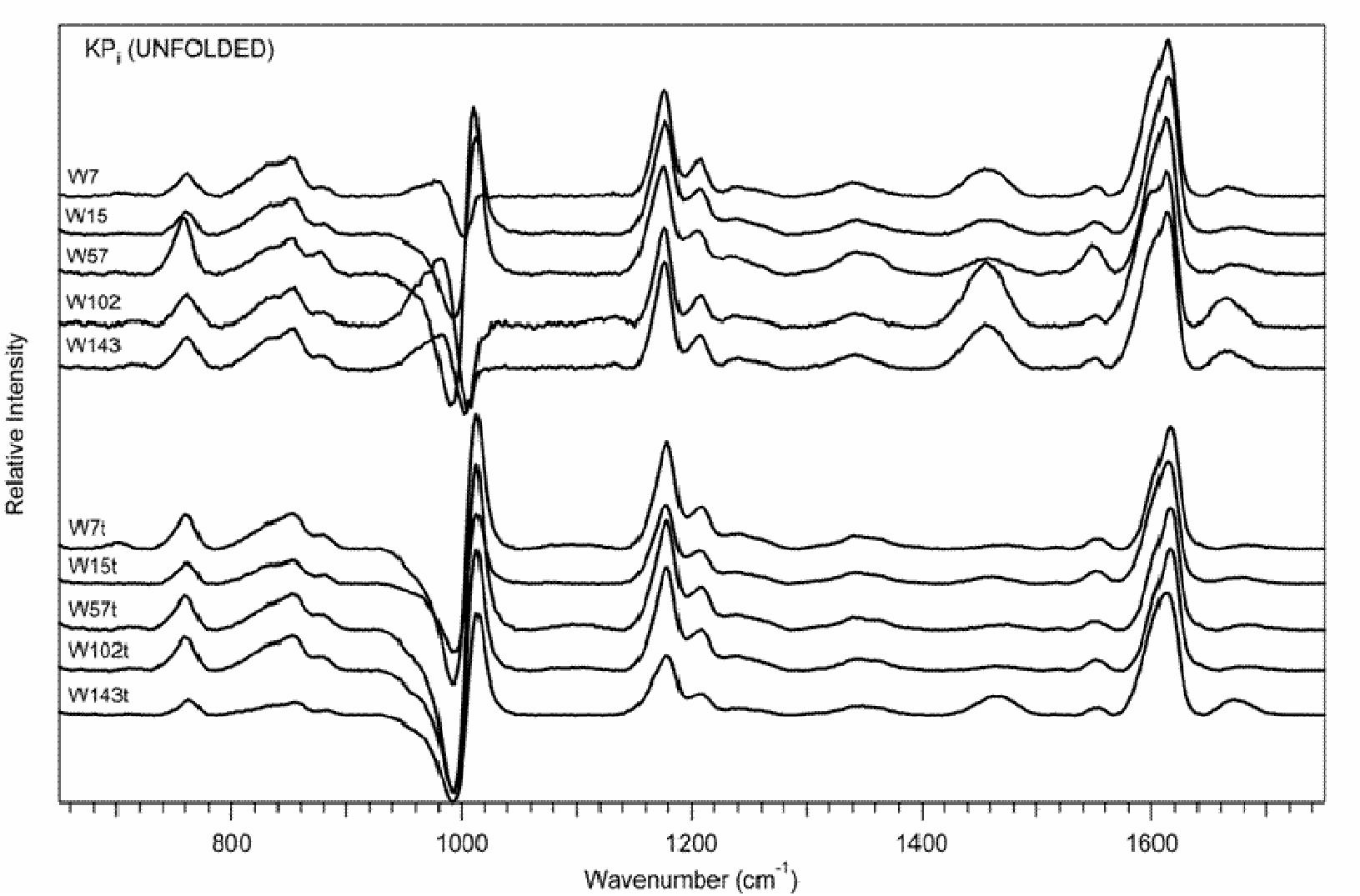

Figure 4.2. UVRR spectra at 228 nm of full-length mutants (top) and truncated mutants (bottom) unfolded in KP_i.

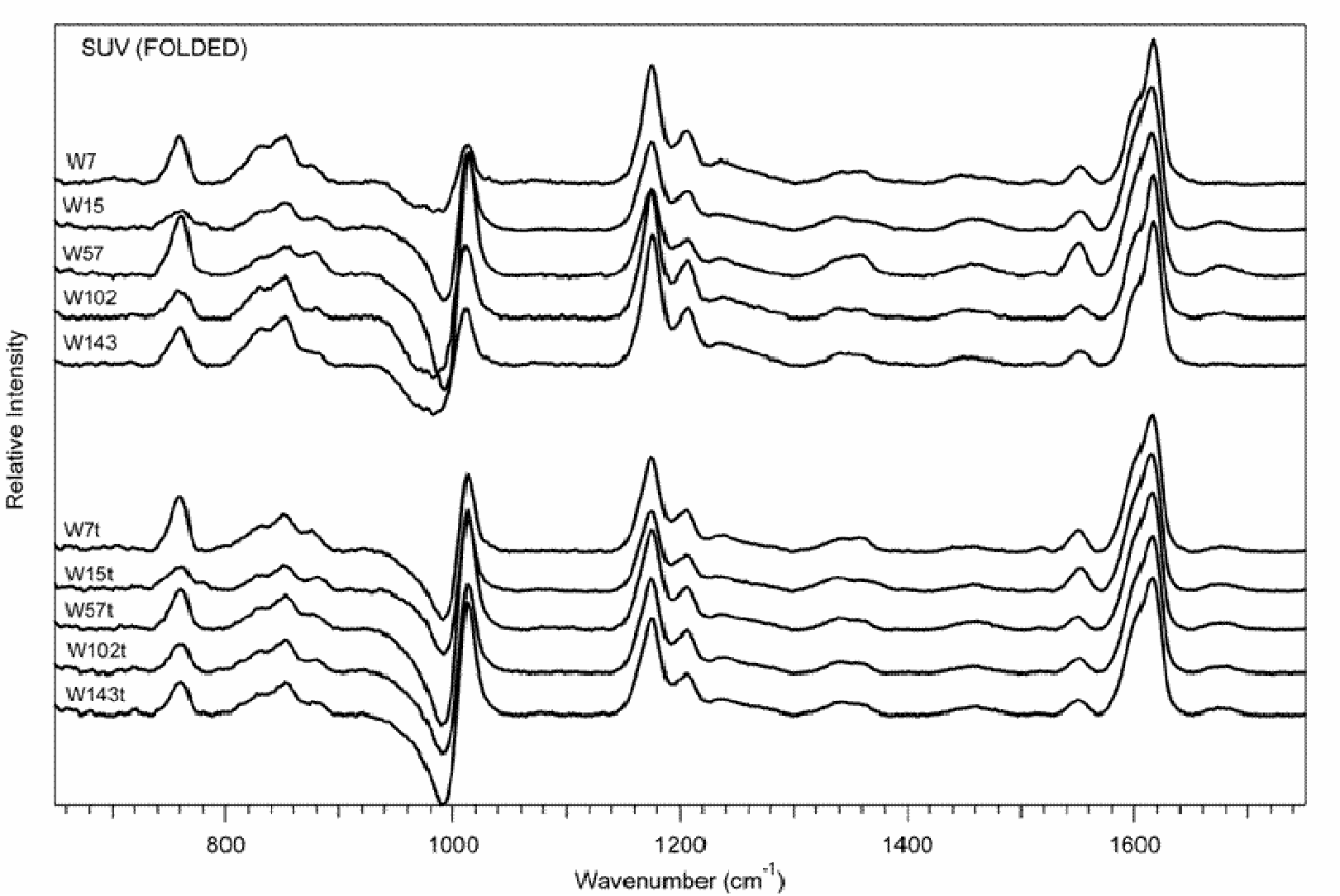

Figure 4.3. UVRR spectra at 228 nm of full-length mutants (top) and truncated mutants (bottom) folded in SUVs.

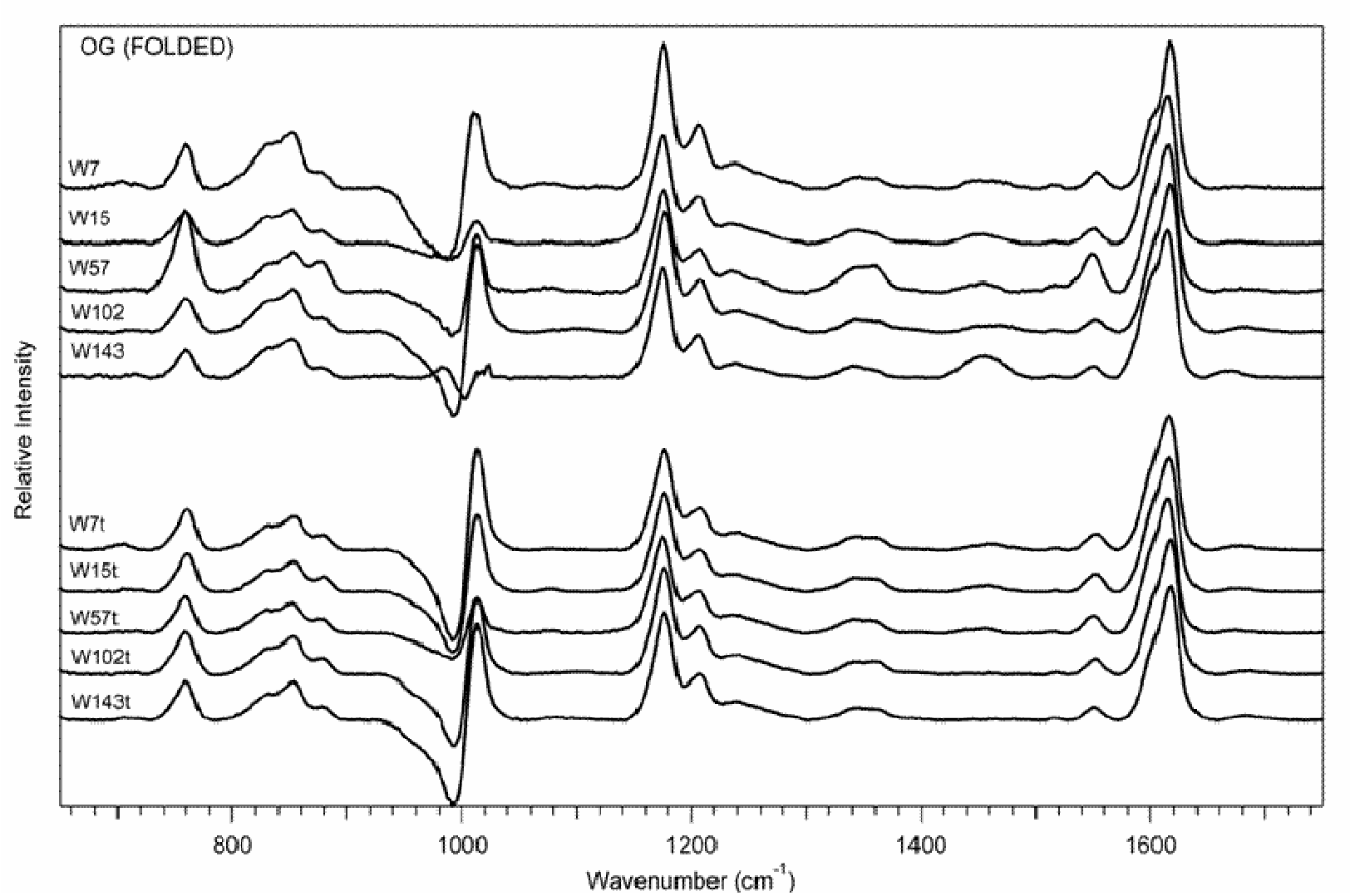

Figure4.4.UVRR spectra at 228 nm of full-length mutants (top) and truncated mutants (bottom) folded in OG.

fourth peak (~810 cm^{-1}) was added to compensate for the extra width. All widths and positions of the decomposition were allowed to vary to observe any changes in frequencies or widths. Figure 4.5 shows an example of OmpA wild-type decomposed into respective tyrosine and tryptophan modes. The results of the decomposition peak positions, widths, and amplitudes for each mutant are listed in Tables 4.1 and 4.2 and given in the appendix (Figures 5.1-5.6). Figure 4.6 shows a close-up of the W17 mode for wild-type and OmpA mutants in KP_i, SUV, and OG.

A frequency range of 876–880 cm^{-1} is observed for the full-length mutants and wild-type, while the truncated mutants show a slightly higher frequency range of 876-882 cm^{-1}. These ranges indicate medium to no hydrogen-bonding in the unfolded and folded protein states, respectively. None of the mutants show a low frequency indicative of strong hydrogen bonding character in either the folded or unfolded states. W15 and W15t have the highest frequencies (880 cm^{-1} and 881 cm^{-1}) of the full-length and truncated mutants in SUVs. This is in contradiction to the crystal structure, which suggests the possible existence of a hydrogen bond between the heteroatom of indole in tryptophan residue 15 and the carbonyl oxygen of asparagine residue 33, when folded (Figure 4.7). One explanation could be the difference in structure upon folding in SUVs versus the detergent used in the crystal structure. Moreover, the difference in hydrogen bonding between the crystal structure and folded protein has been witnessed in other proteins using UVRR.[6] Also the crystal structure data provides information on the state of hydrogen bonding at the N_1H site but the strength of hydrogen

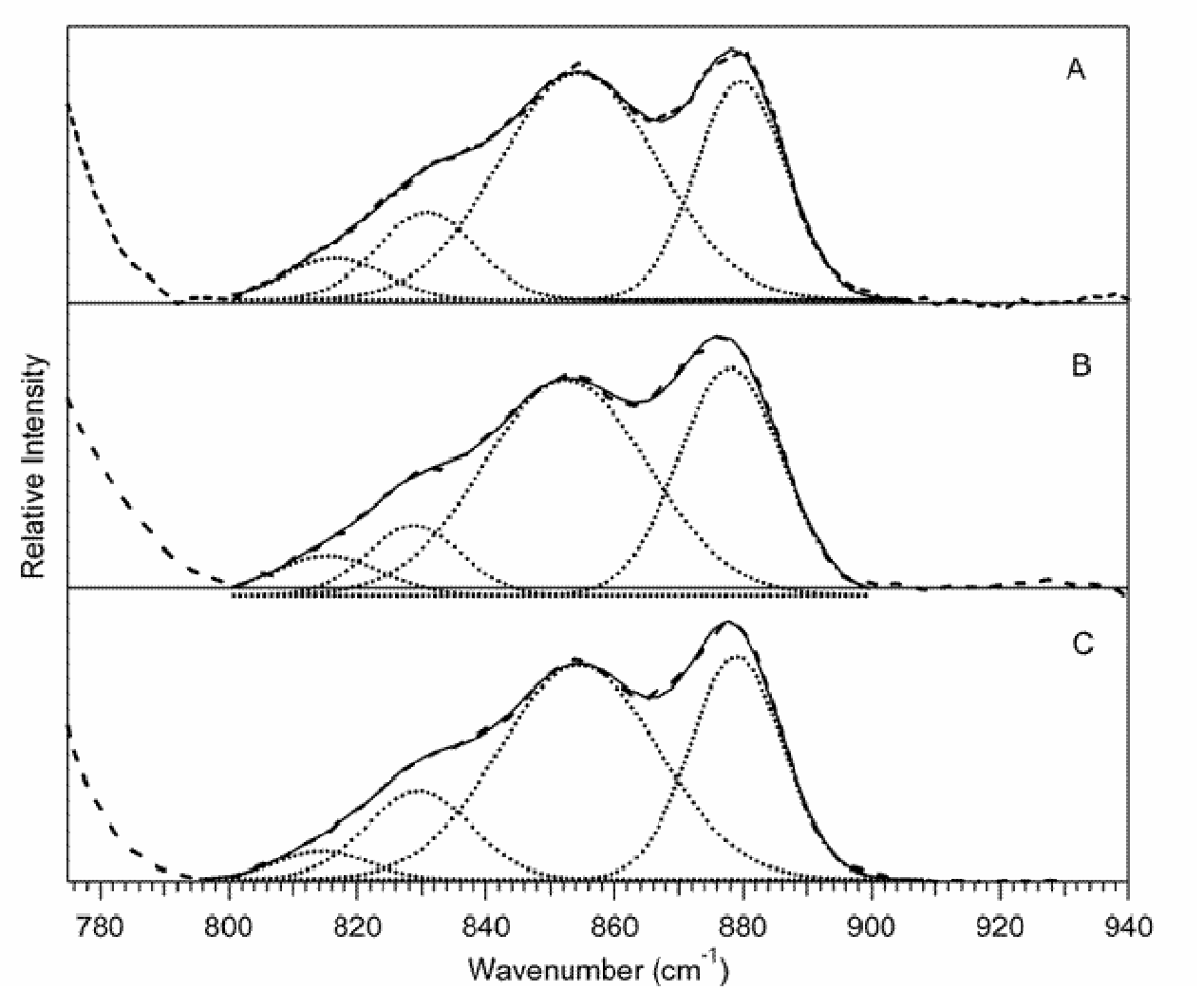

Figure 4.5. UVRR spectra of wild-type in KP_i (A), in SUVs (B), and in OG (C), showing the W17 mode (dashed) and the Gaussian decomposition (dotted) and overall peak fit (solid).

Table 4.1. Gaussian decompositions of the ~800-900 cm^{-1} region of the tyrosine Fermi doublet (Y1 + 2Y16a) and tryptophan W17 mode for the full-length mutants and wild-type.

Protein	Extra Peak		Y1 + 2Y16a (~832 cm^{-1})		Y1 + 2Y16a (~854 cm^{-1})		W17	
	Peak Center (cm^{-1})	Width (cm^{-1})	Peak Center (cm^{-1})	Width (cm^{-1})	Peak Center (cm^{-1})	Width (cm^{-1})	Peak Center (cm^{-1})	Width (cm^{-1})
W0 (KP_i)	814	23	833	23	853	19	-	-
W0 (SUV)	808	16	830	27	852	18	-	-
W0 (OG)	284	52	834	25	853	16	-	-
W7 (KP_i)	810	22	832	27	854	21	879	18
W7 (SUV)	809	12	830	27	853	21	876	18
W7 (OG)	804	23	834	35	854	17	877	19
W15 (KP_i)	812	25	833	24	854	21	879	17
W15 SUV)	811	6.6	831	26	853	19	880	22
W15 (OG)	812	21	830	21	852	22	878	17
W57 (KP_i)	807	19	834	32	856	19	878	18
W57 (SUV)	813	12	830	21	853	23	878	19
W57 (OG)	816	28	831	21	853	24	878	17
W102 (KP_i)	808	2.4	834	35	855	18	879	19
W102 (SUV)	812	13	830	24	852	20	879	15
W102 (OG)	808	16	834	35	855	18	878	18
W143 (KP_i)	816	27	834	23	854	20	879	17
W143 (SUV)	810	14	831	27	853	18	876	20
W143 (OG)	807	8.7	832	34	854	18	878	17
WT (KP_i)	817	18	831	18	854	29	880	16
WT (SUV)	815	19	829	17	852	30	878	18
WT (OG)	815	16	830	19	854	29	879	17

Table 4.2 Gaussian decompositions of the ~800-900 cm^{-1} region of the tyrosine Fermi doublet (Y1 + 2Y16a) and tryptophan W17 mode for the truncated mutants.

Protein	Extra Peak		Y1 + 2Y16a (~832 cm^{-1})		Y1 + 2Y16a (~854 cm^{-1})		W17	
	Peak Center (cm^{-1})	Width (cm^{-1})	Peak Center (cm^{-1})	Width (cm^{-1})	Peak Center (cm^{-1})	Width (cm^{-1})	Peak Center (cm^{-1})	Width (cm^{-1})
W7t (KP_i)	812	23	833	27	855	22	880	18
W7t (SUV)	821	44	831	24	853	20	876	18
W7t (OG)	818	34	834	25	855	20	879	18
W15t (KP_i)	816	27	832	19	853	25	880	15
W15t SUV)	823	25	830	14	852	24	881	19
W15t (OG)	811	13	830	23	853	22	880	16
W57t (KP_i)	811	22	836	35	856	20	879	19
W57t (SUV)	810	13	830	26	853	20	877	21
W57t (OG)	814	26	830	22	852	22	877	17
W102t (KP_i)	810	22	836	37	856	16	879	17
W102t (SUV)	812	17	830	20	852	21	879	17
W102t (OG)	807	11	833	34	854	18	878	18
W143t (KP_i)	807	21	838	38	858	27	882	17
W143t (SUV)	819	23	831	16	852	23	880	17
W143t (OG)	806	17	832	32	854	19	878	18

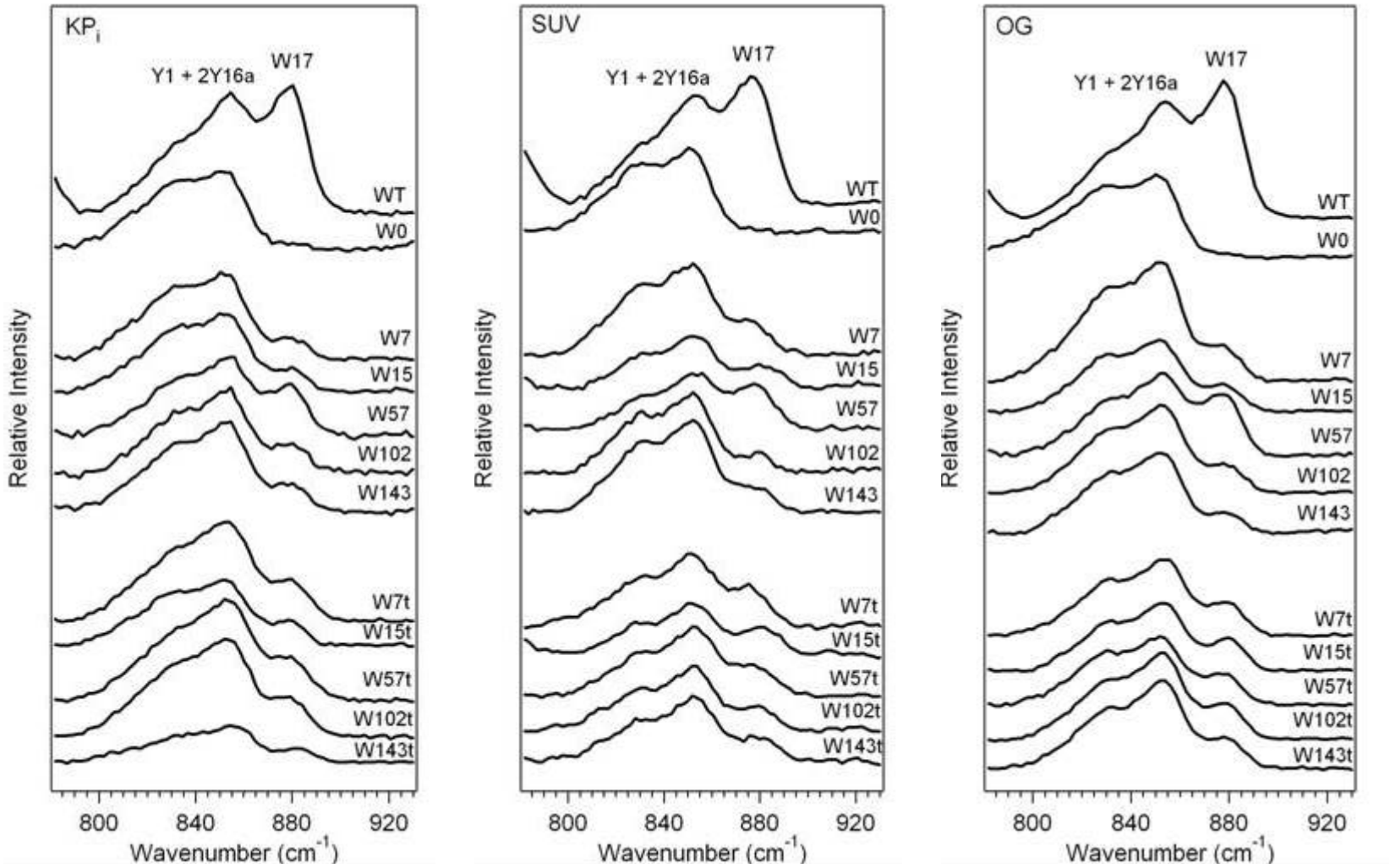

Figure 4.6. UVRR spectra showing close-up of W17 mode for wild-type and mutants in various conditions.

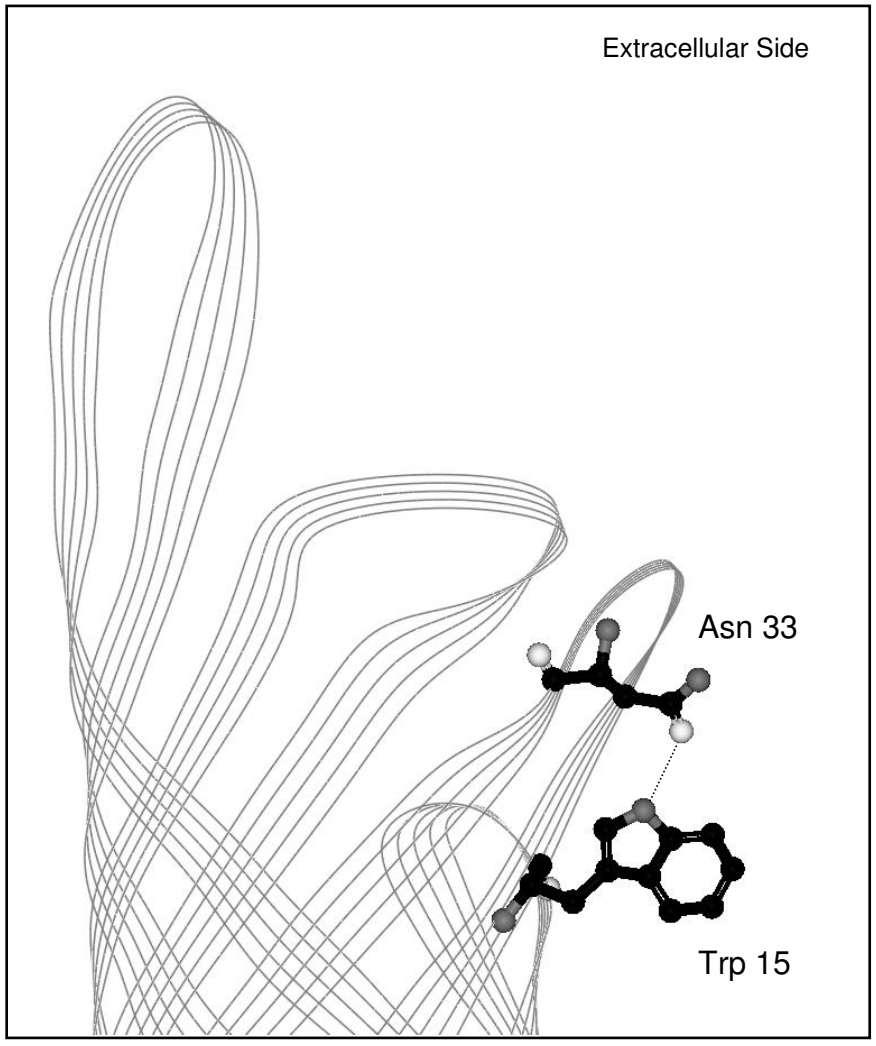

Figure 4.7. Transmembrane domain of OmpA showing the locations of W15 and N33 with a possible hydrogen bond between the heteroatom of W15 and the carbonyl of N33 (dotted line). PDB file 1QJP.

bonding cannot be quantitatively evaluated.[5] Furthermore, most of the peaks are found around 878-880 cm^{-1}, occurring within an error of ± 2 cm^{-1}, so it is unclear which mutants have stronger hydrogen bonds. Regardless, UVRR provides an estimate of the strength of hydrogen bonding. None of the OmpA wild-type or mutants in the unfolded or folded conformation demonstrate strong hydrogen bonding character through the N_1H indole site in tryptophan.

4.3 The W7 Mode

The W7 mode contains information on the hydrophobic environment surrounding tryptophan. Fermi resonance creates a doublet of the W7 mode into two peaks centered at ~1340 cm^{-1} and ~1361 cm^{-1}. The relative intensity (R) of the ratio, $I_{1361}/I_{1340,}$ is indicative of the environment of indole.[6, 7] Experiments with indole in various solvents have been conducted with an excitation at 488 nm and have shown R values that range from 0.65 – 0.92 in hydrophilic solvents, 1.02-1.11 in benzene, and 1.23-1.32 in saturated hydrocarbons.[7] Higher intensity ratios signify greater hydrophobicity. Even though this ratio is wavelength dependent, excitation at lower wavelengths, such as in the ultraviolet region, may provide a more accurate analysis of R, since signal from tryptophan is resonance-enhanced and there is no overlap from other bands, such as the C-H bend around 1340 cm^{-1}, seen with 488 nm excitation. There remains a strong relationship between relative intensity and hydrophobicity.

A tyrosine Y19b mode (~1340cm^{-1}) appears under the tryptophan Fermi resonance of the W7 mode (~1340 and 1361 cm^{-1}). In order to remove contribution from tyrosine in this region OmpA W0 was subtracted from each of

the mutants to obtain tryptophan only spectra (Figure 4.8). The subtracted spectra of OmpA wild-type and all the mutants can be seen in the appendix (Figures 5.7-5.9). The tyrosine Y9a mode, ~1180 cm^{-1}, was used as a guide to subtract the 1180 cm^{-1} region to zero. The 1180 cm^{-1} peak is mostly due to the tyrosine Y9a mode. Phenylalanine has an F9a mode around 1180 cm^{-1} but contributes only ~1/8 or less to this peak and was considered negligible. Therefore, the intensity ratio of 1180 cm^{-1} to 1340 cm^{-1} have the same relative contribution from tyrosine, making the subtraction of the 1180 cm^{-1} peak a good indicator for removal of tyrosine contribution at ~1340 cm^{-1}. After tryptophan-only spectra were obtained, decomposition into Gaussians, centered at 1340 cm^{-1} and 1361 cm^{-1}, were calculated. These peak positions were fixed at a width of 20 cm^{-1}. Decomposition of OmpA in KP_i, SUV, and OG are seen in Figures 4.9, 4.10 and 4.11. Amplitudes of the two Gaussian peaks are given in Table 4.3 with the relative ratio of I_{1361}/I_{1340}.

With R values of 1.9 and 1.8 for W7 and W102 in SUVs, respectively, and 1.8 and 2.5 in OG, W7 and W102 are in the most hydrophobic areas relative to the other full-length mutants. W7t and W102t in SUVs also show the greatest hydrophobicity, with ratios of 1.4 and 1.2. In OG W102t and W143t are the most hydrophobic with values of 2.1 and 2.4. However, W7t follows W102t with an R of1.9. In general, residues 7 and 102 are folded in the most hydrophobic regions. It is likely that residue 102 sits in a hydrophobic pocket inside the β-barrel.

In SUVs, R values of 1.0, 1.3 and 1.7 were found for W15, W57, and W143, while the values in OG are 1.3, 1.3, and 1.1. R values of 1.0, 1.1 and 1.1

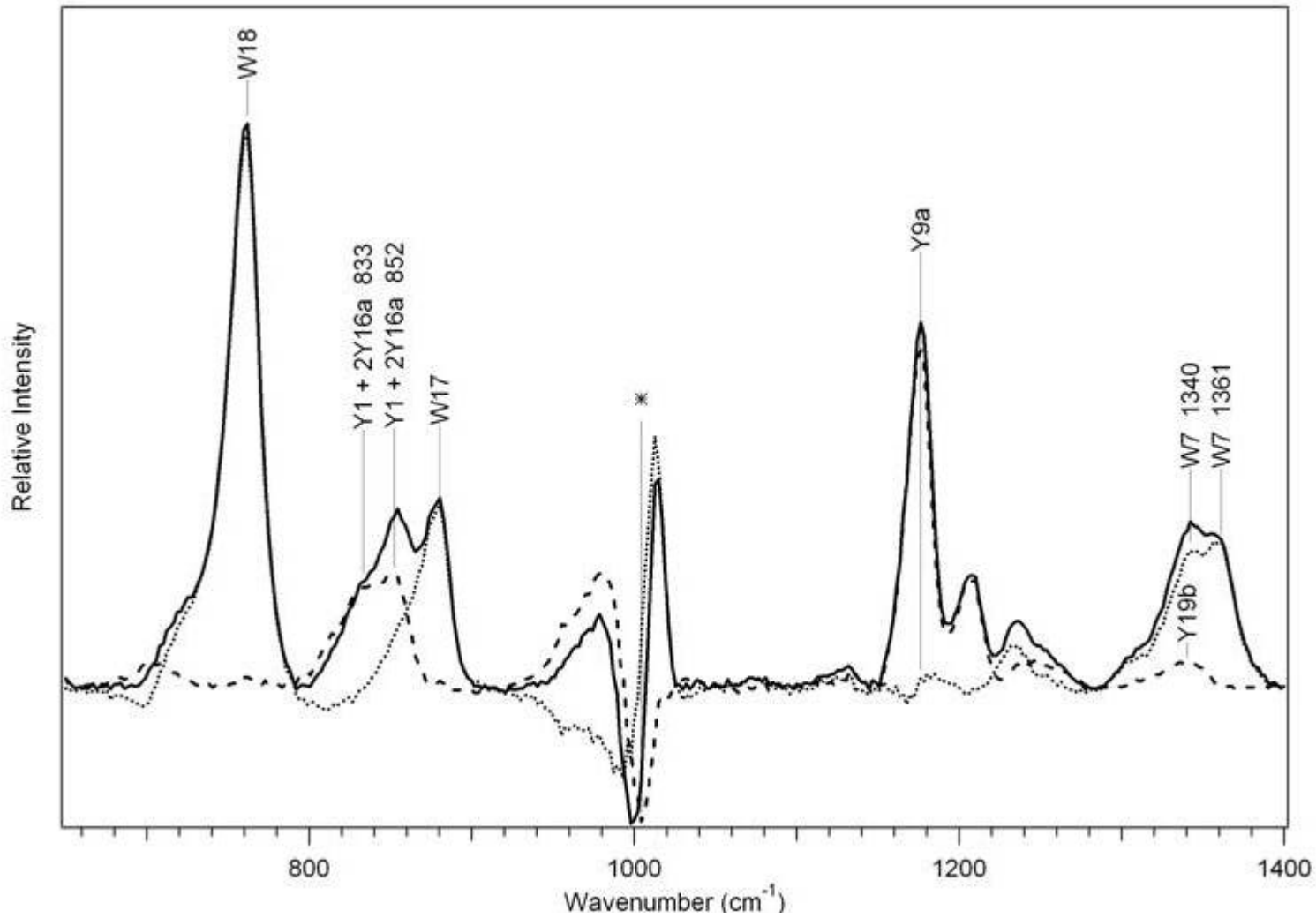

Figure 4.8. Subtraction of tyrosine mode Y19b seen in W0 (dashed) from wild-type (solid) to produce a tryptophan only spectrum (dotted) in the 1340-1361 cm^{-1} region. Tryptophan modes W18, W17, and W7 persist after subtraction of the tyrosine combination mode Y1 + 2Y16a, Y9a mode, and Y19b mode.

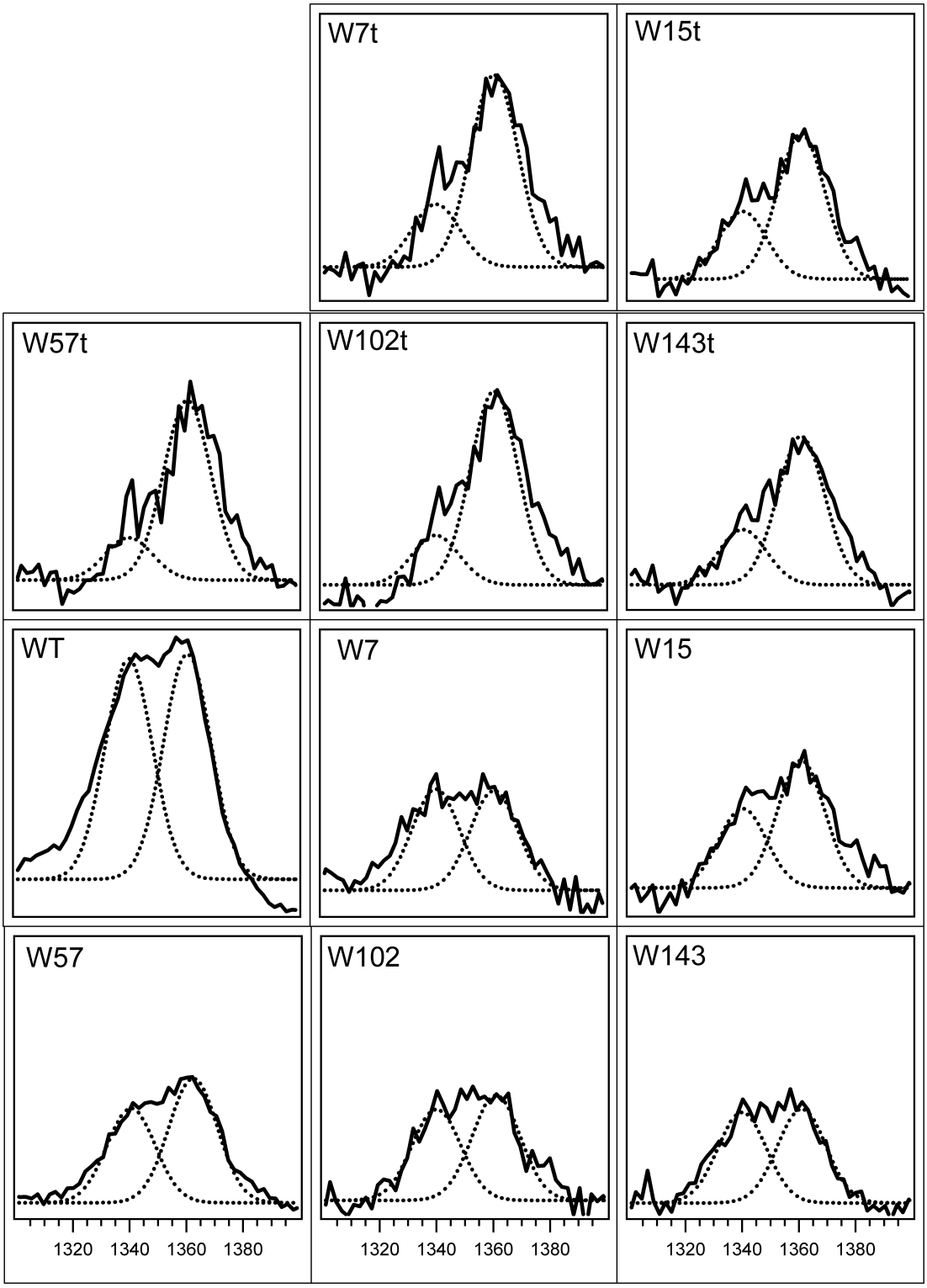

Figure 4.9. UVRR spectra of OmpA wild-type and single-trp mutants unfolded in KP_i (solid) showing relative intensities of the 1340 cm^{-1} and 1361 cm^{-1} peak with Gaussian decompositions of the W7 mode Fermi doublet (dotted). The x-axis is wavenumber (cm^{-1}) and the y-axis is relative intensity.

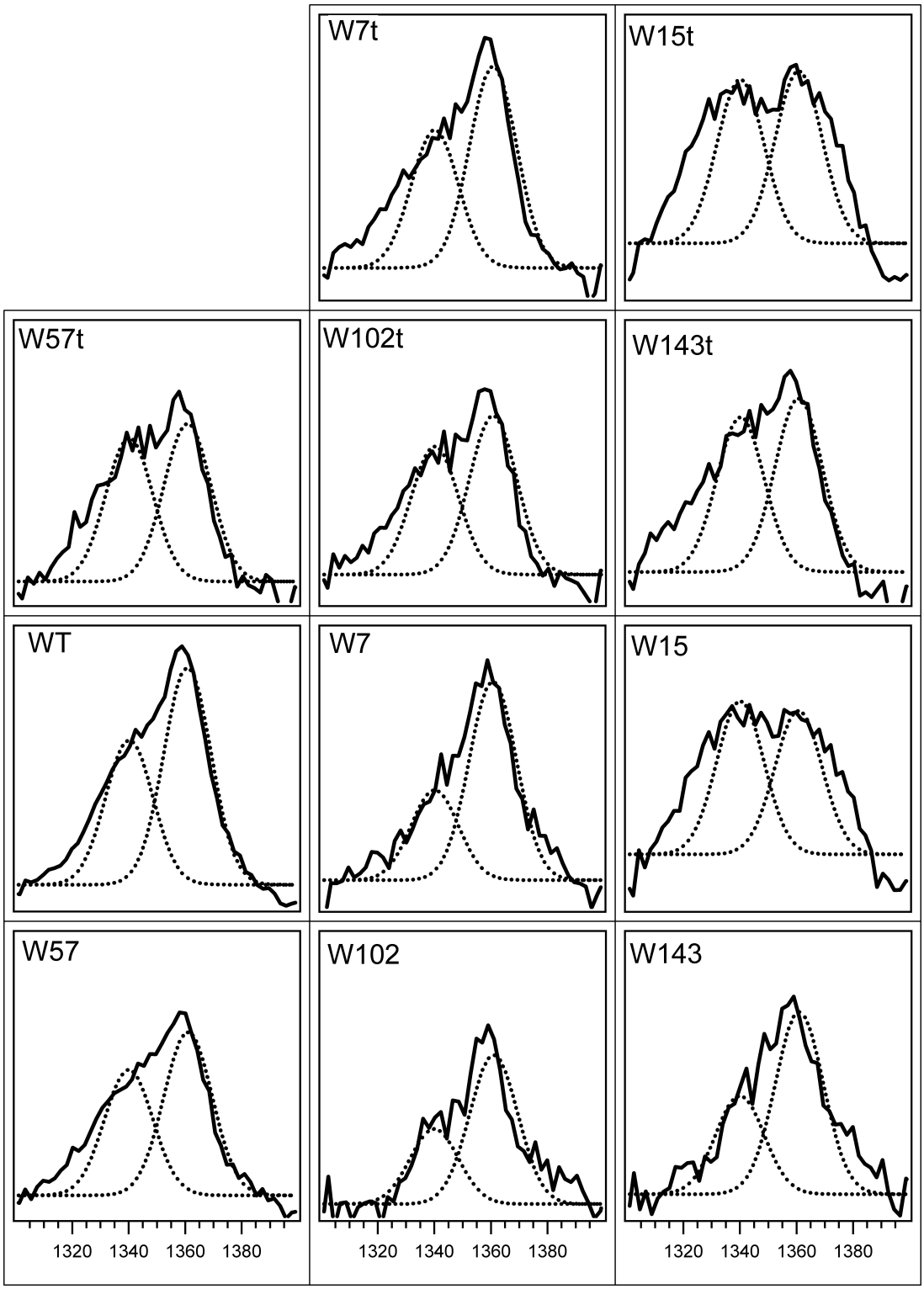

Figure 4.10. UVRR spectra of OmpA wild-type and single-trp mutants folded in SUVs (solid), showing relative intensities of the 1340 cm^{-1} and 1361 cm^{-1} peaks with Gaussian decompositions of the W7 mode Fermi doublet (dotted).The x-axis is wavenumber (cm^{-1}) and the y-axis is relative intensity.

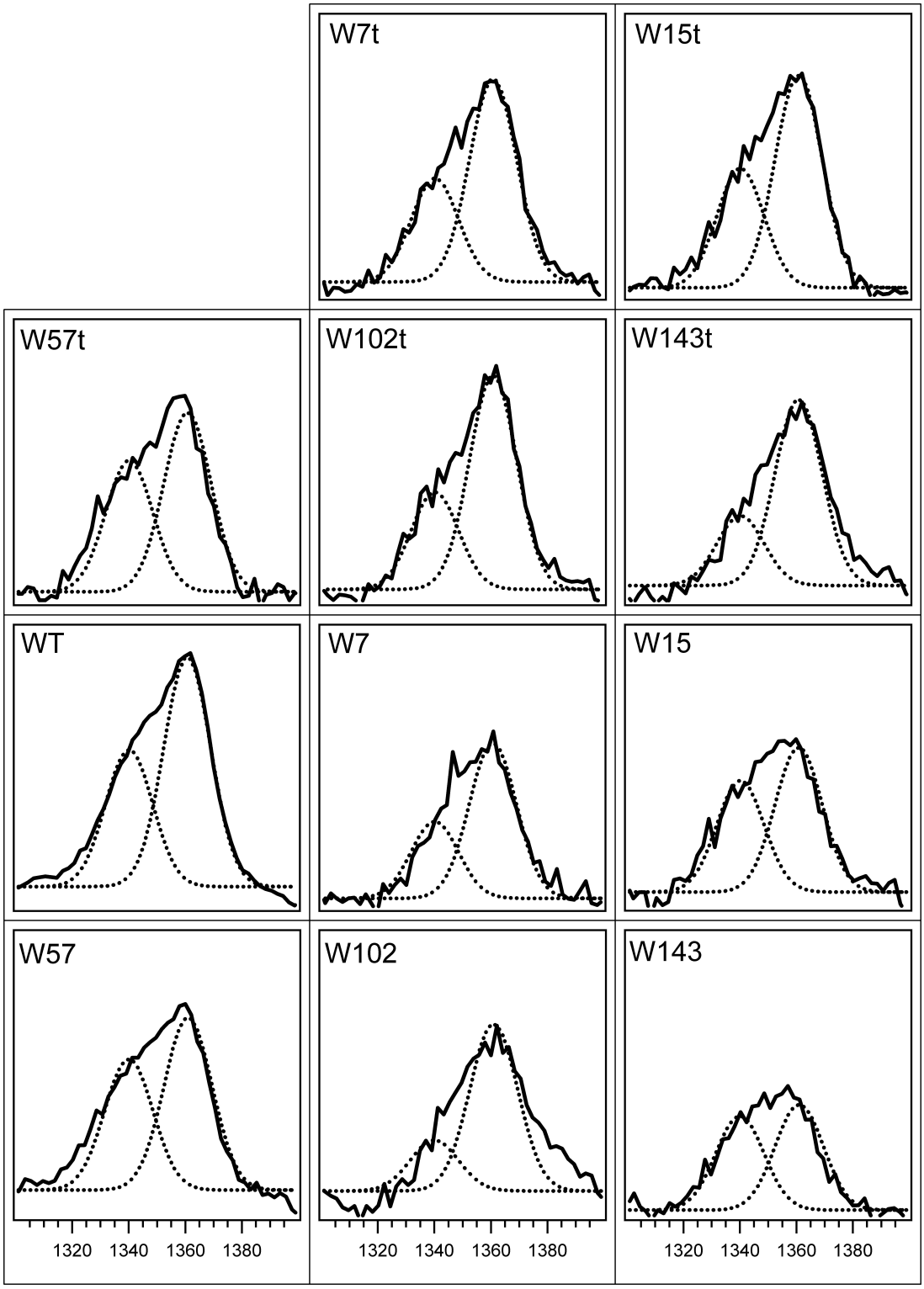

Figure 4.11. UVRR spectra of OmpA wild-type and single-trp mutants folded in OG (solid), showing relative intensities of the 1340 cm^{-1} and 1361 cm^{-1} peaks with Gaussian decompositions of the W7 mode Fermi doublet (dotted). The x-axis is wavenumber (cm^{-1}) and the y-axis is relative intensity.

Table 4.3. Intensity values from the Gaussian decompositions of the W7 Fermi doublet for OmpA wild-type and mutants with the relative intensity ration I_{1361}/I_{1340} in KP_i, SUVs, and OG.

	KP_i			**SUVs**			**OG**		
Protein	Intensity 1361 cm^{-1}	Intensity 1340 cm^{-1}	**R (I_{1361}/I_{1340})**	Intensity 1361 cm^{-1}	Intensity 1340 cm^{-1}	**R (I_{1361}/I_{1340})**	Intensity 1361 cm^{-1}	Intensity 1340 cm^{-1}	**R (I_{1361}/I_{1340})**
W7	0.044	.044	**1.0**	0.081	0.042	**1.9**	0.056	0.031	**1.8**
W15	0.054	0.037	**1.5**	0.071	0.074	**1.0**	0.060	0.045	**1.3**
W57	0.120	0.090	**1.3**	0.014	0.011	**1.3**	0.160	0.127	**1.3**
W102	0.044	0.038	**1.1**	0.057	0.031	**1.8**	0.068	0.027	**2.5**
W143	0.038	0.037	**1.0**	0.073	0.043	**1.7**	0.040	0.035	**1.1**
WT	0.027	0.026	**1.0**	0.310	0.210	**1.5**	0.310	0.200	**1.6**
W7t	0.079	0.033	**2.4**	0.099	0.072	**1.4**	0.078	0.042	**1.9**
W15t	0058	0.031	**1.9**	0.081	0.078	**1.0**	0.079	0.045	**1.8**
W57t	0.073	0.024	**3.0**	0.064	0.059	**1.1**	0.068	0.050	**1.4**
W102t	0.077	0.025	**3.1**	0.067	0.056	**1.2**	0.081	0.039	**2.1**
W143t	0.061	0.026	**2.3**	0.073	0.066	**1.1**	0.073	0.031	**2.4**

were determined for W15t, W57t, and W143t in SUVs. In OG, the values were 1.8, 1.4, and 2.4. Residues 15 and 57 have similar R values in both SUV and OG. W143 in OG and W143t in SUVs remain in a similar environment to its horizontal neighbor residues 15 and 57 but W143 in SUVs and W143t in OG are exceptions and do not agree. The high value of W143 in SUVs is surprising but agrees with the unusually high value of the truncated version of W143t in OG.

The ratios given in SUVs show the most consistent data sets between the full-length and truncated mutants. The greatest hydrophobic environment is seen in tryptophan residue 7. The following scale shows the greatest to least hydrophobicity based on the R values in SUVs: W7 > W102 > W143 > W57 > W15 and W7t > W102t > W143t> W57t> W15t. This consistency of hydrophobicity between the full-length and truncated mutants shown above is not seen to the same degree in the OG data. The scale of hydrophobicity of the OmpA mutants obtained in OG is: W102 > W7 > W15 = W57 >W143 for the full-length mutants and W143t > W102t > W7t > W15t > W57t for the truncated mutants. There is an overall consistently in the hydrophobicity between the full-length and truncated mutants in OG, except W143 is shown as being the least hydrophobic and W143t being the most hydrophobic. If the hydrophobicity can be related to adopting a particular folded conformation then this data suggests there may be slightly different folded structures between W143 and W143t in OG. Not only is it possible that the truncated mutants fold somewhat differently from the full-length mutants due to the difference in hydrophobicity values but perhaps the mutants also fold differently in OG versus SUVs, as witnessed by the differences

in the hydrophobicity values and scale.

The R values for wild-type in SUVs and OG are 1.5 and 1.6. These values are similar to each other and suggest overall similarities in hydrophobicity of the two folded structures in SUVs and OG. It is interesting to point out, the average R value of the full-length single-trp mutants is 1.5 in SUVs and is 1.6 in OG, which are the exact R values given for wild-type. The R values of wild-type parallel the average R values of the single-trp mutants suggesting that wild-type shows hydrophobic contributions from each of the single-trp mutants.

In KP_i, the mutants display a wide range of R values, attributed to the lack of well-defined structure in KP_i. However, the full-length mutants in KP_i have much lower R values than when folded in SUVs or OG. This is consistent with a picture of lower hydrophobicity in aqueous solutions.

In contrast, the truncated mutants in KP_i appear to do something very intriguing. The R values of the truncated mutants approximately double or triple the values obtained for the full-length mutants. The values are much larger than the values for any of the OmpA mutants folded in SUVs and OG. This suggests that when the periplasmic tail is cleaved the tryptophan residues are in a highly hydrophobic region, implying strong hydrophobic collapse of this transmembrane domain. This difference could open the door to new and exciting unfolded structures.

An additional method for viewing hydrophobicity is steady-state fluorescence spectroscopy. This technique is utilized to monitor tryptophan emission of folded and unfolded states of OmpA, described in chapter 1.

Tryptophan in a hydrophobic environment shows a maximum wavelength (λ_{max}) of ~330 nm, while tryptophan emission in a hydrophilic environment exhibits a red shifted maximum of ~355 nm. Table 4.4 compares the maximum tryptophan emission of OmpA wild-type and single-trp mutants to the relative intensity (R).

Table 4.4. Comparison of hydrophobic environments between the relative intensity (R) obtained from UVRR and fluorescence emission maximum (λ_{max}).

	KP_i		SUVs		OG	
Protein	**λ_{max} (nm)**	**R (I_{1361}/I_{1340})**	**λ_{max} (nm)**	**R (I_{1361}/I_{1340})**	**λ_{max} (nm)**	**R (I_{1361}/I_{1340})**
W7	354	1.0	323	1.9	337	1.8
W15	353	1.5	331	1.0	335	1.3
W57	353	1.3	333	1.3	339	1.3
W102	354	1.1	332	1.8	337	2.5
W143	354	1.0	332	1.7	337	1.1
WT	355	1.0	334	1.5	336	1.6
W7t	353	2.4	328	1.4	335	1.9
W15t	354	1.9	331	1.0	332	1.8
W57t	353	3.0	332	1.1	335	1.4
W102t	353	3.1	330	1.2	335	2.1
W143t	353	2.3	332	1.1	334	2.4

The values of the tryptophan emission maximum and the relative intensity of the 1361 cm^{-1} peak to the 1340 cm^{-1} peak show no obvious correlation. While there is no agreement of hydrophobicity between the values of the emission maximum and R value, there does appear to be an agreement in the overall trend. Based on the emission values the hydrophobicity scale for the full-length mutants in KP_i is: W15 = W57 > W102 = W7 = W143. The hydrophobicity scale

based on R values is: W15 > W57 > W102 > W7 =W143. The truncated mutants in KP_i based on emission maximum are: W102t = W57t = W7t = W143t > W15t and based on R value is: W102t > W57t > W7t > W143t > W15t. In SUVs the following hydrophobicity scale is given for emission maximum and R value for the full-length and truncated mutants: W7 > W15> W102 = W143 > W57, W7 > W102 > W143 > W57 > W15, W7t > W102t > W15t > W57t = W143t, and W7t > W102t > W57t = W143t > W15t. Overall the hydrophobicity of the mutants in KP_i and SUVs agrees between the fluorescence and UVRR data, with the exception of W15 and W15t in SUVs. The hydrophobicity between the tryptophan emission maximum and R value of mutants in OG, however, shows no general overall agreeable trend.

4.4 The W3 Mode

The W3 mode reflects the absolute torsion angle, $|\chi^{2,1}|$, about the C2-C3-Cβ-Cα linkage (Figure 4.12). As the Cα and C2 atoms move away from each other the angle of $|\chi^{2,1}|$ increases and the frequency decreases.[5] Gaussian fits of the W3 mode in KP_i, SUVs, and OG for wild-type and mutants are shown in Figures 4.13, 4.14, 4.15, and the results are given in Table 4.5 . Both width and frequency were varied, where 82% of the widths fell between 18 and 22 cm^{-1}. The angles obtained from the Raman spectra are compared to the angles given from the crystal structure for the truncated mutants, since the crystal structure was obtained using the truncated version of OmpA (Table 4.6).

A range of 88°-100°, for the angles calculated are consistent with the range of values in the crystal structure from 83°-102°, except tryptophan 15. The

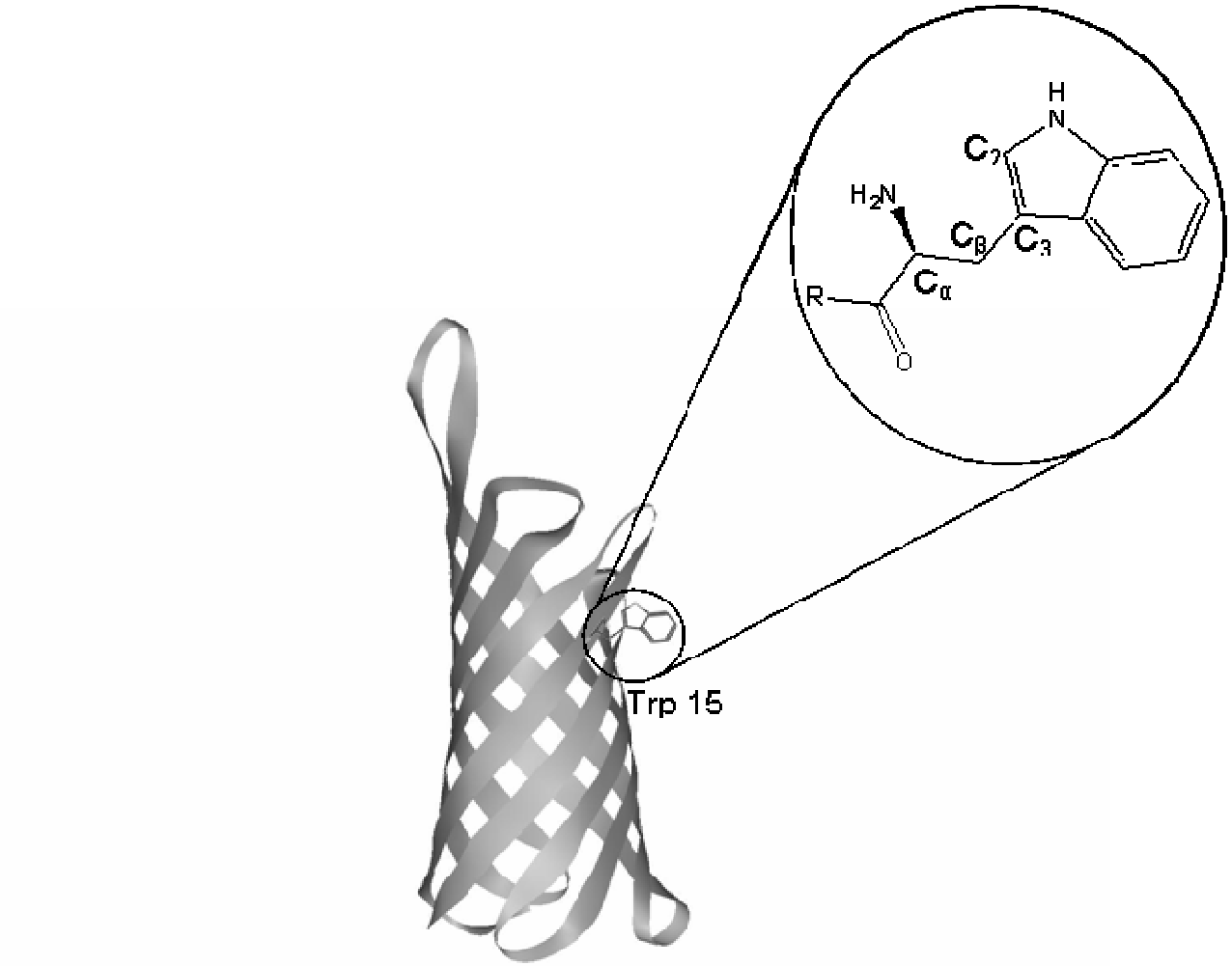

Figure 4.12. Crystal structure of the transmembrane domain of OmpA, showing tryptophan residue15.Periplasmic tail not shown. An expanded region is shown with the dihedral angle .C2-C3-Cβ-Cα. PDB file 1QJP.

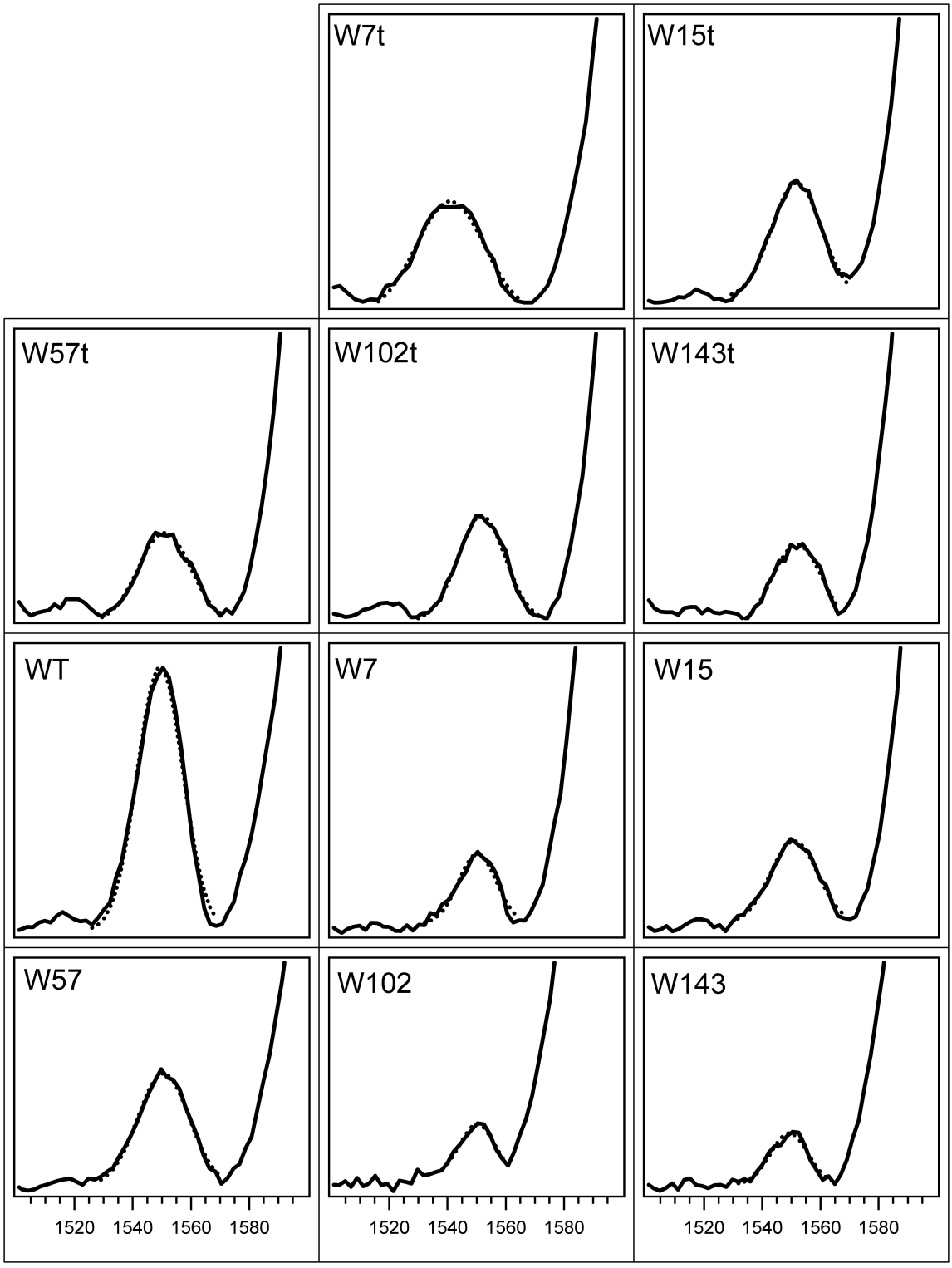

Figure 4.13. UVRR spectra of OmpA wild-type and single-trp mutants unfolded in KP_i (solid), showing ~1550 cm^{-1} peak with Gaussian fit of the W3 mode (dotted). The x-axis is wavenumber (cm^{-1}) and the y-axis is relative intensity.

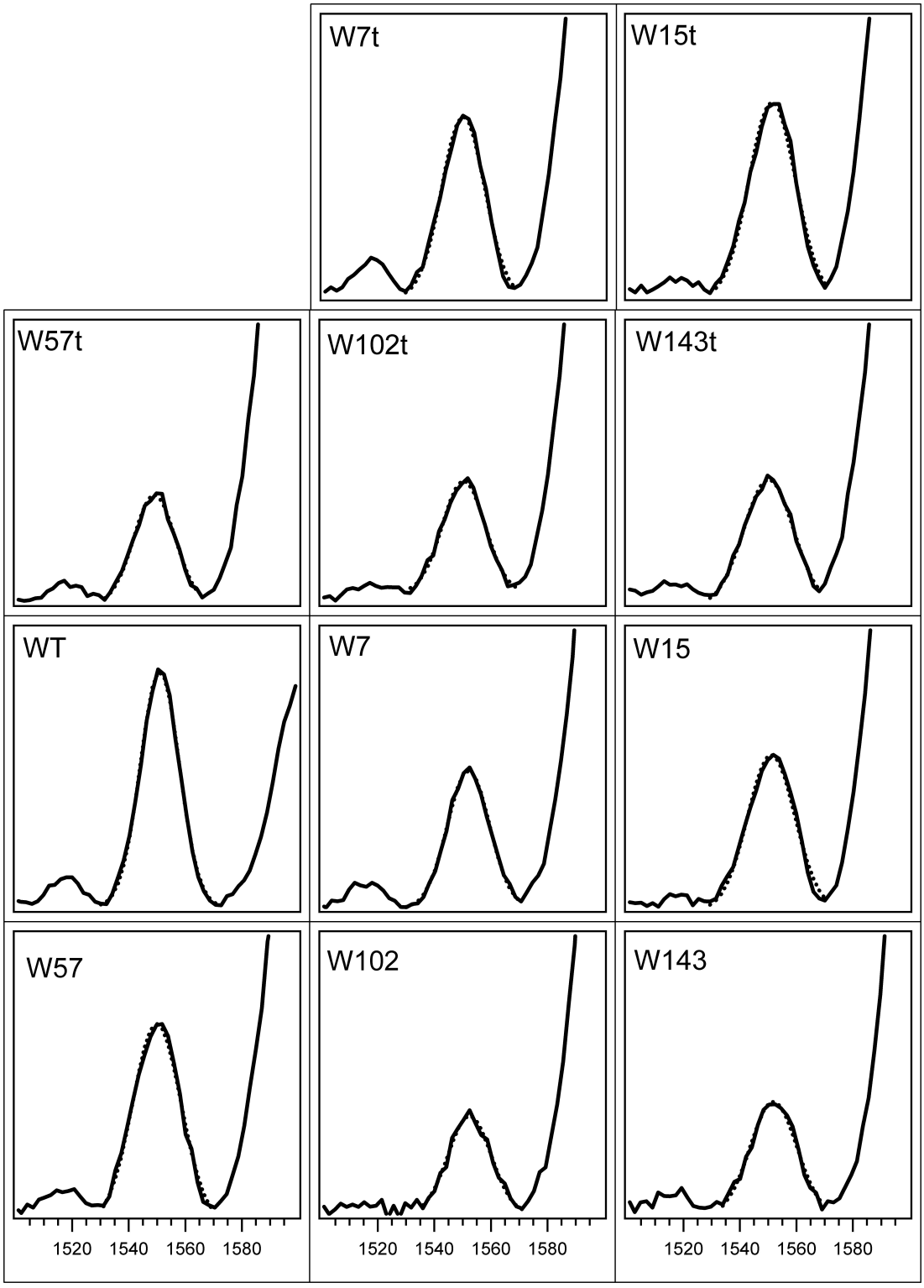

Figure 4.14. UVRR spectra of OmpA wild-type and single-trp mutants folded in SUVs (solid), showing ~1550 cm^{-1} peak with Gaussian fits of the W3 mode (dotted). The x-axis is wavenumber (cm^{-1}) and the y-axis is relative intensity.

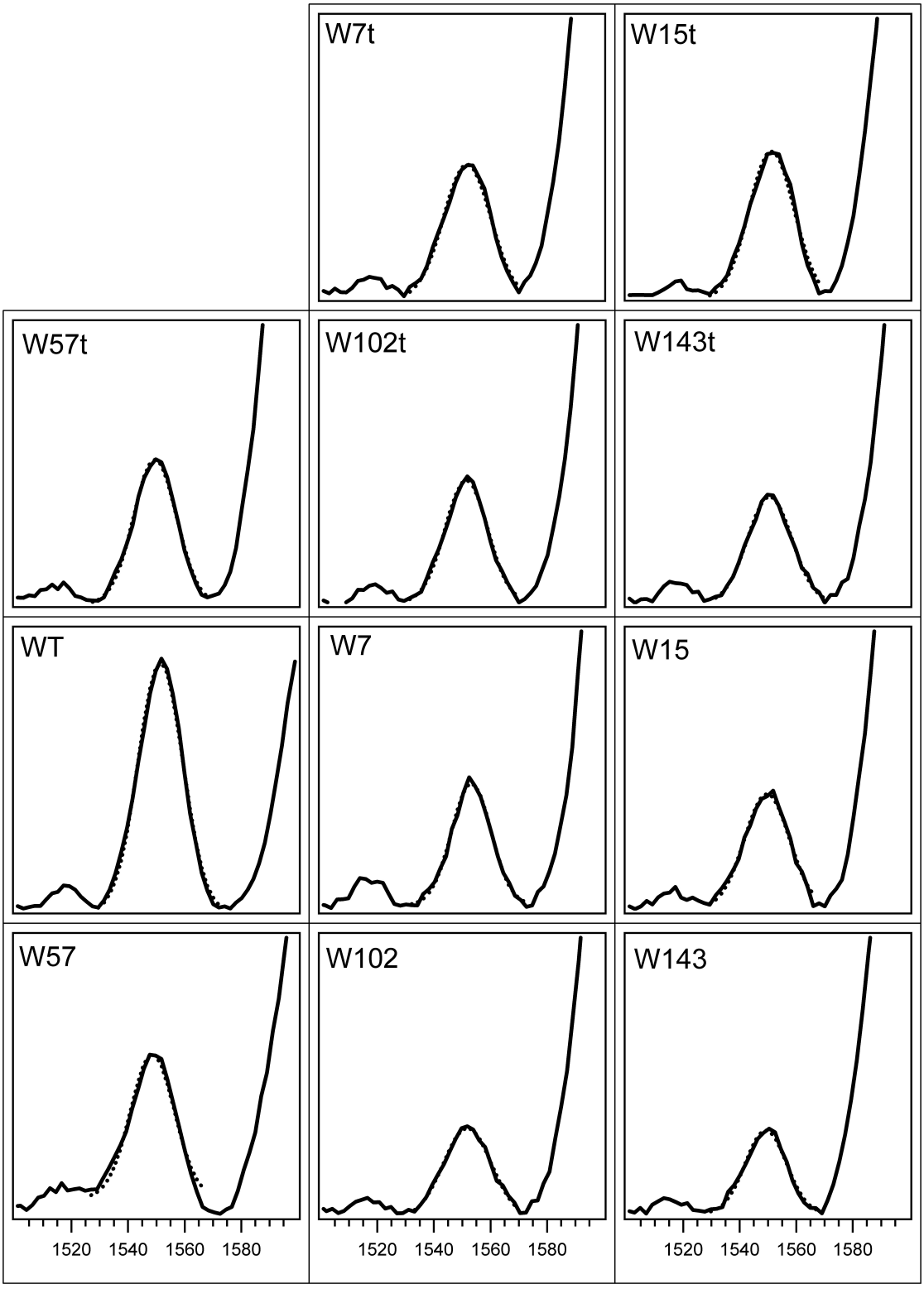

Figure 4.15. UVRR spectra of OmpA wild-type and single-trp mutants folded in OG (solid), showing ~1550 cm^{-1} peak with Gaussian fits of the W3 mode (dotted). The x-axis is wavenumber (cm^{-1}) and the y-axis is relative intensity.

Table 4.5. Gaussian fit of peak centers and widths of OmpA wild-type and mutants for the W3 mode. The calculated $|\chi^{2,1}|$ dihedral angle is given.

	KP_i			SUVs			OG		
Protein	Peak Center (cm^{-1})	Width (cm^{-1})	**Angle (°)**	Peak Center (cm^{-1})	Width (cm^{-1})	**Angle (°)**	Peak Center (cm^{-1})	Width (cm^{-1})	**Angle (°)**
W7	1550	15	**93**	1552	18	**99**	1553	17	**100**
W15	1551	20	**95**	1551	20	**95**	1550	19	**93**
W57	1551	21	**95**	1550	20	**93**	1549	18	**88**
W102	1550	14	**93**	1552	18	**99**	1552	20	**99**
W143	1549	15	**88**	1552	19	**99**	1549	17	**88**
WT	1549	19	**88**	1551	16	**95**	1552	19	**99**
W7t	1553	22	**100**	1550	18	**93**	1551	19	**95**
W15t	1552	21	**99**	1551	20	**95**	1552	18	**99**
W57t	1551	21	**95**	1549	18	**88**	1550	18	**93**
W102t	1552	19	**99**	1550	18	**93**	1551	19	**95**
W143t	1552	21	**99**	1550	21	**93**	1552	20	**99**

Table 4.6. Angles of folded OmpA mutants in SUVs and OG compared to angle given in the crystal structure. The crystal structure is of the truncated OmpA and therefore there are no angles for the full-length mutants. The angle of OmpA in KP_i is compared to the angles of the folded mutants and in parenthesis is denoted with an increase in angle (i), a decrease in angle (d), or the same angle (s) to the angle of unfolded OmpA mutants in KP_i.

Protein	Angle (°) in SUVs	Angle (°) in OG	Angle (°) in Crystal Structure
W7	99 (i)	100(i)	-
W15	95 (s)	93(d)	-
W57	93 (d)	88(d)	-
W102	99 (i)	99(s)	-
W143	99 (i)	88(s)	-
W7t	93 (d)	95(d)	93
W15t	95(d)	99(s)	45
W57t	88(d)	93(d)	93
W102t	93(d)	95(d)	93
W143t	93(d)	99(sw)	102

crystal structure shows a 45° angle for tryptophan 15 compared to the angle given by the Raman spectra of 95°-99° folded in SUVs and OG.

The angles between the mutants folded in SUVs and OG are different. These variations in angle between SUVs and OG illustrate a slight difference in the folded structures of the OmpA mutants in SUVs or OG. The difference in angles between the truncated and full-length mutants may provide evidence that there is slightly different folding between truncated and full-length mutants where the cleaving of the periplasmic tail does affect the folded structure.

The crystal structure gives values of 93°, 93°, and 102° for W57t, 102t and W143t. The angles in SUVs and OG are 88° and 93° for W57t, 93° and 95° for W102t, and 93° and 99° for W143t. These values are in close agreement with the crystal structure. However, the angles of W7t and W15t in SUVs and OG are different than the crystal structure. The crystal structure of W7t gives an angle of 83°, while the angle in SUVs is 93° and 95° in OG. The angle of W7t could reflect the difference in micelle used in the crystal structure (n-octyltetraoxyethylene) compared to SUVs and OG. W15t has angles of 95° and 99° in OG and SUVs, compared to 45°, given by the crystal structure. This could also be attributed to the difference in structure of the micelle used for crystallization or the difference between the crystal structure versus the structure in solution. Consideration of the W17 mode supports different structures for the crystal and solution forms of OmpA. Specifically, the crystal structure indicates a 45° angle as well as hydrogen bonding of the indole N_1-H to asparagine 33, Figure 4.16. Here we observe a 95-99° degree angle in solution and evidence for

minimal to no hydrogen bonding. It is possible that the 95-99° in solution prevents formation of a hydrogen bond. Since the UVRR data provides the absolute $|\chi^{2,1}|$ angle there are two possible configurations of W15t in SUVs, +95° and -95°. Figures 4.17 and 4.18 show how the distance between the W15t heteroatom to the carbonyl of N33t changes with the two possible $\chi^{2,1}$ angles. Both the 95° and -95° representations of W15t in SUVs show an increase in distance between W15t and N33t. This change in angle from the crystal structure supports a decrease in the possible hydrogen bonding of the N_1H site of W15t to the carbonyl of N33t, where a hydrogen bond seems unlikely.

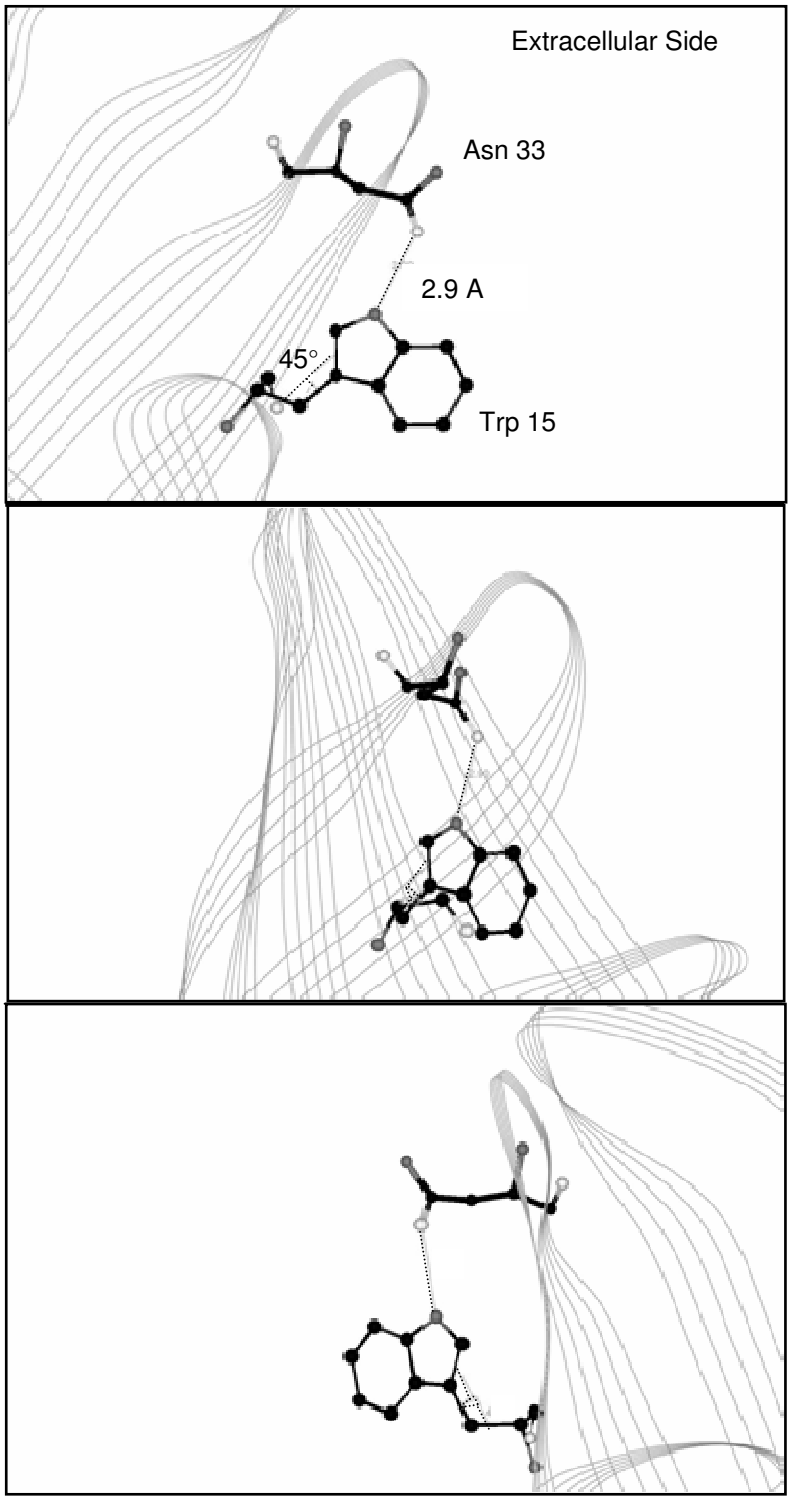

Figure 4.16. Various views of OmpA showing W15 with an angle of 45° about the C2-C3-Cβ-Cα linkage and a possible hydrogen bond between the heteroatom of W15 and the carbonyl of N33 of 2.9 A. PDB file 1QJP.

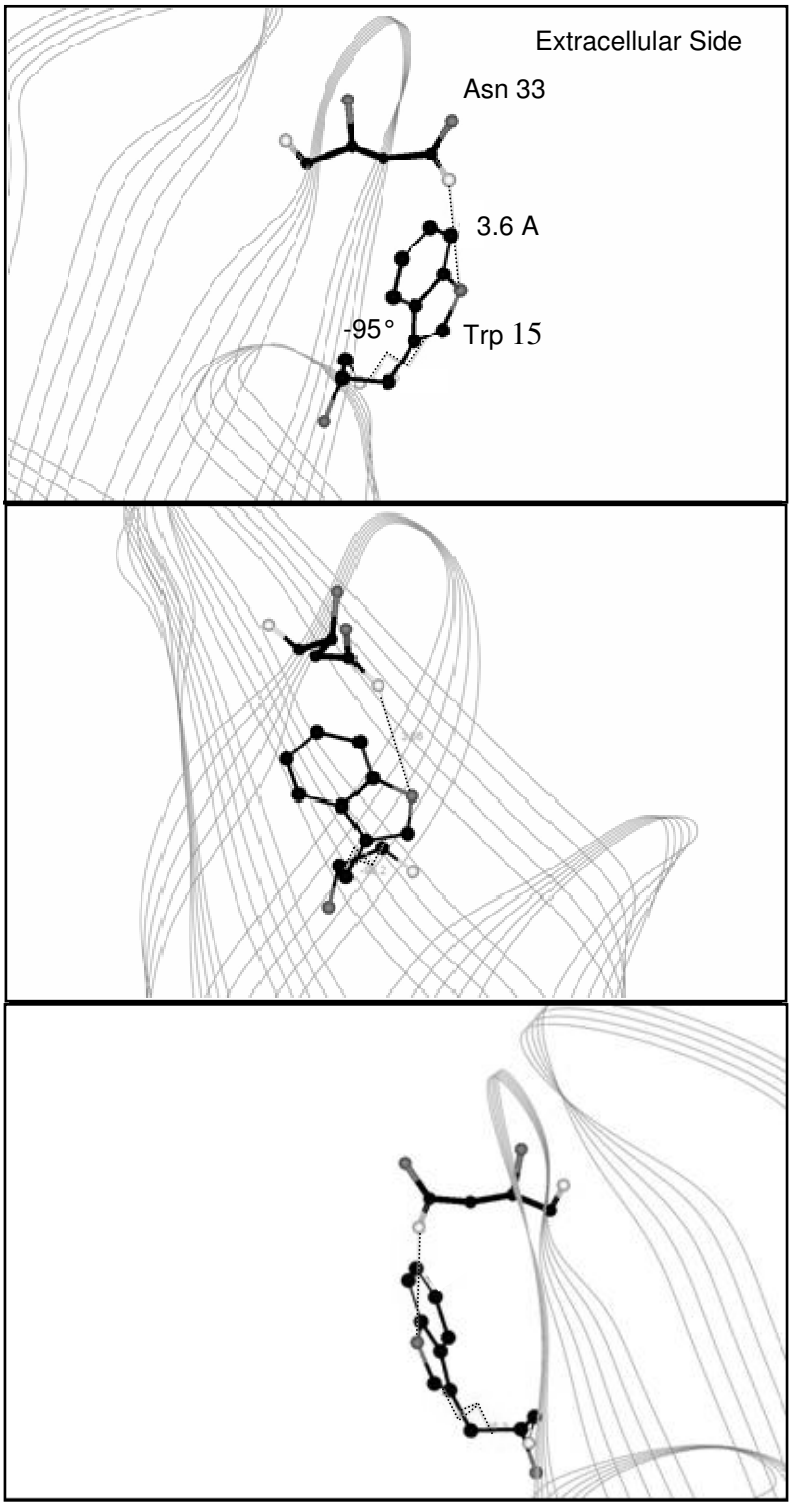

Figure 4.17. Various views of OmpA showing W15 with an angle of -95° about the C2-C3-Cβ-Cα linkage and a possible hydrogen bond between the heteroatom of W15 and the carbonyl of N33 of 3.5 A. PDB file 1QJP.

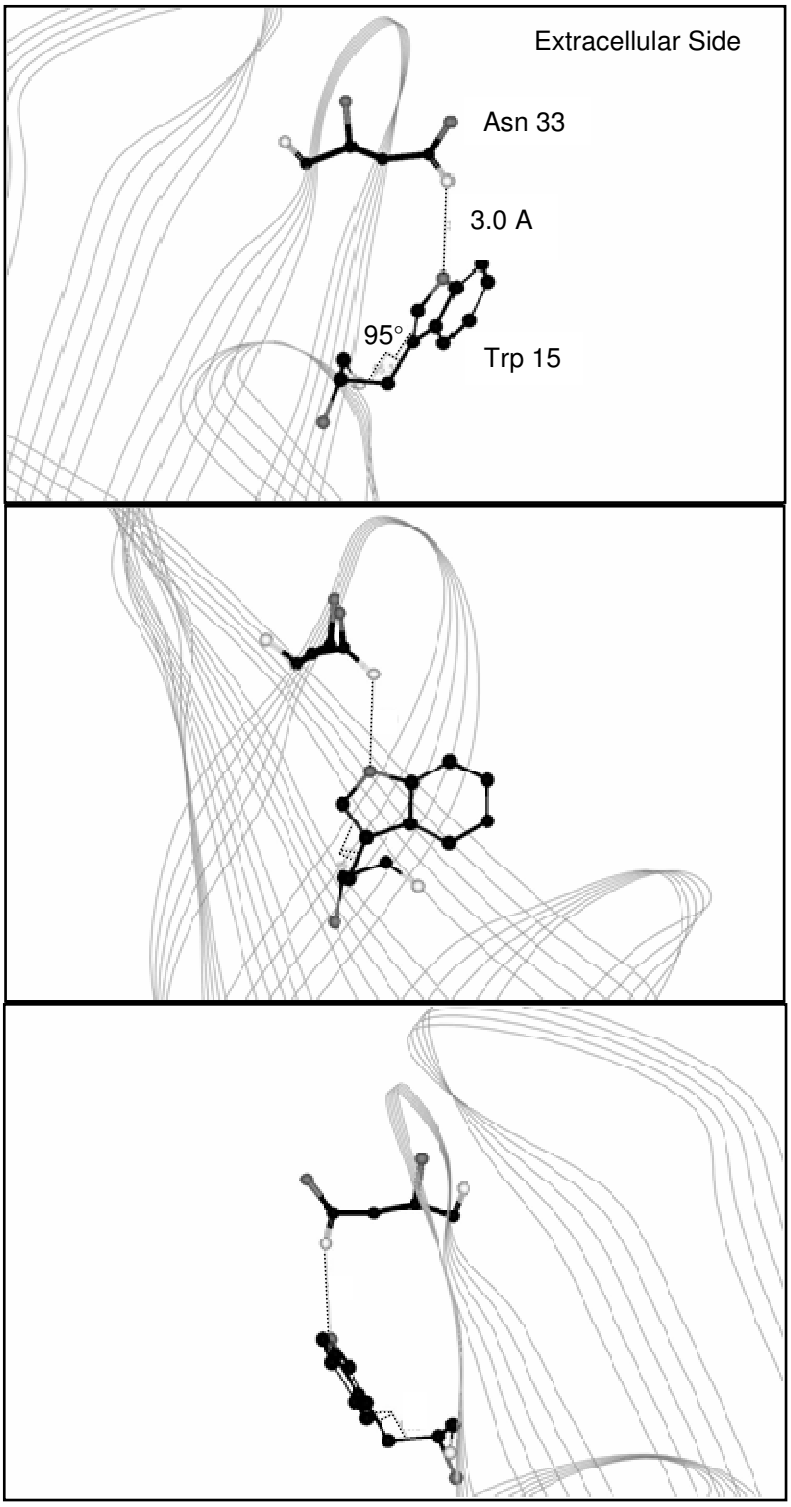

Figure 4.18. Various views of OmpA showing W15 with an angle of +95° about the C2-C3-Cβ-Cα linkage and a possible hydrogen bond between the heteroatom of W15 and the carbonyl of N33 of 3.0 A. PDB file 1QJP.

4.5 Conclusion

The degree of hydrogen bonding is seen by a frequency shift in the W17 band. There may be differences in hydrogen bonding between the crystal structure and the tryptophan side chains in solution, particularly tryptophan 15, which suggests this region does not form a hydrogen bond with any nearby residues. Most of the frequencies appear from 878-880 cm^{-1}, which indicates medium to no hydrogen bonding for the indole site on tryptophan.

The relative intensity ratio (I_{1361}/ I_{1340}), R, of the Fermi doublet of W7 indicates changes in hydrophobicity of the local environment. Hydrophobic interaction with the indole on tryptophan causes the intensity of the ratio to increase. Overall, tryptophan residues 15, 57, and 143 in the full-length and truncated mutants give R values that are within the same degree of hydrophobicity, with the exception of W143 in SUVs and W143t in OG, which show remarkably higher hydrophobicities. Residues 7 and 102 show the most amount of hydrophobic interaction. Residue 102 is likely buried in a hydrophobic pocket in the barrel. The truncated mutants in KP_i are more hydrophobic than any of the folded conformations, suggesting that cleaving the periplasmic tail causes the protein to collapse in solution.

The frequency of the W3 mode changes as the dihedral angle of the C2-C3-Cβ-Cα linkage changes, making it possible to extract the absolute torsion angle, $|\chi^{2,1}|$. The angles found in the OmpA mutants were compared to the crystal structure where it was found that the angle of W15t in the crystal structure (45°) does not match the angles calculated in SUV (95°) and OG (99°). The W17

and W3 modes suggest that hydrogen bond interaction and conformation of W15t is different between the crystal structure and structure folded in SUVs and OG. The angles vary between mutants in SUVs and OG and vary between truncated and full-length mutants suggesting slight variations upon folding in vesicles or detergent and minor folding differences when the periplasmic tail is cleaved.

References

1. H.D. Hong, S. Park, R.H.F. Jimenez, D. Rinehart, and L.K. Tamm. "Role of Aromatic Side Chains in the Folding and Thermodynamic Stability of Integral Membrane Proteins," *J. Am. Chem. Soc.* 129, 26, 8320-8327, 2007.

2. H. Takeuchi, N. Watanabe, Y. Satoh, and I. Harada. "Effects of Hydrogen-Bonding on the Tyrosine Raman Bands in the 1300-1150 cm^{-1} Region," *J. Raman Spectrosc.* 20, 4, 233-237, 1989.

3. J.A. Killian and G. von Heijne. "How Proteins Adapt to a Membrane-water Interface," *Trends Biochem. Sci.* 25, 9, 429-434, 2000.

4. R.G. Efremov, A.V. Feofanov, and I.R. Nabiev. "Effect of Hydrophobic Environment on the Resonance Raman-Spectra of Tryptophan Residues in Proteins," *J. Raman Spectrosc.* 23, 2, 69-73, 1992.

5. T. Miura, H. Takeuchi, and I. Harada. "Tryptophan Raman Bands Sensitive to Hydrogen-Bonding and Side-Chain Conformation," *J. Raman Spectrosc.* 20, 10, 667-671, 1989.

6. T. Miura, H. Takeuchi, and I. Harada. "Characterization of Individual Tryptophan Side-Chains in Proteins using Raman-Spectroscopy and Hydrogen-Deuterium Exchange Kinetics," *Biochemistry (N.Y.)* 27, 1, 88-94, 1988.

7. I. Harada, T. Miura, and H. Takeuchi. "Origin of the Doublet at 1360 and 1340 cm^{-1} in the Raman-Spectra of Tryptophan and Related-Compounds," *Spectrochimica Acta Part A-Molecular and Biomolecular Spectroscopy* 42, 2-3, 307-312, 1986.

8. H. Takeuchi. "Raman Structural Markers of Tryptophan and Histidine Side Chains in Proteins," *Biopolymers* 72, 5, 305-317, 2003.

Appendix

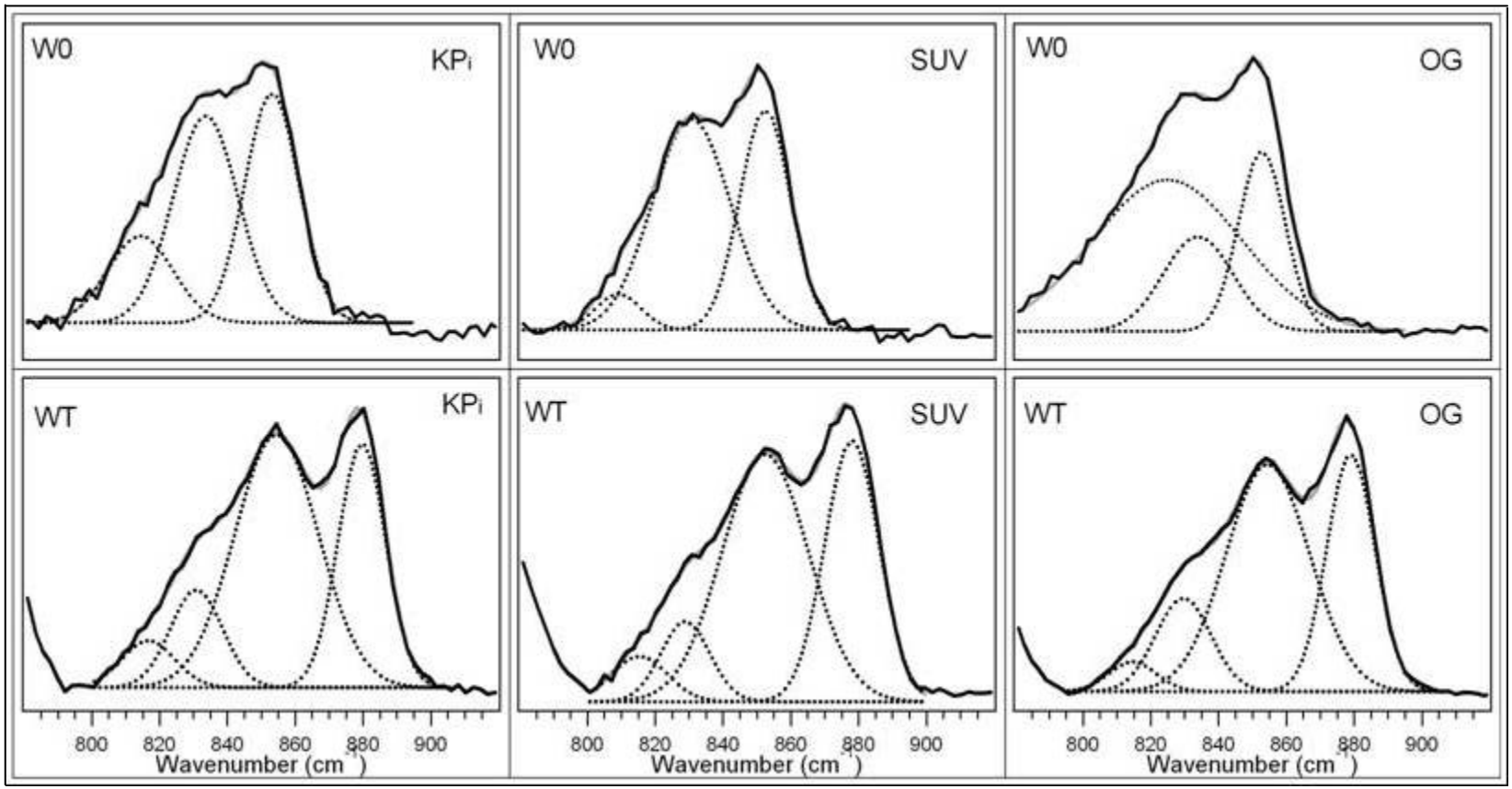

Figure 2. Gaussian decompositions of the 800-900 cm^{-1} region or W0 and WT in KP_i, SUVs, and OG.

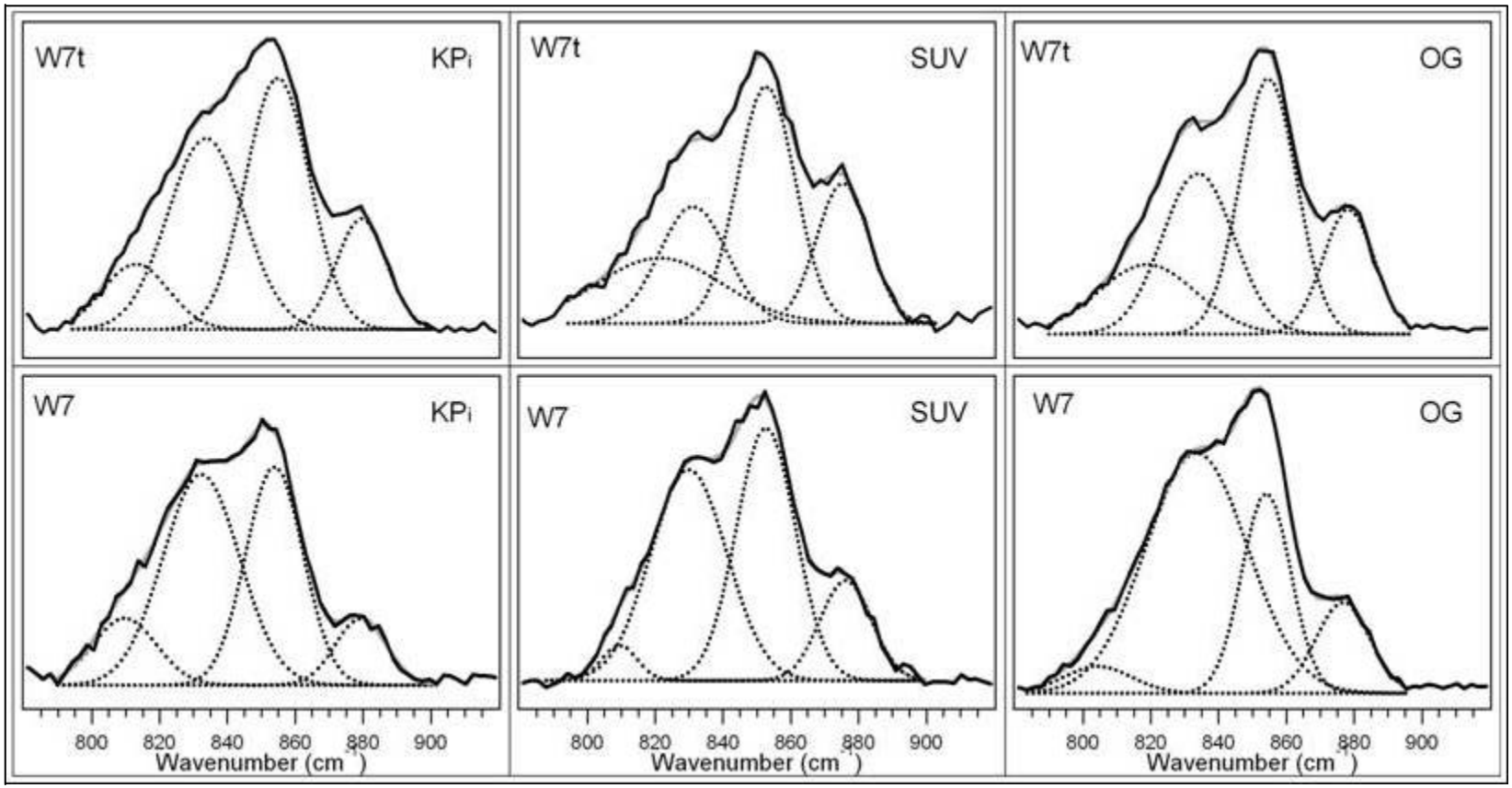

Figure 3. Gaussian decompositions of the 800-900 cm^{-1} region for W7t and W7 in KP_i, SUVs, and OG.

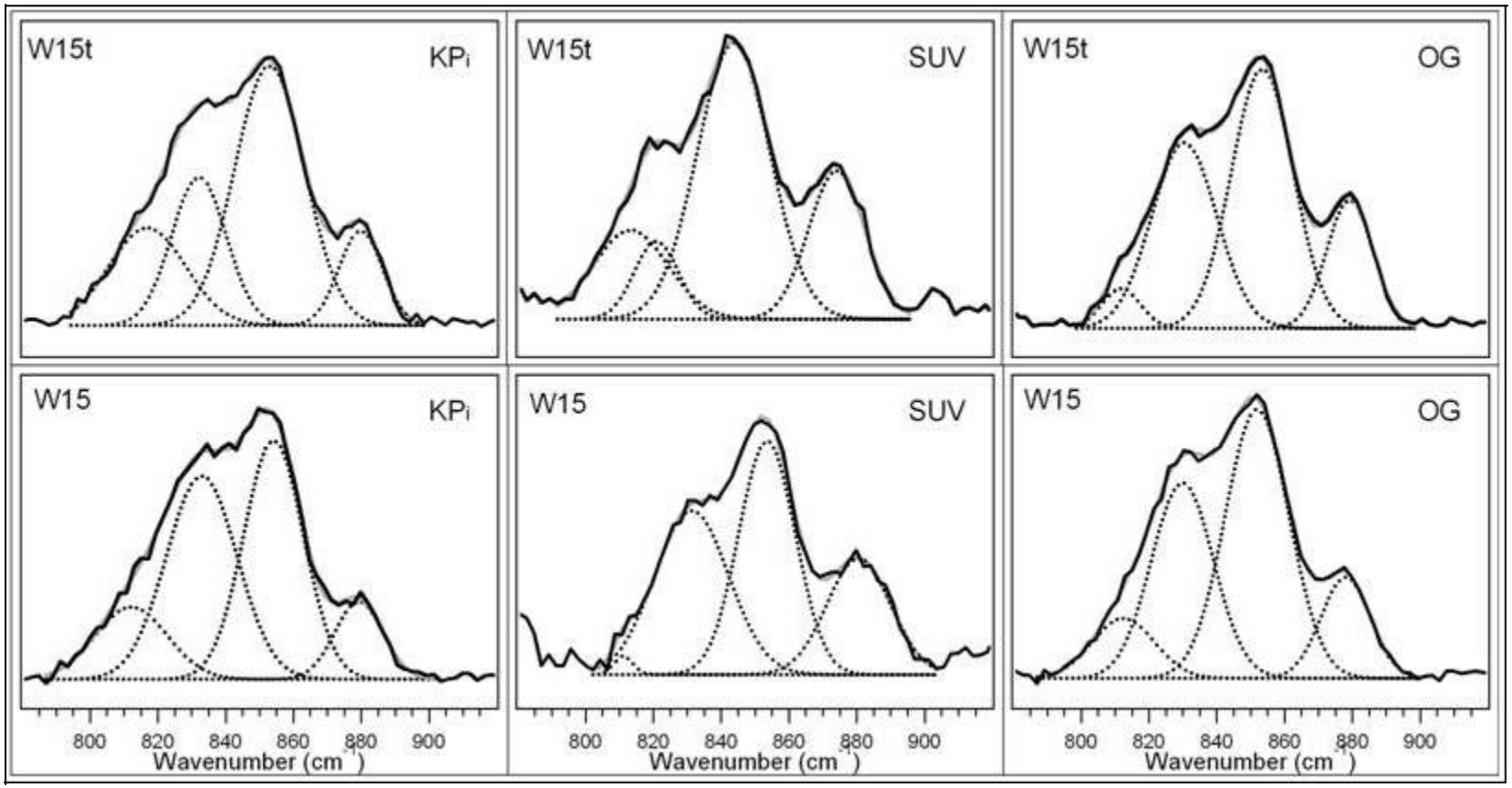

Figure 4. Gaussian decompositions of the 800-900 cm^{-1} region for W15t and W15 in KP_i, SUVs, and OG.

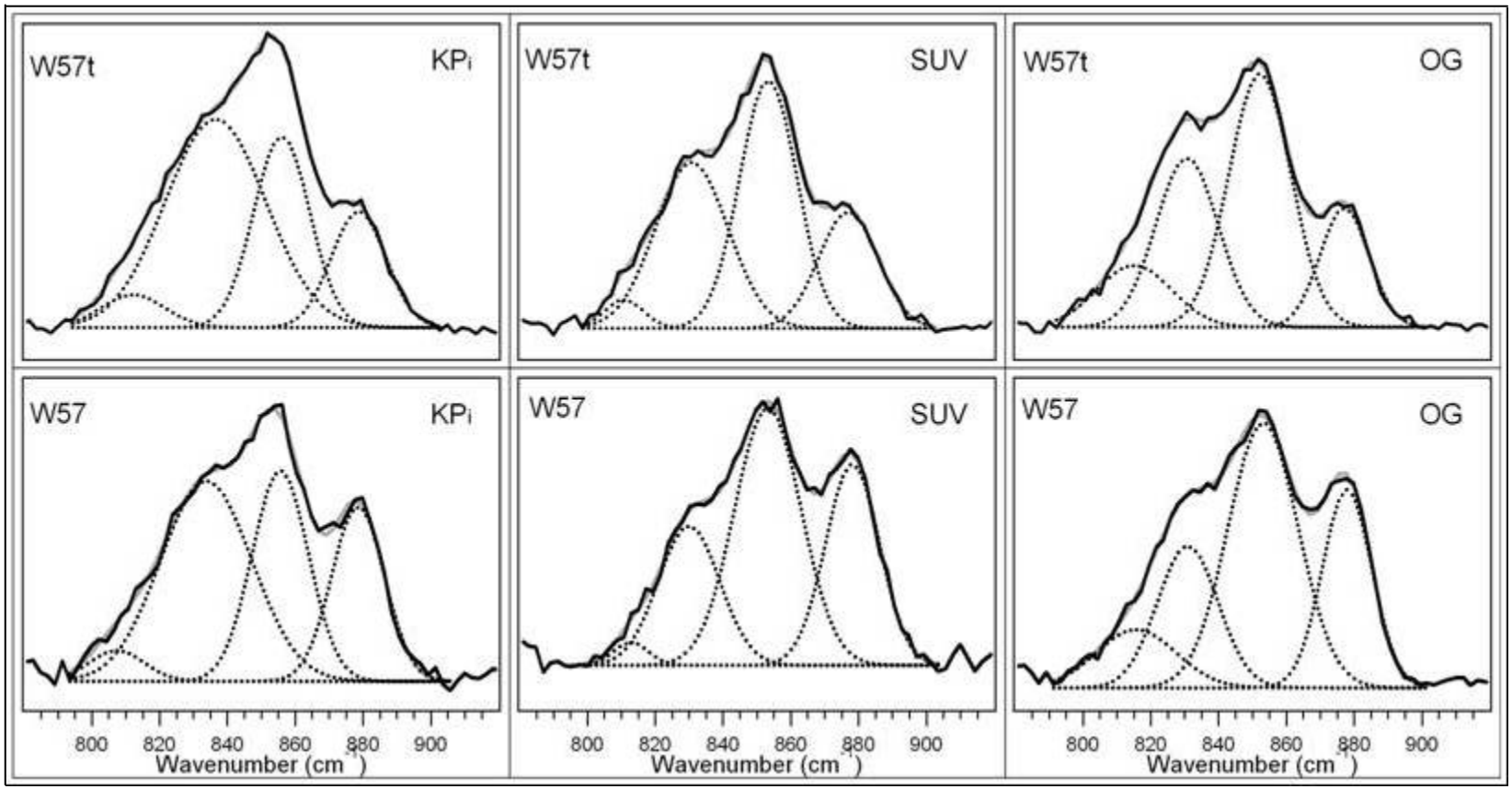

Figure 5. Gaussian decompositions of the 800-900 cm^{-1} region for W57t and W57 in KP_i, SUVs, and OG.

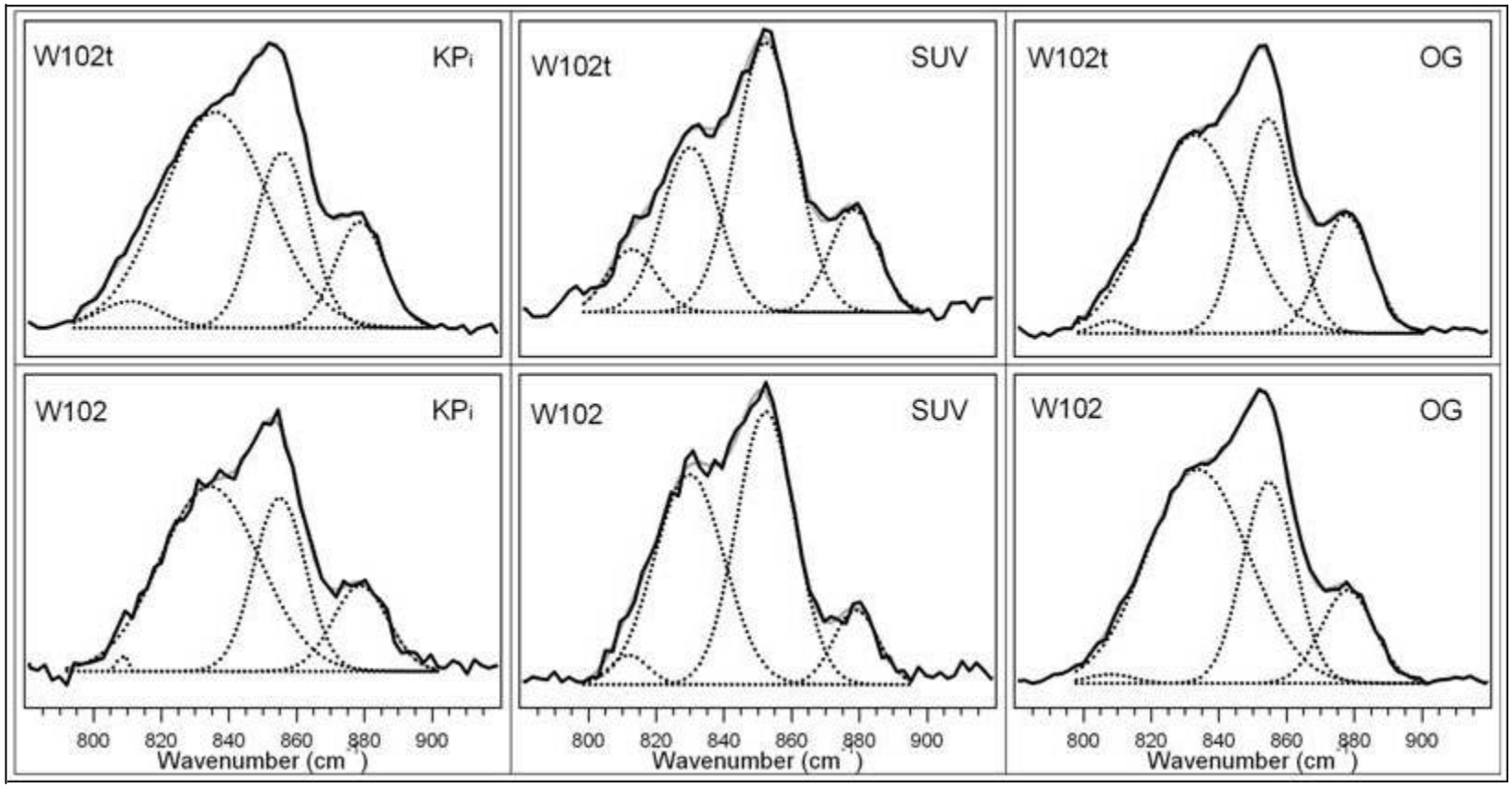

Figure 6. Gaussian decompositions of the 800-900 cm^{-1} region for W102t and W102 in KP_i, SUVs, and OG.

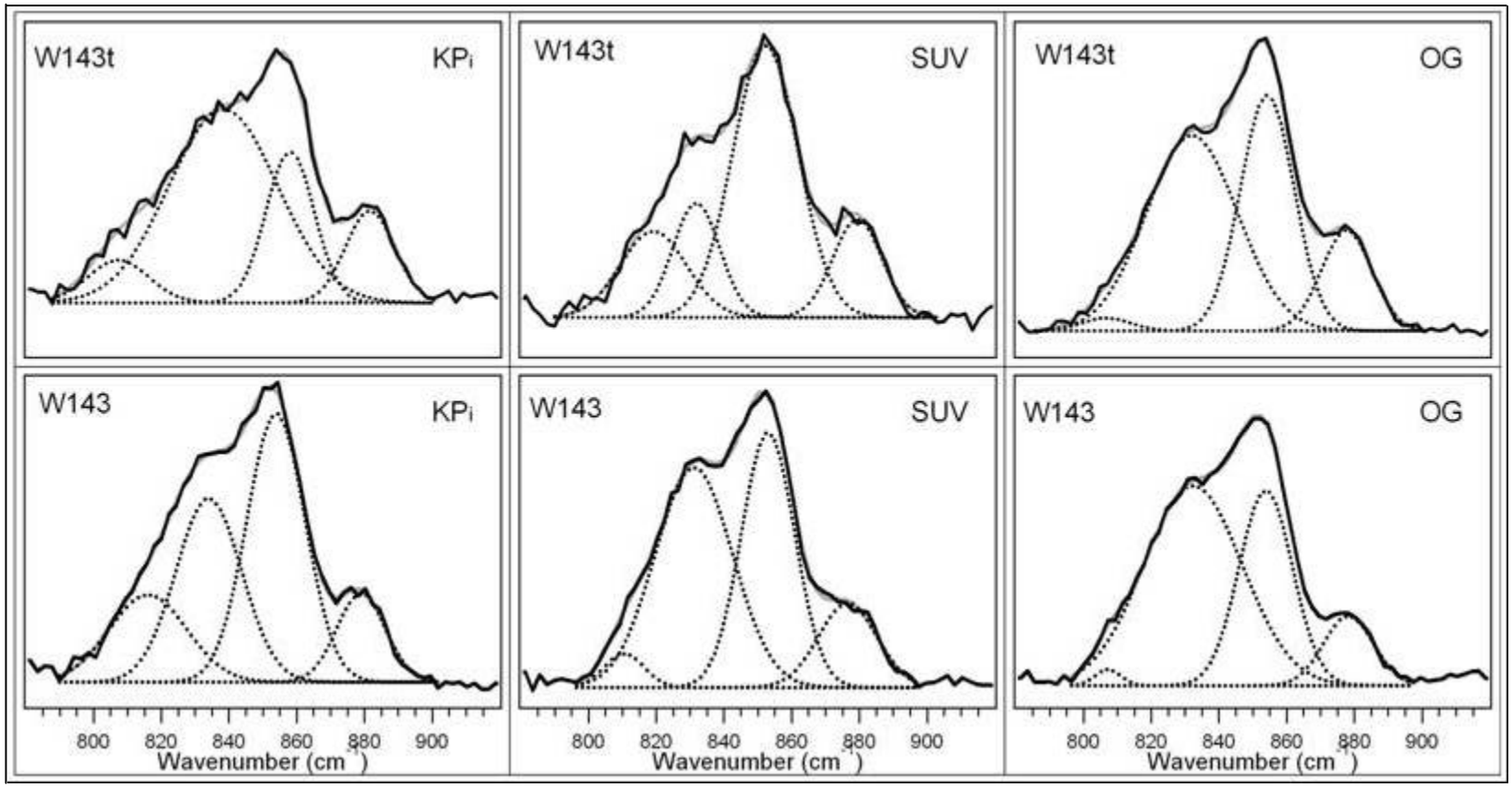

Figure 7. Gaussian decompositions of the 800-900 cm^{-1} region for W143t and W143 in KP_i, SUVs, and OG.

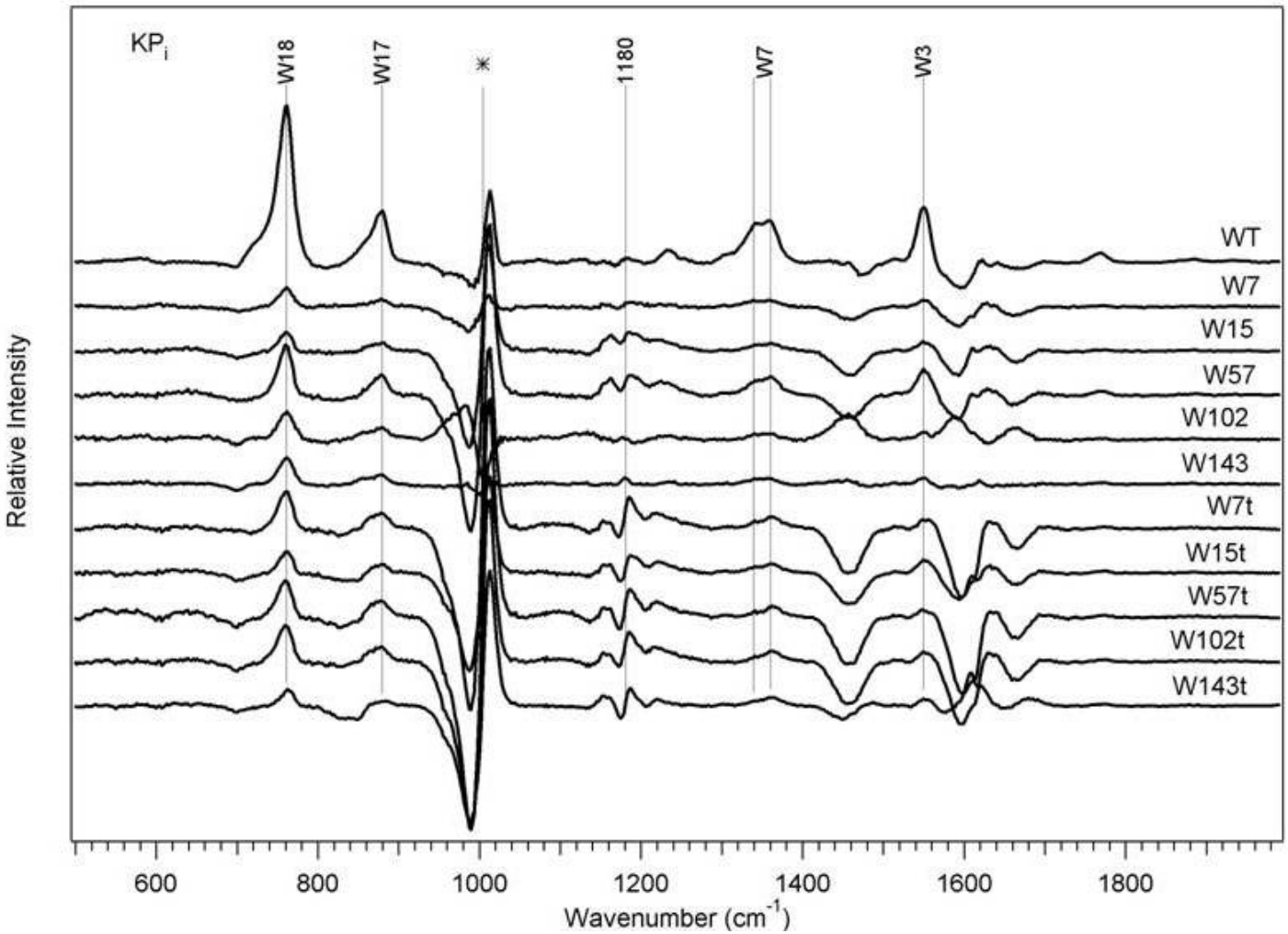

Figure 8. Subtraction of tyrosine mode Y19b (~1180 cm^{-1}) produces a tryptophan only spectrum in the 1340-1361 cm^{-1} region.

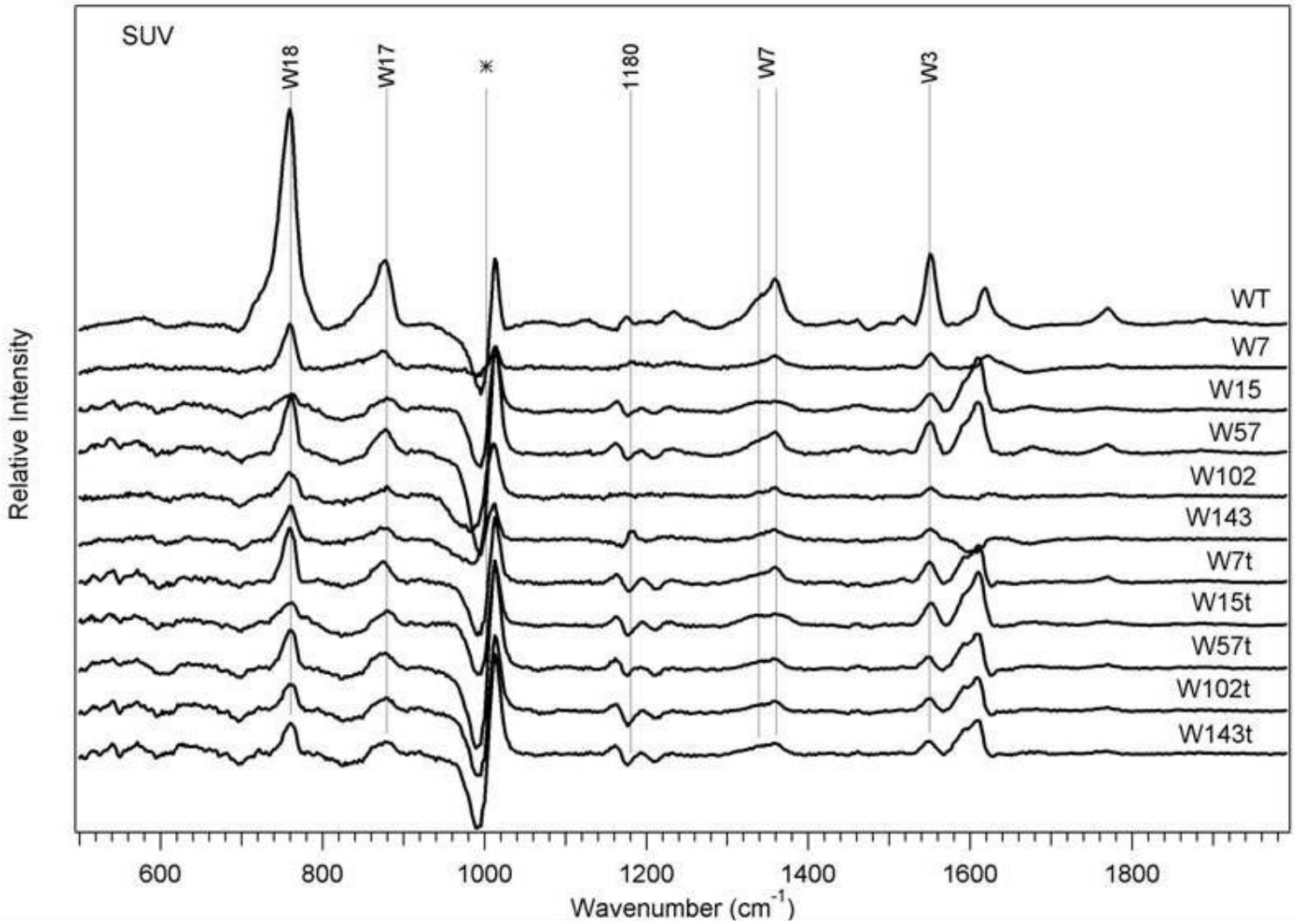

Figure 9. Subtraction of tyrosine mode Y19b (~1180 cm^{-1}) produces a tryptophan only spectrum in the 1340-1361 cm^{-1} region.

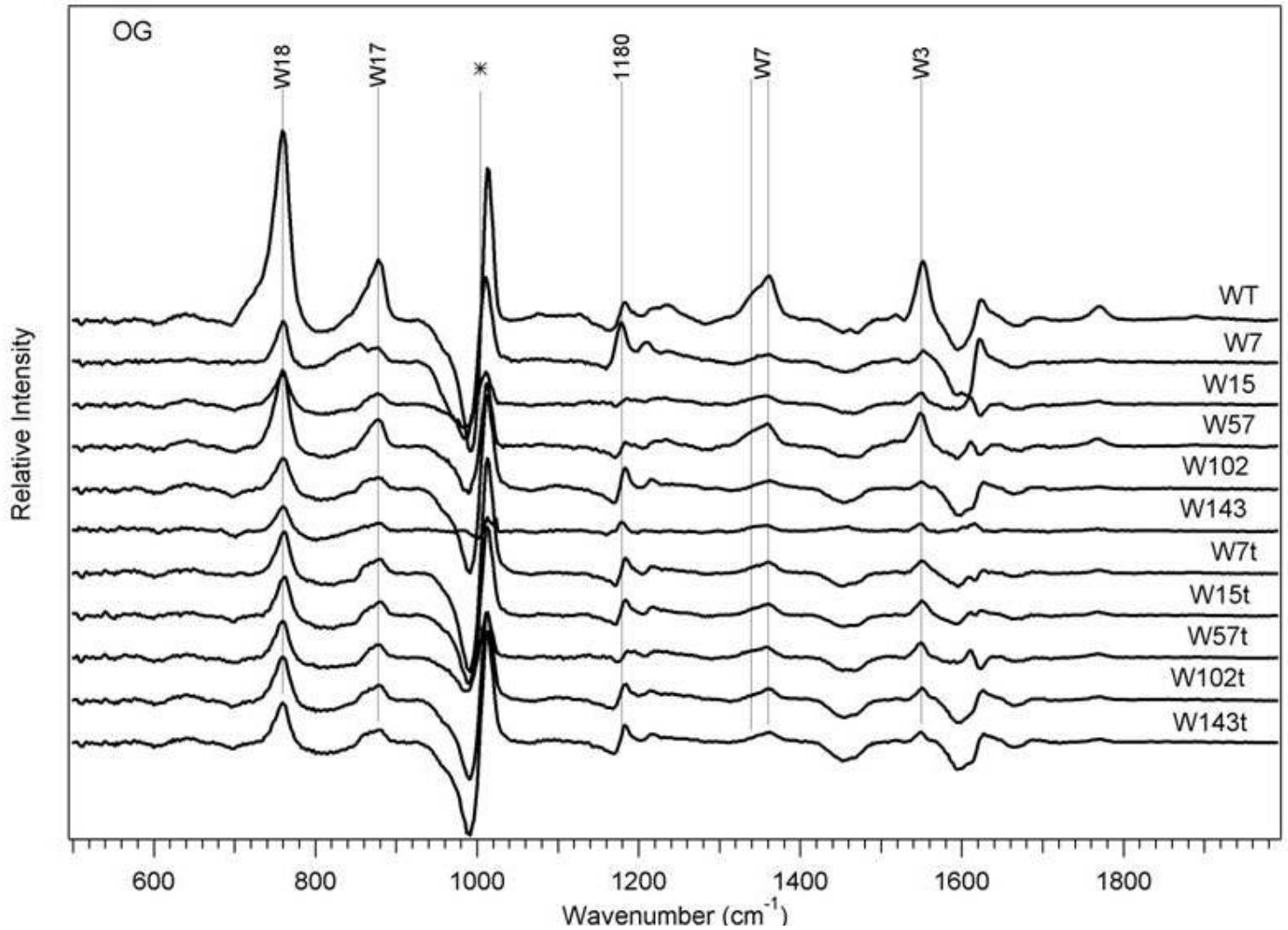

Figure 10. Subtraction of tyrosine mode Y19b (~1180 cm^{-1}) produces a tryptophan only spectrum in the 1340-1361 cm^{-1} region.